



TECHNISCHE
UNIVERSITÄT
DARMSTADT

Fachbereich Physik
Institut für Kernphysik

*Analysis of three-body effects in the
in-medium similarity renormalization group*

Master's thesis

by Matthias Heinz

Submitted: October 13, 2020

Examiners:

Prof. Achim Schwenk, Ph.D.

Dr. Alexander Tichai

Analysis of three-body effects in the in-medium similarity renormalization group

Master's thesis by Matthias Heinz

First examiner report: Prof. Achim Schwenk, Ph.D.

Second examiner report: Dr. Alexander Tichai

Submitted on October 13, 2020

Analyse von Dreiteilcheneffekten in der in-medium Ähnlichkeitsrenormierungsgruppe

Masterthesis von Matthias Heinz

1. Gutachten: Prof. Achim Schwenk, Ph.D.

2. Gutachten: Dr. Alexander Tichai

Tag der Einreichung: 13. Oktober, 2020

This work is licensed under a Creative Commons “Attribution
4.0 International” license.



Erklärung zur Abschlussarbeit gemäß § 22 Abs. 7 und § 23 Abs. 7 APB TU Darmstadt

Hiermit versichere ich, Matthias Heinz, die vorliegende Master-Thesis gemäß § 22 Abs. 7 APB der TU Darmstadt ohne Hilfe Dritter und nur mit den angegebenen Quellen und Hilfsmitteln angefertigt zu haben. Alle Stellen, die Quellen entnommen wurden, sind als solche kenntlich gemacht worden. Diese Arbeit hat in gleicher oder ähnlicher Form noch keiner Prüfungsbehörde vorgelegen.

Mir ist bekannt, dass im Falle eines Plagiats (§ 38 Abs. 2 APB) ein Täuschungsversuch vorliegt, der dazu führt, dass die Arbeit mit 5,0 bewertet und damit ein Prüfungsversuch verbraucht wird. Abschlussarbeiten dürfen nur einmal wiederholt werden.

Bei der abgegebenen Thesis stimmen die schriftliche und die zur Archivierung eingereichte elektronische Fassung gemäß § 23 Abs. 7 APB überein.

English translation for information purposes only:

Thesis statement pursuant to § 22 paragraph 7 and § 23 paragraph 7 of APB TU Darmstadt

I herewith formally declare that I, Matthias Heinz, have written the submitted Master's thesis independently pursuant to § 22 paragraph 7 of APB TU Darmstadt. I did not use any outside support except for the quoted literature and other sources mentioned in the paper. I clearly marked and separately listed all of the literature and all of the other sources which I employed when producing this academic work, either literally or in content. This thesis has not been handed in or published before in the same or similar form.

I am aware, that in case of an attempt at deception based on plagiarism (§ 38 paragraph 2 APB), the thesis would be graded with 5,0 and counted as one failed examination attempt. The thesis may only be repeated once.

In the submitted thesis the written copies and the electronic version for archiving are pursuant to § 23 paragraph 7 of APB identical in content.

Darmstadt, den 13. Oktober 2020

(Matthias Heinz)

Abstract

The in-medium similarity renormalization group (IMSRG) is an *ab initio* many-body method used to great success to solve the time-independent Schrödinger equation in medium-mass nuclear systems. Its computational cost scales polynomially in the size of the truncated model space, and its formalism is highly flexible, leading to multiple variants that have been developed to extend its original closed-shell formulation to open-shell systems.

The current state-of-the-art implementations truncate the IMSRG equations at the normal-ordered two-body level, the first non-trivial order in the expansion. In this work, we seek to systematically study the effects of extending this truncation to the normal-ordered three-body level, the so-called IMSRG(3) approximation. Exploitation of symmetries is essential to making IMSRG(3) calculations tractable. We present the reduced J -scheme IMSRG(3) working equations, which we arrive at by applying angular-momentum reduction to the IMSRG(3) for spherical systems.

We use our implementation of the J -scheme IMSRG(3) to investigate three-body contributions that first appear in the IMSRG(3) in light and medium-mass nuclei. We introduce approximate IMSRG(3) truncations that leave out the most expensive parts of the IMSRG(3). We find that in ^4He and ^{16}O in a restricted $e_{\text{max}} = 2$ model space, these approximate IMSRG(3) truncation schemes deliver small, sub-percent corrections to the ground-state energies and larger corrections to radii. Further, by investigating the behavior under the removal or inclusion of certain terms, we see that the organization by computational cost used to set up our approximate truncation schemes is poorly motivated and some computationally more expensive terms provide larger corrections to ground-state energies than the cheaper terms in the truncation. This work is a key step towards high-precision many-body calculations of medium-mass nuclei in the IMSRG.

Acknowledgements

This work was made possible by many people, more than I can reasonably mention here, but I want acknowledge the contributions of the key players here. I am grateful to my supervisors, Achim Schwenk and Alex Tichai. Achim is the main reason I came to Darmstadt. In my time here, he has taught me a lot in both the classroom and research settings. He has passed on a lot of knowledge and great intuition, and his deep knowledge on so many diverse topics motivates me to broaden my horizons and look beyond my immediate current interests. Achim also has made a lot of opportunities available to me during my time as a Master's student. In particular, I am extremely grateful for the opportunity to attend summer schools at Michigan State University and the ECT*. Alex has been an excellent collaborator on this work, and without his supervision and feedback the project would not have come nearly as far. Alex has brought deep knowledge of nuclear many-body physics and diverse perspectives to research discussions related to this work, and I am excited to continue working with him on improving upon the results presented here.

I would also like to thank my collaborators Kai Hebeler and Jan Hoppe, who also played a supervisory role in my research. Working with Kai on similarity renormalization group projects allowed me to initially find solid footing when I arrived in Darmstadt, and since then he has always been an excellent point of reference for conversations ranging from work-life balance to high-performance computing, from nuclear interactions and few-body systems to nuclear matter. Jan played a crucial role in helping me benchmark many parts of my implementations and was always available to talk through conceptual and technical problems I ran into. Jan also generated on fairly short notice nearly all of the matrix elements used as input in the calculations in this thesis.

In addition to my immediate collaborators, this work was positively influenced by the stimulating research environment I am in. I am grateful to the STRONGINT research group, where folks are happy to discuss all sorts of topics and provide an atmosphere that facilitates creative research. I would like to thank in particular my former and current officemates, Corbinian, Sabrina, Sebastian, and Victoria, who were typically the first people I would approach with questions or new ideas. I would also like to thank the people besides my supervisors that read through and gave feedback on parts or all of this thesis, Jan, Kai, Lars, and Mirko. Lars and Rodric also provided some useful templates for the title page and custom bibliography styles that are used in the thesis. Beyond the STRONGINT group, I am grateful to the many pleasant and helpful people I have

gotten to know in the context of the Institut für Kernphysik and the CRC 1245. Finally, I am grateful to Dick Furnstahl and the OSU low-energy theory group for helping me develop during my undergraduate time into a confident and capable nuclear physicist and continuing to make me feel comfortable whenever I return.

On a personal level, my path through life and also through the year of this thesis has only been possible thanks to the support of my parents, Ulrich Heinz and Christiane Heinz-Neidhart, and my younger brother, Michael Heinz. Of course, I would be nowhere without my parents, but in particular their emotional support during the time of the current pandemic has enabled me to focus on my work. I will always be grateful for how they guided me through life and the many opportunities they have provided me. My brother Michael is simultaneously my best friend and one of my greatest inspirations. I am glad that I can always look to him for motivation and turn to him whenever I need advice, help, or just a listening ear.

I am thankful to Stephanie Müller for all of her assistance during the process of moving to Darmstadt and in the time since. I am thankful to my siblings, Jutta Schröter, Richard Heinz, and Jürgen Dambeck, for answering my many questions about life in Germany and how things work.

Last but not least, I would like to thank my friends. I value the diverse set of perspectives and interests they bring to my life, and I appreciate that we are able to have uninhibited fun when we spend time together.

This work is supported in part by the Deutsche Forschungsgemeinschaft (DFG, German Research Foundation) – Projektnummer 279384907 – SFB 1245.

Contents

Contents	ix
List of Tables	xi
List of Figures	xiii
1 Introduction	1
1.1 Goals	3
1.2 Outline	4
2 Nuclear forces	7
2.1 Nuclear forces from chiral effective field theory	7
2.2 Similarity renormalization group evolution of nuclear forces	10
2.3 Representations of nuclear potentials	12
2.3.1 Jacobi momentum space	13
2.3.2 Jacobi harmonic-oscillator space	14
2.3.3 Single-particle harmonic-oscillator space	15
3 Many-body basics and many-body expansion methods	17
3.1 Second quantization	17
3.2 Normal ordering	20
3.2.1 General properties	20
3.2.2 Vacuum normal ordering	22
3.2.3 In-medium normal ordering	22
3.3 The Hartree-Fock method	25
3.4 Many-body perturbation theory	27
3.5 Non-perturbative techniques	30
4 The in-medium similarity renormalization group	33
4.1 Basic formalism	33
4.2 Truncation schemes	35
4.2.1 IMSRG(2)	36
4.2.2 IMSRG(3)	37
4.3 Generator selection	39

4.4	The Magnus expansion	43
4.5	Application to ${}^4\text{He}$	46
5	Angular-momentum coupling for the IMSRG	49
5.1	Wigner-Eckart theorem	49
5.2	Angular-momentum reduction for scalar operators	51
5.2.1	Operator representation	51
5.2.2	Coupled many-body expressions	55
5.2.3	Coupled fundamental commutators	57
5.2.4	Validation of numerical implementation	61
5.3	Outlook towards tensor operators	62
6	Results	63
6.1	Model space and Hamiltonian details	63
6.2	Truncation schemes	65
6.3	IMSRG(3)- N^7 results	67
6.4	Approximate IMSRG(3) truncation-scheme analysis	71
7	Summary and outlook	73
A	m-scheme fundamental commutators for the IMSRG(3)	75
A.1	$[A^{(1)}, B^{(1)}]$	75
A.2	$[A^{(1)}, B^{(2)}]$	76
A.3	$[A^{(2)}, B^{(2)}]$	76
A.4	$[A^{(1)}, B^{(3)}]$	76
A.5	$[A^{(2)}, B^{(3)}]$	77
A.6	$[A^{(3)}, B^{(3)}]$	77
B	Simplification strategies for coupled fundamental commutators	79
B.1	Using antisymmetry of input operator matrix elements	79
B.2	Using antisymmetry of output operator matrix elements	80
C	IMSRG(3) for the pairing Hamiltonian	83
	Bibliography	85

List of Tables

6.1	List of IMSRG(3) fundamental commutators ordered by computational cost. Right columns indicate whether the commutator is included in various approximate IMSRG(3) truncation schemes (see text for details).	65
6.2	Jacobi-NCSM results for the ground-state energy of ${}^4\text{He}$ as a function of the truncation parameter N_{max} for the NN-only EM 1.8 potential and the NN+3N EM 1.8/2.0 potential. $N_{\text{max}} = \infty$ values are based on an exponential extrapolation using the values of $E_{{}^4\text{He}}$ for $N_{\text{max}} \geq 12$	67

List of Figures

1.1	The nuclear landscape, with stable and unstable atomic nuclei denoted by the black and green squares, respectively, and a theoretical prediction of the limit of bound nuclei indicated by the red bands.	2
1.2	Chart of nuclides showing in red nuclei for which <i>ab initio</i> calculations involving two- and three-body interactions had been done in 2009 (top left) to 2018 (bottom right). Only calculations for which convergence with respect to basis size was achieved are included in the charts.	3
2.1	The contributions to NN, 3N, and 4N interactions in chiral EFT up to order $N^4\text{LO}$. Solid lines indicate nucleon propagators. Dashed lines indicate pion propagators. The number of new LECs for the new interaction contributions at each new order is shown in the top right corner.	8
2.2	The total proton-neutron scattering cross section calculated order by order at different energies using chiral potentials with 68% and 95% degree of belief intervals indicated by the thick and thin error bars obtained via Bayesian uncertainty quantification.	10
2.3	An example of an SRG-evolved potential using the chiral EMN NN potential at $N^4\text{LO}$ in the $^3\text{S}_1$ part of the $^3\text{S}_1$ - $^3\text{D}_1$ channel.	12
3.1	The partial sums (left) and order-by-order contributions (right) for an MBPT calculation of the ground-state energy of ^{16}O using a harmonic-oscillator reference state (top) and a Hartree-Fock reference state (bottom). The red, blue, and yellow points are for $N_{\text{max}} = 2, 4$, and 6 , the basis truncation parameter for the approach used.	29
4.1	Schematic diagram showing the minimal decoupling scheme taken in the IMSRG.	39
4.2	The left panel shows $E(s=0)$ and $E(s \rightarrow \infty)$ for an IMSRG(2) calculation of ^4He for $\hbar\Omega$ ranging from 16 MeV to 32 MeV. The interaction used is the EM NN interaction with a regulator cutoff $\Lambda = 500$ MeV and SRG-evolved to $\lambda = 1.8 \text{ fm}^{-1}$. The right panel shows the flowing energy $E(s)$ along with the energy with second- and third-order MBPT corrections included for $\hbar\Omega = 32$ MeV. The right panel is similar for the different $\hbar\Omega$ of the left panel.	47

6.1	IMSRG(2) ground-state energies (top row) and charge radii (bottom row) of ${}^4\text{He}$ for the NN-only EM 1.8 potential (left column) and the NN+3N EM 1.8/2.0 potential (right column) as a function of the oscillator frequency $\hbar\Omega$ for the HF and NAT bases. The HF basis is constructed in $e_{\text{max}} = 2$, and the NAT basis is constructed in $e_{\text{max}} = 14$, with $E_{3\text{max}} = 16$ for the NN+3N case, before being truncated to $e_{\text{max}} = 2$ for the IMSRG(2) calculation.	68
6.2	Ground-state energies (top row) and charge radii (bottom row) of ${}^4\text{He}$ for the NN-only EM 1.8 potential (left column) and the NN+3N EM 1.8/2.0 potential (right column) as a function of the oscillator frequency $\hbar\Omega$ for the NAT basis obtained via IMSRG(2) and IMSRG(3)- N^7 calculations. The NAT basis is constructed in $e_{\text{max}} = 14$, with $E_{3\text{max}} = 16$ for the NN+3N case, before being truncated to $e_{\text{max}} = 2$ for the IMSRG calculations.	69
6.3	Ground-state energies (top row) and charge radii (bottom row) of ${}^4\text{He}$ for the NN-only EM 1.8 potential (left column) and the NN+3N EM 1.8/2.0 potential (right column) as a function of the oscillator frequency $\hbar\Omega$ for the HF basis obtained via IMSRG(2) and IMSRG(3)- N^7 calculations. The HF basis is constructed in $e_{\text{max}} = 2$	70
6.4	Ground-state energies of ${}^{16}\text{O}$ for the NN-only EM 1.8 potential resulting from IMSRG calculations using the IMSRG(2) and various approximated IMSRG(3) truncation schemes (see text for details). Calculations were done at an oscillator frequency of 20 MeV, and a NAT reference state was used. The NAT basis is constructed in $e_{\text{max}} = 14$ before being truncated to $e_{\text{max}} = 2$ for the various many-body calculations.	72
C.1	The correlation energy E_{corr} for the solution of the pairing Hamiltonian obtained via exact diagonalization, IMSRG(2), and IMSRG(3) for $-1 \leq g \leq 1$	84

Chapter 1

Introduction

Nuclear physics aims to understand systems where the structure and dynamics are dominated by the strong interaction, one of the four fundamental forces of nature. The goals of nuclear science are well-described by the overarching open questions identified by the U.S. National Academy of Science in *Exploring the Heart of Matter* [1]:

1. How did matter come into being and how does it evolve?
2. How does subatomic matter organize itself and what phenomena emerge?
3. Are the fundamental interactions that are basic to the structure of matter fully understood?
4. How can the knowledge and technological progress provided by nuclear physics best be used to benefit society?

At the heart of this work is the second question, with the focus of our attention being on the structure of atomic nuclei.

Atomic nuclei consist of protons and neutrons, collectively referred to as nucleons. The interaction between nucleons is dominated by the strong interaction, and nuclei as self-bound systems of nucleons form as the result of the strong interaction overcoming a strong kinetic repulsion due to nucleons being fermions and obeying the Pauli exclusion principle. Emergent out of the interplay between these two effects, with contributions from the weak and electromagnetic interactions, is the nuclear landscape, shown in Fig. 1.1. All of these isotopes arise out of the same basic physics, with constituent nucleons interacting via basic two- and three-particle interactions.

Ab initio nuclear theory aims to realize this understanding of the nuclear landscape in theoretical calculations, determining first the interactions between nucleons in a way that is connected to the fundamental theory of the strong interaction and then modeling nuclei using only the interactions between nucleons as input. Using only these interactions as inputs means that *ab initio* methods have far-reaching predictive power with a large range

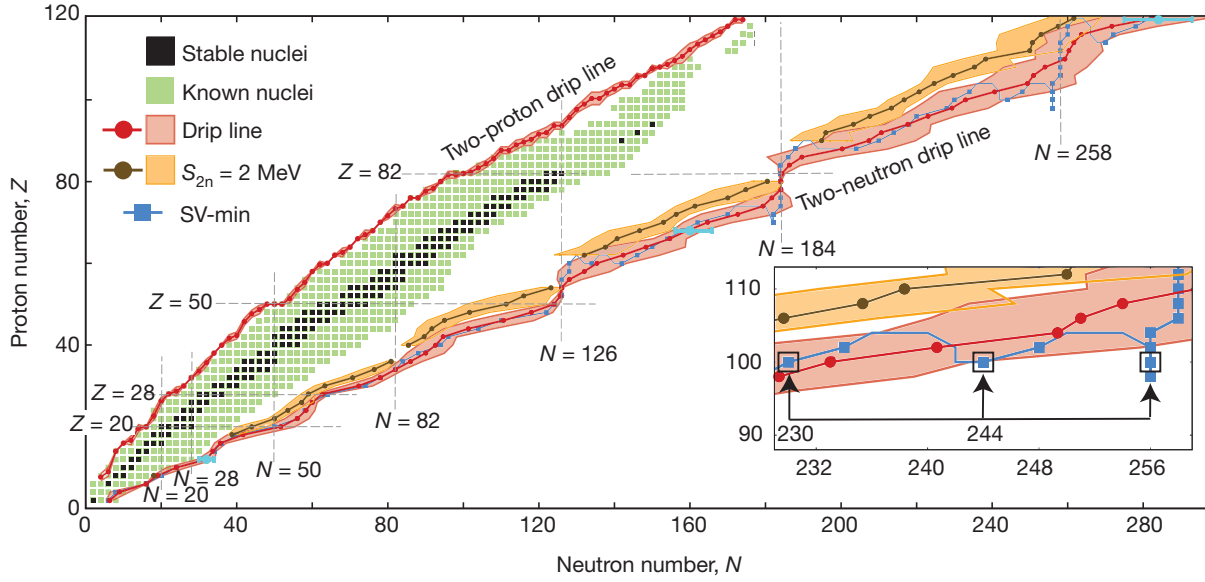


Figure 1.1: The nuclear landscape, with stable and unstable atomic nuclei denoted by the black and green squares, respectively, and a theoretical prediction of the limit of bound nuclei indicated by the red bands. Figure taken from Ref. [2].

of applicability. An additional requirement for the *ab initio* approach is that the methods used are in a theoretical limit exact and thus systematically improvable for any practical approximation. This feature also allows the *ab initio* approach to in principle deliver robust uncertainty estimates, allowing for the meaningful comparison between experiment and theory and also between different *ab initio* theoretical approaches.

Over the past two decades, the range of *ab initio* results has expanded rapidly, as is shown in Fig. 1.2. This change was driven by a shift in our understanding of *low-energy* nuclear physics, both in the determination of nuclear interactions and in the subsequent modeling of nuclei. The essential change in our understanding of nuclear forces is encapsulated in the effective field theory (EFT) and renormalization group (RG) methods. Underlying both of these ideas is the concept of limited resolution in low-energy physics and the realization that behavior at short distances (small wavelengths or high energies) does not affect the big picture at long distances. Effective field theory methods connect to underlying fundamental theories explicitly setting the scale to include essential long-distance physics and generating the most general expansion for the short-distance physics in terms of contact interactions [4–7]. Renormalization group methods allow for varying of the resolution scale, decoupling or integrating out high-energy details to produce an efficient low-resolution description of the system at hand [8–10]. These two obviously synergistic methods have worked together to produce low-resolution nuclear forces rooted in the fundamental theory of quantum chromodynamics.

With these new, more efficient low-energy nuclear forces and the ever increasing avail-

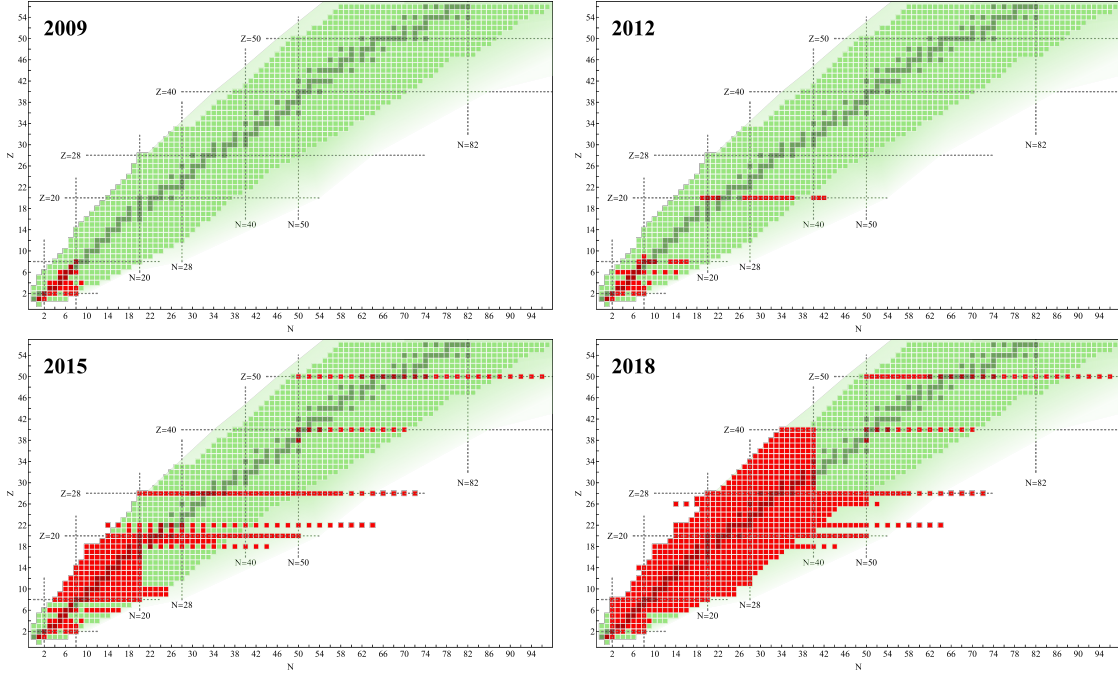


Figure 1.2: Chart of nuclides showing in red nuclei for which *ab initio* calculations involving two- and three-body interactions had been done in 2009 (top left) to 2018 (bottom right). Only calculations for which convergence with respect to basis size was achieved are included in the charts. Figure courtesy of Heiko Hergert [3].

able computational resources, the parallel development of nuclear many-body methods was uncapped. New developments on well-established methods, such as the coupled cluster approach, and the introduction of new methods, such as the in-medium similarity renormalization group, have carried *ab initio* nuclear theory to its present state. A crucial role was played by the developments on many-body expansion methods, such as coupled cluster or the in-medium similarity renormalization group, whose computational cost scales polynomially in the system size rather than exponentially like exact diagonalization approaches or Monte Carlo simulations. These methods are the best candidates available for extending the reach of *ab initio* nuclear theory to the heavy-mass region and the neutron-rich medium-mass region.

1.1 Goals

The focus of this work is the in-medium similarity renormalization group (IMSRG) [11]. As indicated by its name, it brings the RG approach of decoupling low- and high-energy states to the many-body problem, seeking to decouple the state of a system from its elementary excitations. It is flexible in that it can target both ground states and low-lying excited states and calculate energies as well as expectation values for other operators, and

while its original formulation centers on describing closed-shell nuclei, multiple variants are able to model open-shell nuclei as well [12–16].

The current state-of-the-art IMSRG approaches truncate the formalism at the IMSRG(2) level, the first non-trivial truncation where up to normal-ordered two-body operators are kept in the equations. This truncation has been quite successful, but for the purposes of reaching higher precision and allowing for quantification of many-body uncertainties, extending the truncation to the IMSRG(3) level is of great interest. In practice, the general IMSRG(3) is computationally too expensive to allow for a systematic study in even the smallest systems and model spaces. By considering only closed-shell systems, one can apply spherical symmetry to reduce the IMSRG(3) based on the shared symmetries of the system, the Hamiltonian, and computational basis. For the IMSRG, this formulation is less restrictive than one may expect, as the valence-space IMSRG can be used to produce an effective shell-model Hamiltonian that can be fed into a shell-model code and predict the properties of open-shell nuclei as well [12, 13, 17]. In this work, we perform the angular-momentum reduction of the IMSRG(3). We aim to use this to systematically study the improvements offered by the IMSRG(3) for the ground-state properties of light and medium-mass nuclei.

1.2 Outline

The remainder of this thesis is structured as follows:

- In Chapter 2, we introduce some aspects of the theory of nuclear forces. We focus on the modern approaches to deriving nuclear forces and the construction and generation of low-resolution Hamiltonians that improve the convergence of many-body calculations.
- In Chapter 3, we introduce the many-body formalism that underlies the IMSRG. We introduce some related many-body methods that also build on this formalism to help position the IMSRG in the greater space of available many-body methods.
- In Chapter 4, we discuss the IMSRG in detail. We discuss the general formalism and the IMSRG(2) and IMSRG(3) truncations. We also discuss generator choice, which sets how the IMSRG decouples low and high energies, and the Magnus expansion, an extension that makes the IMSRG easier to solve and easier to apply to other observables. We show some benchmark results for our implementation of the IMSRG(2) for ${}^4\text{He}$.
- In Chapter 5, we introduce the angular-momentum reduction formalism. We apply this formalism to the IMSRG(3) and some auxiliary many-body operations. The result is the IMSRG(3) in a spherically symmetric basis, which is computationally more efficient and allows us to solve the flow equations for light and medium-mass nuclei in small model spaces.

- In Chapter 6, we discuss the contributions of the IMSRG(3) truncation to ground-state properties of nuclei using the optimized spherically-reduced IMSRG(3). We consider how the IMSRG(3) handles different reference state choices, and we investigate what the effects of individual contributions to the IMSRG(3) are.
- In Chapter 7, we summarize our results and offer an outlook for the next steps in exploring three-body effects in the IMSRG.

Chapter 2

Nuclear forces

For low-energy nuclear physics, the goal is to understand the structure and dynamics of systems with nucleons as constituents. Thus, a key input into any theoretical calculations of such systems is the interactions between nucleons. However, quantum chromodynamics (QCD), the theory of the strong interaction, is given in terms of quarks and gluons, not nucleons. Moreover, at low energies the strong interaction coupling constant $\alpha_s(q^2)$ becomes large, preventing a fundamental closed-form solution for the interactions between color-neutral hadrons.

As a result, various approaches to determining the interactions between nucleons have been developed. One such approach is the phenomenological expansion of the interaction between two nucleons into terms with different spin, isospin, and angular-momentum dependences. The (position- and momentum-dependent) strength of each of these terms is then fit to nucleon-nucleon scattering data, giving rise to, for example, the AV18 potential [18]. This approach has several features that make it undesirable for *ab initio* nuclear theory. First, it does not connect to the underlying fundamental theory. Second, this approach does not prescribe a way to arrive at consistent three-nucleon forces. Additionally, the fitting procedure often includes scattering data at relatively high energies when compared to the expected kinetic energy of nucleons in nuclei or nuclear matter, making such phenomenological interactions highly non-perturbative.

In this chapter, we discuss chiral effective field theory as an alternative to the phenomenological determination of nuclear forces and the similarity renormalization group as a method to generally “soften” interactions for many-body calculations. Then we discuss some details regarding different bases in which one can represent nuclear potentials.

2.1 Nuclear forces from chiral effective field theory

A modern approach to deriving nuclear potentials is chiral effective field theory. The EFT approach allows one to systematically construct a field theory that approximates a more fundamental theory in a low-energy domain [5–7]. In this appropriately chosen

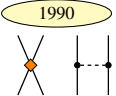
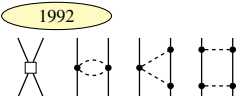
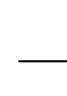
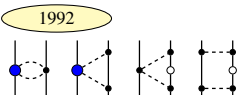
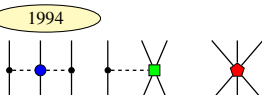
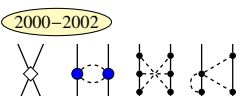
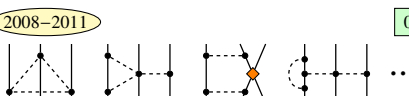
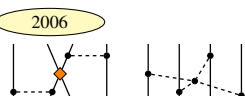
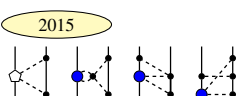
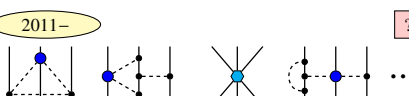
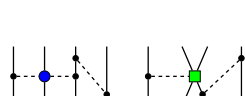
	NN	3N	4N
LO $\mathcal{O}(Q^0/\Lambda^0)$	 <div>1990</div> <div>2</div>	—	—
NLO $\mathcal{O}(Q^2/\Lambda^2)$	 <div>1992</div> <div>7</div>	 <div>1992, 1994</div>	—
N ² LO $\mathcal{O}(Q^3/\Lambda^3)$	 <div>1992</div> <div>0</div>	 <div>1994</div> <div>2</div>	—
N ³ LO $\mathcal{O}(Q^4/\Lambda^4)$	 <div>2000–2002</div> <div>12</div>	 <div>2008–2011</div> <div>0</div>	 <div>2006</div> <div>0</div>
N ⁴ LO $\mathcal{O}(Q^5/\Lambda^5)$	 <div>2015</div> <div>0</div>	 <div>2011–</div> <div>?</div>	 <div>?</div>

Figure 2.1: The contributions to NN, 3N, and 4N interactions in chiral EFT up to order N⁴LO. Solid lines indicate nucleon propagators. Dashed lines indicate pion propagators. The number of new LECs for the new interaction contributions at each new order is shown in the top right corner. Figure taken from Ref. [19].

domain, one can use the most efficient degrees of freedom to formulate the theory. The construction of the theory relies on knowing the symmetries (exact and approximate) of the underlying theory. Constructing the most general Lagrangian consistent with these underlying symmetries yields the most general S -matrix [4].

To construct an effective field theory, one identifies the degrees of freedom one wants to work with and identifies a high-momentum scale Λ of the underlying theory that characterizes physics no longer resolved by the EFT [5]. The EFT then should be an efficient, approximately complete description of the relevant physics at momenta Q small compared to Λ . The chosen degrees of freedom are used to construct the most general Lagrangian consistent with the underlying symmetries, which will have an infinite number of terms each with their own coefficients, the so-called low-energy constants (LECs). The EFT can then be used to calculate observables up to some precision in an expansion in Q/Λ , made systematic by a power-counting approach.

For chiral EFT, the underlying theory is QCD in the light-quark sector (here this means only up and down quarks), where the Lagrangian has an approximate chiral symmetry $SU(2)_L \times SU(2)_R$ in the limit of vanishing quark masses and no electroweak interactions [5]. This symmetry is spontaneously broken, giving rise to the pion as the Goldstone boson associated with the broken $SU(2)_A$ symmetry, as well as explicitly broken by the non-zero

quark masses [20]. A logical choice of degrees of freedom is then nucleons and pions. The high-momentum scale Λ_b is set by the lightest meson not included in our degrees of freedom, the ρ meson with a mass of $m_\rho \approx 770$ MeV [7]. The low-momentum scale is a collective scale given by $\max(Q, m_\pi)$.

The resulting potential contributions from chiral EFT have either explicit pion exchanges or contact interactions with LECs describing short-range physics unresolved by the EFT, as shown in Fig. 2.1. The first consistent three-nucleon (3N) interactions appear at next-to-next-to-leading order (N^2 LO), and the first four-nucleon (4N) interactions appear at next-to-next-to-next-to-leading order (N^3 LO). Among the features that make EFTs so powerful is that they allow for clear error estimates [21–23], given proper power counting, by considering the order-by-order convergence of observables and seeing that the orders left out due to a truncation at order N should contribute something like

$$\Delta O^{(N)} \sim O\left(\frac{\max(Q, m_\pi)}{\Lambda_b}\right)^{N+1}, \quad (2.1)$$

where O is the exact result for some observable of interest (see Fig. 2.2).

For potentials from chiral EFT, at each order a finite number of undetermined LECs are introduced with the new contributions to the potential. For nucleon-nucleon (NN) interactions, these can be determined by fitting to *low-energy* scattering data. For 3N interactions, the relevant LECs must be fit to three-body or four-body observables. Typical choices for these observables at N^2 LO, where two three-body LECs, c_D and c_E , need to be fit, are the triton binding energy and either the triton half-life or the ^4He charge radius [19]. Additionally, some contributions at later orders in the expansion only depend on LECs from previous orders. For example, the 3N force contributions at N^3 LO require no new LECs to be fit.

Some comments are now in order regarding interactions as used in this thesis. The derivation of potentials requires the explicit regularization of momenta to make divergent integrals over intermediate momenta convergent. This introduces a dependence on the regularization scheme and scale used, which is an artifact of the finite order of our EFT. Each additional order in the EFT cancels the scale dependence of the previous order, and in the limit of infinite order all observables should not depend on the cutoff scale and scheme used (within reason). For every interaction used we state the order, the regularization scale, and the family of interactions, which specifies the regularization scheme used.

We primarily use two families of interactions. The first set is a family of interactions with NN interactions given up to N^3 LO, which was worked out by Entem and Machleidt in 2003 [24]. These interactions are denoted by EM when they are used. The second set was worked out by Entem, Machleidt, and Nosyk in 2017 and provides NN interactions up to N^4 LO [25]. These interactions are denoted by EMN. From 2007 through 2011, the 3N interactions were worked out [26–28], and the consistent (in terms of power counting and regularization scheme) 3N potentials with these families up to N^3 LO were presented in 2015 by Hebeler *et al.* [29]. At N^3 LO, the chiral power counting dictates the inclusion

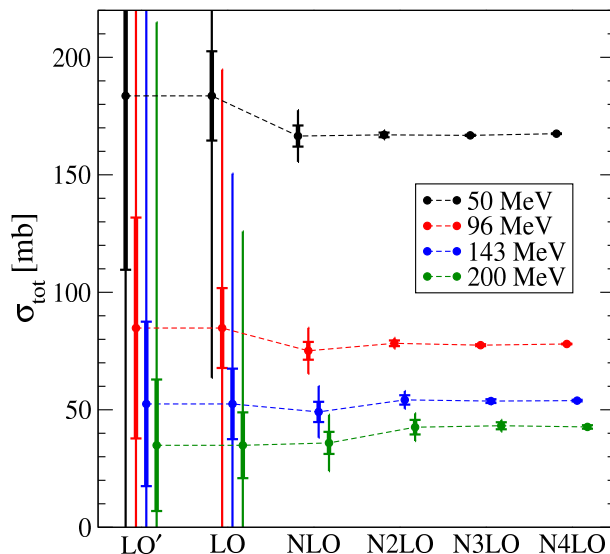


Figure 2.2: The total proton-neutron scattering cross section calculated order by order at different energies using potentials from Ref. [23] with 68% and 95% degree of belief intervals indicated by the thick and thin error bars obtained via Bayesian uncertainty quantification [21]. Figure taken from Ref. [21].

of 4N forces (see Fig. 2.1). However, this is generally *not* done because the inclusion of 4N forces in calculations is prohibitively expensive and past results have shown that they contribute at the sub-1% level [30, 31].

Chiral EFT essentially resolves all of the shortcomings of phenomenological potentials mentioned previously. There are still many open questions regarding the derivation of potentials via chiral EFT and their consistent application in many-body calculations. For example, there are multiple schools of thought regarding what the correct power counting for nuclear potentials is [32–34]. Additionally, the uncertainties from the regularization scheme and scale for nuclear potentials are still most likely dominant in many-body calculations. However, the rapid expansion of the range of *ab initio* calculations over the past two decades has been in no small part due to the introduction of chiral potentials and the development of auxiliary tools to aid in their application to many-body calculations.

2.2 Similarity renormalization group evolution of nuclear forces

The similarity renormalization group (SRG) is a method that has been used to great success to “soften” nuclear interactions [9, 35, 36]. The key idea of the SRG is the generation of a continuous unitary transformation of a given Hamiltonian H ,

$$H(s) = U(s) H U^\dagger(s), \quad (2.2)$$

where s is the continuous flow parameter. The resulting flow equation gives the evolution of the Hamiltonian

$$\frac{dH(s)}{ds} = [\eta(s), H(s)], \quad (2.3)$$

with $\eta(s) = U(s)dU^\dagger(s)/ds$ and we choose $H(0) = H$. An “appropriate” choice of the anti-Hermitian generator η can generate a unitary transformation such that $H(s)$ evolves, for example, towards a diagonal form. This leads to a decoupling of low- and high-energy states in the Hamiltonian, allowing for a truncation in momentum space or a discretized basis without distorting low-energy observables.

The evaluation of the commutator in the SRG flow equation generates higher-body forces in the evolved Hamiltonian, even if the initial Hamiltonian consists only of two- and three-body forces. This means that the fully unitary SRG evolution of an A -body Hamiltonian requires the evaluation of the flow equation in the A -body basis. For all but the smallest systems, this is computationally infeasible.

A pragmatic approach uses the SRG restricted to the three-body space to evolve two- and three-body nuclear forces to “softer” forms in momentum space [37], reducing coupling between low- and high-energy states. These evolved potentials are for few-body purposes equivalent to the un-evolved ones, reproducing the few-body binding energies, radii, and NN phase shifts exactly. After truncating the potentials, taking advantage of the decoupling, the few-body observables remain essentially unchanged, and the low-energy NN phase shifts are also preserved.

The typical choice for the generator in the so-called “free-space” SRG in nuclear applications is

$$\eta(s) = [T_{\text{rel}}, H(s)], \quad (2.4)$$

where T_{rel} is the relative kinetic energy of the two- and three-body systems. In two-body Jacobi momentum coordinates, T_{rel} is diagonal, thus the right-hand side of the flow equation clearly has a fixed point if $H(s)$ is ever diagonal. Evaluating the flow equation in momentum space in the two-body case for this choice for η gives

$$\frac{dV_2(s; p, p')}{ds} = -(p^2 - p'^2)^2 V_2(s; p, p') + \int dp'' (p^2 + p'^2 - 2p''^2) V_2(s; p, p'') V_2(s; p'', p'), \quad (2.5)$$

where p and p' are the incoming and outgoing Jacobi momenta of the two-body subsystem (see Section 2.3.1). We also used the conventional choice of leaving the kinetic energy invariant under the SRG evolution. Empirically, one can see that the first term dominates the evolution for far off-diagonal elements in nuclear applications, and so

$$V_2(s; p, p') \approx V_2(0; p, p') \exp(-s(p^2 - p'^2)^2). \quad (2.6)$$

Using a redefinition of the flow parameter

$$\lambda = \frac{1}{s^{1/4}}, \quad (2.7)$$

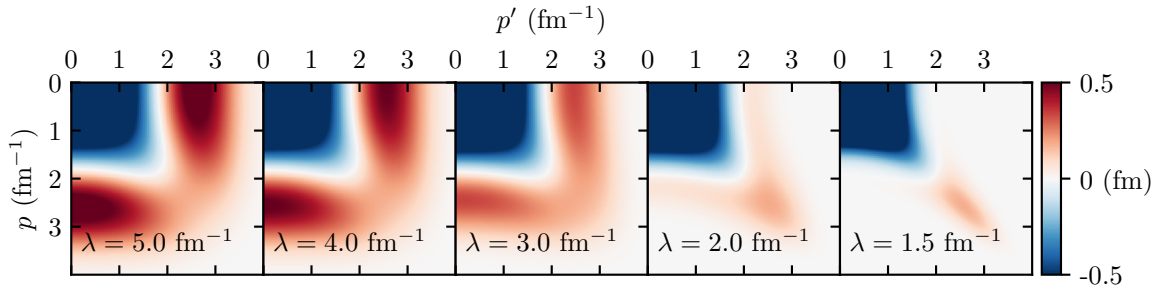


Figure 2.3: An example of an SRG-evolved potential using the chiral NN potential from Ref. [25] at $N^4\text{LO}$ in the $^3\text{S}_1$ part of the $^3\text{S}_1$ - $^3\text{D}_1$ channel.

which has units of fm^{-1} and evolves from $\lambda = \infty$ towards 0, one can see that over the course of the evolution off-diagonal parts of the potential outside a band of width λ begin to be exponentially suppressed [38]. Looking at Fig. 2.3, one can see that this is qualitatively true, and the desired decoupling between low- and high-momentum states is achieved.

These softened interactions can then be fed into many-body frameworks, which benefit strongly from the improved convergence with respect to model-space size. However, the few-body evolution of potentials neglects induced A -body forces, which do contribute in many-body calculations. One way to probe the size of the missing many-body forces is to do calculations with potentials evolved to different values of s or λ and see how much the calculated result depends on the renormalization scale. A strong dependence would indicate significant missing contributions from many-body forces while no dependence would indicate approximate renormalization group invariance, which is ultimately the goal [10].

2.3 Representations of nuclear potentials

The efficient representation of nuclear potentials exploits symmetries of the few-body system and the interactions. In particular, for 3N forces, where the potential can depend in principle on 18 parameters in momentum space $(\vec{k}_1, \vec{k}_2, \vec{k}_3, \vec{k}'_1, \vec{k}'_2, \vec{k}'_3)$, simplifications afforded by these symmetries are essential to being able to evaluate, store, and calculate with these potentials.

The essential symmetries of the free two- and three-nucleon systems (from which the potentials are determined) are [19]

- conservation of the center-of-mass momentum of the system,
- independence on the center-of-mass momentum in the nonrelativistic regime,
- and rotational invariance.

Additionally, one can simplify things dramatically by making the assumption that the masses of all nucleons are the same, a reasonable assumption given that the mass difference between the proton and neutron is less than a per mille [19]. In this approximation in the absence of electroweak interactions, the NN force would also be independent of isospin projection, however the Coulomb interaction breaks this isospin charge symmetry. Also, even without the Coulomb interaction, the chiral EFT expansion explicitly breaks isospin charge symmetry at higher orders, a result of it being constructed in a way that systematically accounts for the breaking of approximate symmetries.

In the following, we discuss some possible representations of NN forces, going from one of the representations most convenient for the evaluation of potentials to the representation of choice for the many-body methods discussed in this thesis. We mention along the way some of the analogous results for 3N forces. A more thorough treatment of this topic can be found in Ref. [19].

2.3.1 Jacobi momentum space

Going from single-particle momenta to Jacobi and center-of-mass momenta, like

$$\vec{k}_1, \vec{k}_2 \rightarrow \vec{p}, \vec{P}_{2N}, \quad (2.8)$$

$$\vec{k}_1, \vec{k}_2, \vec{k}_3 \rightarrow \vec{p}, \vec{q}, \vec{P}_{3N}, \quad (2.9)$$

allows one to factor out and ignore the center-of-mass degrees of freedom of the system. The Jacobi and center-of-mass momenta are defined as

$$\vec{p} \equiv \frac{\vec{k}_1 - \vec{k}_2}{2}, \quad (2.10)$$

$$\vec{P}_{2N} \equiv \vec{k}_1 + \vec{k}_2, \quad (2.11)$$

$$\vec{q} \equiv \frac{2\vec{k}_3 - \vec{P}_{2N}}{3}, \quad (2.12)$$

$$\vec{P}_{3N} \equiv \vec{k}_1 + \vec{k}_2 + \vec{k}_3. \quad (2.13)$$

For NN forces, this gives us two-body states of the form

$$|\vec{p} s_1 m_{s_1} s_2 m_{s_2} t_1 m_{t_1} t_2 m_{t_2}\rangle, \quad (2.14)$$

where $s_i = 1/2$, m_{s_i} , $t_i = 1/2$, m_{t_i} are the i -th particle's spin, spin projection, isospin, and isospin projection, respectively. In cases where explicit values of isospin projection are used, we adopt the convention that for protons $m_t = 1/2$ and for neutrons $m_t = -1/2$.

To take advantage of rotational invariance, one can decompose the potential into partial-wave channels, with two-body states like

$$|p [l (s_1 s_2) S] J m_J T m_T\rangle, \quad (2.15)$$

where p is the magnitude of \vec{p} , l is the relative orbital angular momentum of the two-body system, and S , J , m_J , T , m_T are the total spin, total angular momentum, total angular momentum projection, isospin, and isospin projection of the two-body system. The resulting potential

$$\langle p' [l' (s'_1 s'_2) S'] J' m'_J T' m'_T | V_{2N} | p [l (s_1 s_2) S] J m_J T m_T \rangle \quad (2.16)$$

is proportional to $\delta_{JJ'} \delta_{m_J m_{J'}}$ and independent of m_J due to rotational invariance. Additionally, antisymmetry under exchange of particle indices and parity conservation require it to also be proportional to $\delta_{SS'} \delta_{TT'}$ with the additional constraints

$$(-1)^{l+S+T+1} = (-1)^{l'+S+T+1} = 1, \quad (2.17)$$

$$l - l' = -2, 0, 2, \quad (2.18)$$

and charge conservation requires that it also is proportional to $\delta_{m_T m_{T'}}$. For notational convenience, we sometimes collect the partial-wave quantum numbers of states in a collective index α_2 , giving the concise notation for 2N potentials

$$\langle p' \alpha'_2 | V_{2N} | p \alpha_2 \rangle. \quad (2.19)$$

With this, the representation of NN forces has been reduced to two continuous variables, p and p' , and some strongly constrained partial-wave quantum numbers. For 3N forces, there is similar simplification possible, yielding three-body states of the form

$$|pq [(lS) J (\ell s) j] \mathcal{J} \mathcal{M}_{\mathcal{J}} (Tt) \mathcal{T} \mathcal{M}_{\mathcal{T}} \rangle, \quad (2.20)$$

where p , l , S , J , T still refer to the two-particle subsystem as before, q , ℓ , j are the Jacobi momentum, orbital angular momentum, and total angular momentum of the third nucleon relative to the two-body subsystem center-of-mass, and s and t are the spin and isospin of the third nucleon. Here, the 3N potential is, among other things, independent of $\mathcal{M}_{\mathcal{T}}$.

2.3.2 Jacobi harmonic-oscillator space

The transformation to Jacobi harmonic-oscillator (HO) space follows quite simply. Using the radial solutions to the isotropic three-dimensional harmonic oscillator with frequency $\hbar\Omega$, one obtains

$$\langle n' \alpha'_2 | V_{2N} | n \alpha_2 \rangle = \int dp p^2 dp' p'^2 R_{n'v'}(p') R_{nv}(p) \langle p' \alpha'_2 | V_{2N} | p \alpha_2 \rangle. \quad (2.21)$$

The radial solutions are given by

$$R_{nl}(p) = \sqrt{\frac{2(n!)}{(m\hbar\Omega)^{3/2} \Gamma(n+l+3/2)}} (\tilde{p})^l \exp(-\tilde{p}^2/2) L_n^{l+1/2}(\tilde{p}^2), \quad (2.22)$$

where m is the nucleon mass, $\tilde{p} \equiv p/\sqrt{m\hbar\Omega}$ is the dimensionless momentum, and $L_n^k(x)$ are the generalized Laguerre polynomials. For 3N forces, the Jacobi momenta q and q' must also be transformed, giving two more integrals.

In the infinite model-space limit, this transformation is exact, and the dependence on the basis frequency $\hbar\Omega$ disappears. However, for practical calculations a basis truncation n_{\max} must be introduced, which implicitly introduces an ultraviolet (UV) cutoff and an infrared (IR) cutoff on the potential. The UV cutoff is due to high frequencies requiring HO wave functions beyond the truncation to be resolved. The IR cutoff is due to the basis frequency $\hbar\Omega$ setting the minimum frequency reproducible by wave functions in the basis.

For a given truncation, the optimal $\hbar\Omega$ can be determined by making use of the variational principle, which states that for the true ground state the energy functional $E[|\psi\rangle]$ is stationary under infinitesimal variations of $|\psi\rangle$. In this case, one can look at the approximate ground state by solving the two- or three-body system (for example, via exact diagonalization). For the optimal $\hbar\Omega$, the ground-state energy will be minimal, guaranteed by the variational principle to be no less than the true ground-state energy. Many-body calculations are typically done with operators transformed at several $\hbar\Omega$. For energies the minimum result under this variation is taken to be the result of the calculation, but it is important to note that many many-body methods are *not* variational.

2.3.3 Single-particle harmonic-oscillator space

Many many-body methods used in nuclear physics, in particular also many-body expansion methods, work with operators given in a single-particle basis as input. This means we have a basis of single-particle states

$$\{|a\rangle\} \quad (2.23)$$

spanning the one-body Hilbert space. Then the set of product states

$$|ab\rangle = |a\rangle |b\rangle \quad (2.24)$$

spans the two-body Hilbert space. At this point these states are not appropriately antisymmetrized. At the end of this section, we discuss how to recover the required antisymmetry under exchange of particle indices.

In our case, we work with the single-particle harmonic-oscillator basis with the same frequency $\hbar\Omega$ as used in the transformation above. To be explicit, these states are of the form

$$|n_a(l_a s_a) j_a m_{j_a} t_a m_{t_a}\rangle . \quad (2.25)$$

The two-body single-particle states are then

$$|n_a(l_a s_a) j_a m_{j_a} t_a m_{t_a} n_b(l_b s_b) j_b m_{j_b} t_b m_{t_b}\rangle , \quad (2.26)$$

or, coupled to two-body total angular momentum J ,

$$|n_a n_b [(l_a s_a) j_a (l_b s_b) j_b] J m_J t_a m_{t_a} t_b m_{t_b}\rangle . \quad (2.27)$$

To connect the states in Eq. (2.26) with those in Eq. (2.21), one does a Talmi-Moshinsky transformation. This connects the relative and center-of-mass excitation numbers, n and N , and orbital angular momentum numbers, l and L , with the single-particle excitation numbers, n_a and n_b , and orbital angular momentum numbers, l_a and l_b . The central object of this transformation is the harmonic-oscillator bracket

$$\langle n_a n_b (l_a l_b) \Lambda | n N (l L) \Lambda \rangle , \quad (2.28)$$

where both sets of orbital angular momenta have been coupled to total orbital angular momentum Λ . The properties and evaluation of these brackets is discussed in detail in Refs. [39, 40]. By appropriately decoupling and recoupling angular momenta and applying the harmonic-oscillator brackets, one arrives at NN potential matrix elements of the form

$$\langle ab | V_{2N} | cd \rangle , \quad (2.29)$$

where a , b , c , and d are collective indices that run over the single-particle states in Eq. (2.25).

The matrix elements in Eq. (2.29) do not obey the required antisymmetry of fermions under exchange of particle indices since the product states $|ab\rangle$ are not antisymmetrized. Restoring the required antisymmetry, one obtains the antisymmetrized matrix elements

$$V_{2N,abcd} = \frac{1}{2}(1 - P_{ab})(1 - P_{cd}) \langle ab | V_{2N} | cd \rangle \quad (2.30)$$

$$= (1 - P_{cd}) \langle ab | V_{2N} | cd \rangle , \quad (2.31)$$

where P_{ab} exchanges the indices a and b in the following expression. The simplification above takes advantage of the symmetry

$$\langle ab | V_{2N} | cd \rangle = \langle ba | V_{2N} | dc \rangle , \quad (2.32)$$

arising due to the indistinguishability of the two particles. In the next chapter, we develop the fundamentals of the formalisms that use these matrix elements as input.

Chapter 3

Many-body basics and many-body expansion methods

The goal of many-body quantum mechanics is to solve the A -body time-independent Schrödinger equation. This requires, among other things, the construction of a set of states that span the A -body Hilbert space. For distinguishable particles, taking a set of single-particle states $|p\rangle$ and building A -body product states $|p_1\rangle \dots |p_A\rangle$ would be a reasonable approach. However, the wave function of a system of A nucleons, which are indistinguishable fermions, must be antisymmetric under the exchange of any two particle labels. The explicit antisymmetrization of states going from naive product states quickly becomes unwieldy with growing A .

Second quantization offers an alternative that bakes the required antisymmetry into the formalism. This formalism is the basis for a class of many-body methods called many-body expansion methods, which includes the IMSRG. These methods have the benefit that, instead of scaling combinatorially in A like exact diagonalization approaches, they scale polynomially, taking advantage of knowledge of a good approximate solution to the ground state to reduce the task to finding corrections to this zeroth-order ansatz. In this chapter, we introduce the basics of second quantization and normal ordering, focusing on the case of fermions. Then we discuss some of the more traditional many-body expansion methods before discussing the IMSRG in detail in the next chapter.

3.1 Second quantization

To consider second quantization, one starts by constructing the Fock space, the direct sum of all A -body antisymmetric Hilbert spaces. As a concrete example, for the zero-, one-, and two-body Hilbert spaces, we have the bases $|0\rangle$, $\{|p\rangle\}$, and

$$\left\{ \frac{|p\rangle_1 |q\rangle_2 - |q\rangle_1 |p\rangle_2}{\sqrt{2}} \mid q > p \right\},$$

respectively. These states (and many more) are all in the Fock space, related to one another via field operators.

The field operators are particle creation and annihilation operators that connect states in the A -body antisymmetric Hilbert space to states in the $A + 1$ -body and $A - 1$ -body antisymmetric Hilbert spaces. The creation operator a_p^\dagger creates a particle in the single-particle state $|p\rangle$. Operating on an A -body state with it creates an $A + 1$ -body state with an additional particle in state $|p\rangle$,

$$a_p^\dagger |p_1 \dots p_A\rangle_a = (1 - n_p) |pp_1 \dots p_A\rangle_a , \quad (3.1)$$

where we have explicitly denoted that the states are antisymmetrized. Here, n_p is the occupation number of state $|p\rangle$ in the A -body state, which for fermions, due to the Pauli exclusion principle, can only be 0 or 1. Attempting to create a second particle in an already occupied state annihilates the state.

The annihilation operator a_p annihilates a particle in the single-particle state $|p\rangle$. Operating on an A -body state with it creates an $A - 1$ -body state with a particle in state $|p\rangle$ removed,

$$a_p |pp_2 \dots p_A\rangle_a = n_p |p_2 \dots p_A\rangle_a . \quad (3.2)$$

If no particle with the single-particle state $|p\rangle$ exists in the state, the annihilation operator annihilates the state.

With the field operators, an antisymmetric A -body state can very efficiently be written as

$$|p_1 p_2 \dots p_A\rangle_a = a_{p_1}^\dagger a_{p_2}^\dagger \dots a_{p_A}^\dagger |0\rangle . \quad (3.3)$$

This antisymmetrized product of A particles in A unique single-particle states is frequently referred to as a Slater determinant, owing to the fact that it can be, in its explicitly antisymmetrized form, written as an appropriately normalized determinant [41].

Since these states should be antisymmetric under exchange of particle indices, that is,

$$|p_1 p_2 \dots p_A\rangle_a = - |p_2 p_1 \dots p_A\rangle_a , \quad (3.4)$$

the creation and annihilation operators must anti-commute with themselves,

$$\{a_p^\dagger, a_q^\dagger\} = 0 , \quad (3.5)$$

$$\{a_p, a_q\} = 0 . \quad (3.6)$$

Similarly, one can arrive at the anti-commutation relation between creation and annihilation operators,

$$\{a_p, a_q^\dagger\} = \delta_{pq} . \quad (3.7)$$

With this formalism in place, we are now in a position to discuss the representation of many-body operators in the Fock space. Operators are classified as A -body operators

if they can at most couple A particles. We have used this language frequently so far, but we make it very precise in the following discussion.

Zero-body operators are simple scalars,

$$O^{(0)} = o. \quad (3.8)$$

They have, among other things, in general a non-zero vacuum expectation value.

One-body operators are of the form

$$O^{(1)} = \sum_{pq} O_{pq}^{(1)} a_p^\dagger a_q, \quad (3.9)$$

where $O_{pq}^{(1)}$ are the matrix elements of $O^{(1)}$. One-body operators have two useful properties. First, their vacuum expectation value is 0:

$$\langle 0 | O^{(1)} | 0 \rangle = 0. \quad (3.10)$$

Second, they do not contribute to processes where the incoming (bra) and outgoing (ket) states differ in more than one single-particle state. Some examples of one-body operators are the kinetic energy and an external potential.

Two-body operators are of the form

$$O^{(2)} = \frac{1}{(2!)^2} \sum_{pqrs} O_{pqrs}^{(2)} a_p^\dagger a_q^\dagger a_s a_r. \quad (3.11)$$

Here $O_{pqrs}^{(2)}$ is an antisymmetrized matrix element, with the property

$$O_{pqrs}^{(2)} = -O_{qprs}^{(2)} = -O_{psrq}^{(2)} = O_{rpsq}^{(2)}. \quad (3.12)$$

We note that in Eq. (3.11) the order of the annihilation operators is reversed relative to the indices on the matrix element. The indices p and r and the indices q and s are “paired,” and the product of creation and annihilation operators is structured such that the pairs are nested inside of each other, not adjacent to each other. However, by the antisymmetry of the matrix elements, the matrix element for one pairing determines it for all other pairings of the same creation and annihilation operators. Two-body operators have the properties

$$\langle 0 | O^{(2)} | 0 \rangle = 0, \quad (3.13)$$

$$\langle p | O^{(2)} | q \rangle = 0, \quad (3.14)$$

and they do not contribute to processes where incoming and outgoing states differ in more than two single-particle states. A typical example of a two-body operator is any pairwise interaction, such as the Coulomb interaction or NN nuclear forces.

Three-body operators are of the form

$$O^{(3)} = \frac{1}{(3!)^2} \sum_{pqrstu} O_{pqrstu}^{(3)} a_p^\dagger a_q^\dagger a_r^\dagger a_u a_t a_s. \quad (3.15)$$

Here, $O_{pqrstu}^{(3)}$ are also antisymmetrized matrix elements, with the property

$$O_{pqrstu}^{(3)} = \text{sign}(\sigma_1) \text{sign}(\sigma_2) O_{\sigma_1(pqr)\sigma_2(stu)}^{(3)}, \quad (3.16)$$

where σ_1 and σ_2 are permutations and the $\text{sign}(\sigma)$ prefactors account for the signs of the permutations, that is, whether they are cyclic (with sign 1) or anticyclic (with sign -1). Three-body operators have the properties

$$\langle 0 | O^{(3)} | 0 \rangle = 0, \quad (3.17)$$

$$\langle p | O^{(3)} | q \rangle = 0, \quad (3.18)$$

$$\langle pq | O^{(3)} | rs \rangle = 0, \quad (3.19)$$

and they do not contribute to processes where incoming and outgoing states differ in more than three single-particle states. Examples of three-body operators are 3N nuclear forces. These definitions can be generalized to get the general representation of any A -body operator, and the properties follow analogously.

3.2 Normal ordering

A product of creation and annihilation operators is in normal order if all creation operators appear to the left of all annihilation operators. The normal ordering operation on cA , where c is a scalar coefficient and A is a product of creation and annihilation operators, can be written as

$$N[cA] = \text{sign}(\sigma) c \sigma(A), \quad (3.20)$$

where σ is a permutation that rearranges the product A into normal order. This rearrangement is not unique, but, since each change in the permutation is accompanied by a change in the exchange prefactor, all normal-ordered products resulting from different permutations used in normal ordering are equivalent. Also, note that in general $N[A] \neq A$, since anti-commuting creation and annihilation operators past each other will leave a residual δ_{pq} from their anti-commutation relation.

3.2.1 General properties

Suppose the product of creation and annihilation operators A contains p creation operators and q annihilation operators. Then, unless p and q are both 0, $N[A]$ has a vacuum expectation value of 0. Additionally, $N[A]$ does not contribute to processes where the incoming state has less than q particles or the outgoing state has less than p particles.

We are now interested in considering products of normal-ordered products of creation and annihilation operators. Ultimately, we will use Wick's theorem to systematically evaluate these products [42]. To introduce the theorem, we first need to introduce the notion of a Wick contraction, which for adjacent operators α and β is defined as

$$\overline{\alpha\beta} = \alpha\beta - N[\alpha\beta] . \quad (3.21)$$

The value of the contraction is the vacuum expectation value of $\alpha\beta$. Note that for two operators that are already in normal order their contraction vanishes. This provides an alternative definition of normal ordering, namely a product of two operators is in normal order if its vacuum expectation value is 0 and so its contraction vanishes. This leads to an extension of normal ordering that works for many different vacuum choices, including multi-reference vacuums, which we don't consider any further in this work [43].

We are now equipped to use Wick's theorem to rewrite a general product of creation and annihilation operators in terms of sums of normal-ordered products and contractions [42]:

$$\begin{aligned} ABCDEF \dots = & N[ABCDEF \dots] \\ & + \overline{AB} N[CDEF \dots] - \overline{AC} N[BDEF \dots] + \text{singles} \\ & + \left(\overline{ABCD} - \overline{ACBD} + \overline{ADBC} \right) N[EF \dots] + \text{doubles} \\ & + \dots + \text{full contractions} . \end{aligned} \quad (3.22)$$

The minus signs arise due to the fact that in order to simplify the contraction and pull it out of the normal-ordered product, we must anti-commute the contracted operators such that they are adjacent.

The generalized Wick's theorem states that for a product of two normal-ordered products of creation and annihilation operators, $A = N[A_1 A_2 \dots A_N]$ and $B = N[B_1 B_2 \dots B_M]$, the resulting expression in terms of normal-ordered products is the sum of all normal-ordered terms with 0 to $\min(N, M)$ contractions between the operators in A and B , that is,

$$\begin{aligned} N[A_1 A_2 \dots A_N] N[B_1 B_2 \dots B_M] = & N[A_1 A_2 \dots A_N B_1 B_2 \dots B_M] \\ & + (-1)^{N-1} \overline{A_1 B_1} N[A_2 \dots A_N B_2 \dots B_M] \\ & + (-1)^{N-2} \overline{A_2 B_1} N[A_1 \dots A_N B_2 \dots B_M] \\ & + (-1)^N \overline{A_1 B_2} N[A_2 \dots A_N B_1 \dots B_M] \\ & + (-1)^{N-1} \overline{A_2 B_2} N[A_1 \dots A_N B_1 \dots B_M] \\ & + \text{singles} + \text{doubles} + \dots . \end{aligned} \quad (3.23)$$

Despite the name, this is a special case of Eq. (3.22).

3.2.2 Vacuum normal ordering

In Section 3.2.1, we discussed the properties of normal ordering in general, and while we referenced “the vacuum” several times (for example, in the context of vacuum expectation values), we never specified the specific vacuum involved. Indeed, normal ordering is dependent on the vacuum with respect to which it is done, and there are multiple options for this vacuum. In the following, we focus on normal ordering with respect to the *physical* vacuum $|0\rangle$, that is, the state with no particles present.

The fermion creation and annihilation operators a_p^\dagger and a_p are the *physical* creation and annihilation operators, so normal ordering with respect to the physical vacuum, which we denote by $N_0[\cdot]$, produces products with all creation operators to the left of annihilation operators. Concretely, one can consider adjacent Wick contractions, which should be 0 for pairs of operators already in normal order. Applying the definition that a contraction of two adjacent operators is the vacuum expectation value of the operator product, we find

$$a_p \underset{\text{below}}{a_q^\dagger} = \langle 0 | a_p a_q^\dagger | 0 \rangle = \delta_{pq}, \quad (3.24)$$

where we use the contraction *below* to indicate that we are normal ordering with respect to the physical vacuum. Similarly, we find

$$a_p \underset{\text{below}}{a_q} = 0, \quad (3.25)$$

$$a_p^\dagger \underset{\text{below}}{a_q^\dagger} = 0, \quad (3.26)$$

$$a_p^\dagger \underset{\text{below}}{a_q} = 0, \quad (3.27)$$

indicating that these products are already in normal order, as expected.

As a brief aside, the definitions for the second-quantized form of one-, two-, and three-body operators in Eqs. (3.9), (3.11), and (3.15) are clearly already in normal order with respect to the physical vacuum. This is no longer the case when we normal order with respect to some other vacuum.

3.2.3 In-medium normal ordering

One alternative is normal ordering with respect to an A -body reference state, also called the Fermi vacuum, given by

$$|\Phi\rangle = \prod_{i=1}^A a_{p_i}^\dagger |0\rangle. \quad (3.28)$$

The reference state is only non-zero if A unique single-particle states are occupied (that is, $p_i \neq p_j$ for $i \neq j$). The frequently used occupation numbers n_p for single-particle states in the reference state are then

$$n_p = \begin{cases} 1 & p \in \{p_i\}, \\ 0 & p \notin \{p_i\}. \end{cases} \quad (3.29)$$

When calculating operator matrix elements for an A -body system, every bra or ket state comes with A annihilation or creation operators along with the physical vacuum. A more practical, but equivalent way to go about this is constructing A -body states from the reference state $|\Phi\rangle$, annihilating states occupied in the reference state but unoccupied in the state of interest and creating in their place particles occupied in the state of interest. As an example, an A -body state that differs from the reference state by one single-particle state is given by

$$a_a^\dagger a_i |\Phi\rangle \equiv |\Phi_i^a\rangle. \quad (3.30)$$

One thing to note is that with respect to the reference state, the fermion creation and annihilation operators no longer have certain useful properties. For example, the annihilation operator no longer always annihilates the Fermi vacuum, and the creation operator in some cases *does* annihilate the Fermi vacuum. However, one can define quasiparticle creation and annihilation operators that recover these properties with respect to the reference state, with the annihilation operator given by

$$b_p = \begin{cases} a_p & \text{if } p \text{ is unoccupied in the reference state,} \\ a_p^\dagger & \text{if } p \text{ is occupied in the reference state,} \end{cases} \quad (3.31)$$

and the creation operator being related by conjugation.

These quasiparticle field operators obey all the typical anti-commutation relations and have the usual properties, just with respect to the reference state:

$$\{b_p, b_q^\dagger\} = \delta_{pq}, \quad (3.32)$$

$$\{b_p, b_q\} = 0, \quad (3.33)$$

$$\{b_q^\dagger, b_q^\dagger\} = 0, \quad (3.34)$$

$$b_p |\Phi\rangle = 0, \quad (3.35)$$

$$b_p^\dagger |\Phi\rangle \neq 0. \quad (3.36)$$

The quasiparticle creation operator b_p^\dagger annihilates a particle in the reference state if the state p is occupied, producing a so-called hole state. But when p is unoccupied in the reference state, b_p^\dagger creates a particle. This gives this formalism its name, the particle-hole formalism.

In this thesis so far, we have used indices p, q, r, \dots to indicate that the indices run over all single-particle states. Here we introduce the convention that the indices i, j, k, \dots only run over hole states, that is, states that are occupied in the reference state, and the indices a, b, c, \dots only run over particle states, that is, states that are unoccupied in the reference state.

We are now interested in normal ordering with respect to our reference state, which we denote by $N_\Phi[\cdot]$ and with contractions above the operators. This can be accomplished

via Wick's theorem [see Eq. (3.22)]. We only need to know the values of different Wick contractions. For our quasiparticle field operators, we find

$$\overline{b_p b_q^\dagger} = \delta_{pq} , \quad (3.37)$$

$$\overline{b_p b_q} = 0 , \quad (3.38)$$

$$\overline{b_p^\dagger b_q^\dagger} = 0 , \quad (3.39)$$

$$\overline{b_p^\dagger b_q} = 0 , \quad (3.40)$$

exactly the same as for the physical field operators when normal ordering with respect to the physical vacuum.

The case of physical field operators is more relevant to us, since our operators are given in terms of physical creation and annihilation operators. For the physical field operators, we find

$$\overline{a_p a_q^\dagger} = (1 - n_p) \delta_{pq} , \quad (3.41)$$

$$\overline{a_p a_q} = 0 , \quad (3.42)$$

$$\overline{a_p^\dagger a_q^\dagger} = 0 , \quad (3.43)$$

$$\overline{a_p^\dagger a_q} = n_p \delta_{pq} . \quad (3.44)$$

Assuming we have a Hamiltonian with one-, two-, and three-body operators,

$$H = H^{(1)} + H^{(2)} + H^{(3)} , \quad (3.45)$$

we can normal order it with respect to our reference state by making use of Eq. (3.22) and the contractions above. Doing this yields the following expression for our normal-ordered Hamiltonian \bar{H} :

$$\bar{H}^{(0)} \equiv \sum_i H_{ii}^{(1)} + \frac{1}{2} \sum_{ij} H_{ijij}^{(2)} + \frac{1}{6} \sum_{ijk} H_{ijkijk}^{(3)} , \quad (3.46)$$

$$\bar{H}_{pq}^{(1)} \equiv H_{pq}^{(1)} + \sum_i H_{piqi}^{(2)} + \frac{1}{2} \sum_{ij} H_{pijqij}^{(3)} , \quad (3.47)$$

$$\bar{H}_{pqrs}^{(2)} \equiv H_{pqrs}^{(2)} + \sum_i H_{pqirsi}^{(3)} , \quad (3.48)$$

$$\bar{H}_{pqrstu}^{(3)} \equiv H_{pqrstu}^{(3)} . \quad (3.49)$$

With this we have normal ordered our Hamiltonian with respect to our reference state, obtaining our normal-ordered Hamiltonian. Additionally, we can bring any products of normal-ordered operators to a normal-ordered form by applying the generalized Wick's theorem.

At this point, a few comments are in order about the choice of our reference state $|\Phi\rangle$. The choice of reference state corresponds to a partitioning of our Hamiltonian into a part that is exactly solved by the reference state and a part that contributes corrections to this zeroth-order solution, schematically

$$H = H_0 + H_1, \quad (3.50)$$

as in perturbation theory. A reasonable choice for the reference state corresponds to a choice that solves a problem “approximately” like the problem of interest, for example a spherical harmonic oscillator for spherical bound systems. The normal-ordered zero-body part of the Hamiltonian $\bar{H}^{(0)}$ is the expectation value of the ground-state energy as a result of the partitioning. $\bar{H}^{(1)}$, $\bar{H}^{(2)}$, and $\bar{H}^{(3)}$ do not contribute to this expectation value by construction. To improve the approximation of the physical ground state, one can:

1. improve the single Slater-determinant reference state, as is discussed in Section 3.3,
2. include corrections to the ground-state wave function, for example admixtures of one-particle one-hole excited states $|\Phi_i^a\rangle$, as is discussed in Section 3.4,
3. or extend the reference state to be made up of a linear combination of multiple Slater-determinants, leading to multi-reference many-body formalisms, which we do not discuss in this thesis.

3.3 The Hartree-Fock method

The variational principle states that the true ground state $|\psi\rangle$ globally minimizes the energy functional

$$E[|\psi\rangle] = \frac{\langle\psi|H|\psi\rangle}{\langle\psi|\psi\rangle}. \quad (3.51)$$

However, the ground state will in general not be describable by a single Slater determinant, meaning that we cannot hope to get the exact ground-state energy by normal ordering our Hamiltonian with respect to some optimized reference state. Still, one can optimize the reference state within a space restricted to Slater determinants to get the best possible single Slater determinant approximation to the ground state.

This is the core idea behind the Hartree-Fock method [44–46]. Working from a known single-particle basis $|p\rangle$, one wants to find a new single-particle basis $|p'\rangle$ such that our reference state

$$|\Phi\rangle = |p'_1 \dots p'_A\rangle \quad (3.52)$$

has the minimal energy expectation value, or Hartree-Fock energy,

$$\langle\Phi|H|\Phi\rangle = \bar{H}^{(0)}. \quad (3.53)$$

Rewriting the optimized basis in terms of our original basis,

$$|p'\rangle = \sum_{p'} C_{p'p} |p\rangle , \quad (3.54)$$

where C is a unitary matrix giving the basis transformation, we can expand the Hartree-Fock energy using our Hamiltonian from Eq. (3.45) as

$$\bar{H}^{(0)} = \sum_{i'} H_{i'i'}^{(1)} + \frac{1}{2} \sum_{i'j'} H_{i'j'i'j'}^{(2)} + \frac{1}{6} \sum_{i'j'k'} H_{i'j'k'i'j'k'}^{(3)} , \quad (3.55)$$

where these matrix elements can be connected back to those in our known single-particle basis,

$$H_{i'i'}^{(1)} = \sum_{pq} C_{pi'}^* H_{pq}^{(1)} C_{qi'} , \quad (3.56)$$

$$H_{i'j'i'j'}^{(2)} = \sum_{pqrs} C_{pi'}^* C_{qj'}^* H_{pqrs}^{(2)} C_{ri'} C_{sj'} , \quad (3.57)$$

$$H_{i'j'k'i'j'k'}^{(3)} = \sum_{pqrstu} C_{pi'}^* C_{qj'}^* C_{rk'}^* H_{pqrstu}^{(3)} C_{si'} C_{tj'} C_{uk'} . \quad (3.58)$$

The minimization of $\bar{H}^{(0)}$ gives the Hartree-Fock equations,

$$\sum_q F_{pq} C_{qr} = C_{pr} e_r , \quad (3.59)$$

where F_{pq} is the Fock matrix given by

$$F_{pq} = H_{pq}^{(1)} + \sum_{rsj'} C_{rj'}^* H_{prqs}^{(2)} C_{sj'} + \frac{1}{2} \sum_{rstuj'k'} C_{rj'}^* C_{sk'}^* H_{prsqtu}^{(3)} C_{tj'} C_{uk'} , \quad (3.60)$$

and e_i are Lagrange multipliers ensuring orthonormality of the new single-particle basis. Using that

$$\sum C_{p,i'}^* C_{q,i'} = \rho_{pq} , \quad (3.61)$$

the one-body density in the known single-particle basis, we can simplify Eq. (3.60) to

$$F_{pq} = H_{pq}^{(1)} + \sum_{rs} \rho_{rs} H_{prqs}^{(2)} + \frac{1}{2} \sum_{rstu} \rho_{rt} \rho_{su} H_{prsqtu}^{(3)} . \quad (3.62)$$

These equations are solved self-consistently, where in each iteration k : the density $\rho^{(k-1)}$ of the previous iteration is used to construct the new Fock matrix $F^{(k)}$, $F^{(k)}$ is diagonalized, a new $C^{(k)}$ is constructed from the eigenvectors of $F^{(k)}$, and the density $\rho^{(k)}$ is constructed via Eq. (3.61). To start, we choose $\rho_{pq}^{(0)} = n_p \delta_{pq}$. The iteration terminates when between iterations the $e_i^{(k)}$ change by less than some threshold. At this point, we can transform all operators to our new optimized single-particle basis by applying C appropriately. After this transformation $\bar{H}^{(1)}$ is diagonal with diagonal matrix elements e_i , the single-particle energies.

3.4 Many-body perturbation theory

Many-body perturbation theory (MBPT) has its formal roots in formal perturbation theory, which abstractly gives the perturbation theory formalism. MBPT then specifies certain details about the system and the starting point for perturbation theory and translates the formalism into concrete formulas for order-by-order corrections to the wave function and the energy of a state. In this section we give the key results from formal perturbation theory, discuss the setup for MBPT, and give the formulas for second- and third-order MBPT corrections to the energy. We refer the interested reader to Refs. [47, 48] for a more comprehensive treatment.

To start, one partitions the Hamiltonian

$$H = H_0 + H_1, \quad (3.63)$$

into H_0 , for which the solution to the Schrödinger equation is known exactly with solutions $|\Phi_k\rangle$ and corresponding energies $E_k^{(0)}$, and a perturbation H_1 . One is interested in an expansion of the true eigenstate $|\Psi_k\rangle$ in terms of the unperturbed solutions $|\Phi_k\rangle$. We concentrate our discussion here on an expansion for the ground state, so the ground state of H is denoted $|\Psi\rangle$ and the ground state of H_0 , the starting point of the expansion, is denoted $|\Phi\rangle$ with an unperturbed energy $E^{(0)}$.

The partitioning comes with the definition of the projection operators

$$P = |\Phi\rangle \langle \Phi|, \quad (3.64)$$

$$Q = \sum_{k \neq 0} |\Phi_k\rangle \langle \Phi_k|. \quad (3.65)$$

Working with the so-called intermediate normalization

$$\langle \Psi | \Phi \rangle = 1, \quad (3.66)$$

one can write the ground state of H as

$$|\Psi\rangle = (P + Q) |\Psi\rangle \quad (3.67)$$

$$= |\Phi\rangle + |\chi\rangle, \quad (3.68)$$

where $|\chi\rangle = Q |\Psi\rangle$ is what needs to be solved for.

The result of formal perturbation theory is that using the Rayleigh-Schrödinger resolvent

$$R = \sum_{k \neq 0} \frac{|\Phi_k\rangle \langle \Phi_k|}{E^{(0)} - E_k^{(0)}}, \quad (3.69)$$

the correction to the unperturbed ground state is given by

$$|\chi\rangle = \sum_{n=1}^{\infty} (RH_1)^n |\Phi\rangle_c, \quad (3.70)$$

where the ‘*c*’ subscript indicates that the expansion is connected, which ensures its size extensivity, that is, that calculated observables scale linearly with the size of the system. The corrections to the energy beyond the standard first-order energy correction

$$E^{(1)} = \langle \Phi | H_1 | \Phi \rangle , \quad (3.71)$$

are given by

$$\Delta E = \langle \Phi | H_1 | \chi \rangle \quad (3.72)$$

$$= \langle \Phi | H_1 \sum_{n=1}^{\infty} (RH_1)^n | \Phi \rangle_c . \quad (3.73)$$

As an example, the second-order correction to the energy is

$$E^{(2)} = \sum_{k \neq 0} \frac{\langle \Phi | H_1 | \Phi_k \rangle \langle \Phi_k | H_1 | \Phi \rangle}{E^{(0)} - E_k^{(0)}} . \quad (3.74)$$

This makes it clear that the corrections to the ground state involve the perturbation H_1 connecting the unperturbed ground state in the P -space to excited states in the Q -space before connecting these back to the ground state.

Transitioning to (single-reference) many-body perturbation theory, we define our A -body Hilbert space as comprising our reference state and n -particle n -hole excitations of the reference state:

$$\{ |\Phi\rangle , |\Phi_i^a\rangle , |\Phi_{ij}^{ab}\rangle , |\Phi_{ijk}^{abc}\rangle , \dots \} . \quad (3.75)$$

After normal ordering with respect to $|\Phi\rangle$, we have our normal-ordered zero- through three-body parts of the Hamiltonian, $\bar{H}^{(0)}$, $\bar{H}^{(1)}$, $\bar{H}^{(2)}$, and $\bar{H}^{(3)}$. This choice of basis corresponds to the following partitioning: our unperturbed Hamiltonian is

$$H_0 = \bar{H}^{(0)} + \text{diag}(\bar{H}^{(1)}) \quad (3.76)$$

$$= \bar{H}^{(0)} + \sum_p e_p N_{\Phi} [a_p^\dagger a_p] , \quad (3.77)$$

where $e_p = \bar{H}_{pp}^{(1)}$ are the single-particle energies. The energy of the reference state is given by $\bar{H}^{(0)}$. The energy of an n -particle n -hole excited state $|\Phi_{ij\dots}^{ab\dots}\rangle$ is given by

$$\bar{H}^{(0)} + \epsilon_{ij\dots}^{ab\dots} \quad (3.78)$$

with

$$\epsilon_{ij\dots}^{ab\dots} = (e_a + e_b + \dots) - (e_i + e_j + \dots) . \quad (3.79)$$

The perturbation is then

$$H_1 = \bar{H}^{(1)} - \text{diag}(\bar{H}^{(1)}) + \bar{H}^{(2)} + \bar{H}^{(3)} . \quad (3.80)$$

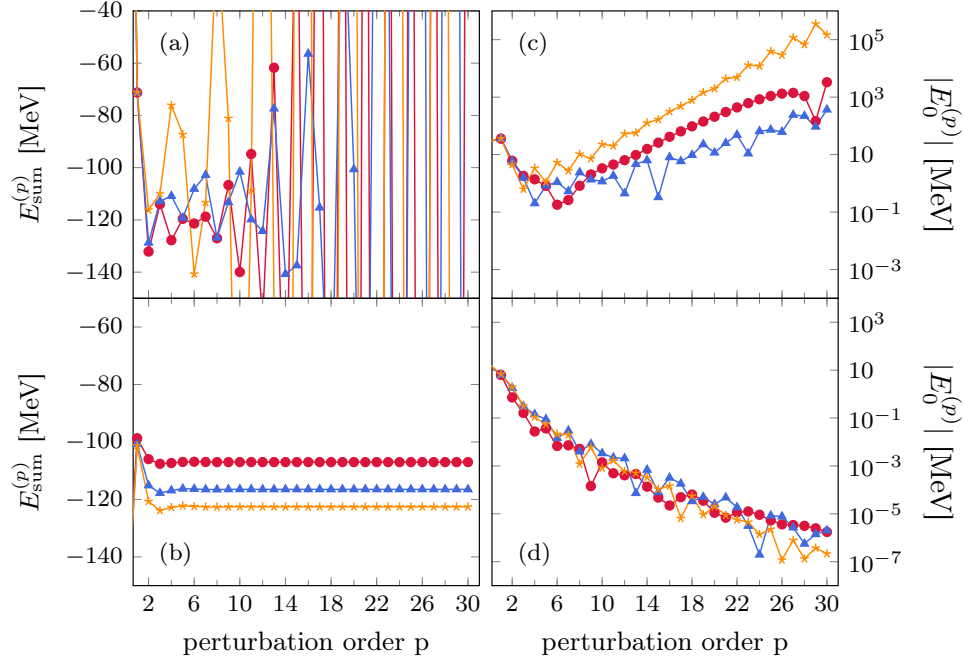


Figure 3.1: The partial sums (left) and order-by-order contributions (right) for an MBPT calculation of the ground-state energy of ^{16}O using a harmonic-oscillator reference state (top) and a Hartree-Fock reference state (bottom). The red, blue, and yellow points are for $N_{\text{max}} = 2, 4$, and 6 , the basis truncation parameter for the approach used. Figure taken from Ref. [49].

Finally, the many-body resolvent is

$$R = -\sum_{ai} \frac{|\Phi_i^a\rangle \langle \Phi_i^a|}{\epsilon_i^a} - \frac{1}{(2!)^2} \sum_{abij} \frac{|\Phi_{ij}^{ab}\rangle \langle \Phi_{ij}^{ab}|}{\epsilon_{ij}^{ab}} - \frac{1}{(3!)^2} \sum_{abcijk} \frac{|\Phi_{ijk}^{abc}\rangle \langle \Phi_{ijk}^{abc}|}{\epsilon_{ijk}^{abc}} + \dots \quad (3.81)$$

We are now in a position to discuss the second- and third-order contributions to the ground-state energy. Using Eq. (3.81) and the properties of normal-ordered operators, the second-order correction to the ground-state energy is given by

$$E^{(2)} = -\sum_{ai} \frac{\bar{H}_{ai}^{(1)} \bar{H}_{ia}^{(1)}}{\epsilon_i^a} - \frac{1}{(2!)^2} \sum_{abij} \frac{\bar{H}_{abij}^{(2)} \bar{H}_{ijab}^{(2)}}{\epsilon_{ij}^{ab}} - \frac{1}{(3!)^2} \sum_{abcijk} \frac{\bar{H}_{abcijk}^{(3)} \bar{H}_{ijkabc}^{(3)}}{\epsilon_{ijk}^{abc}}. \quad (3.82)$$

The first term in this equation is related to a so-called non-canonical diagram that vanishes if we choose the Hartree-Fock (HF) reference state to be our determinant. This is because, as mentioned previously, $\bar{H}^{(1)}$ is by definition diagonal in the HF basis.

At the third order, even considering only canonical diagrams, the number of diagrams possible with two- and three-body operators grows to 17. The complete list of these

diagrams can be found in Ref. [50]. The canonical contributions involving only the normal-ordered two-body Hamiltonian are

$$\begin{aligned}
 E_{2\text{-body only}}^{(3)} = & \frac{1}{8} \sum_{abcdij} \frac{\bar{H}_{ijab}^{(2)} \bar{H}_{abcd}^{(2)} \bar{H}_{cdij}^{(2)}}{\epsilon_{ij}^{ab} \epsilon_{ij}^{cd}} \\
 & + \frac{1}{8} \sum_{abijkl} \frac{\bar{H}_{ijab}^{(2)} \bar{H}_{abkl}^{(2)} \bar{H}_{klij}^{(2)}}{\epsilon_{ij}^{ab} \epsilon_{kl}^{ab}} \\
 & - \sum_{abcijk} \frac{\bar{H}_{ijab}^{(2)} \bar{H}_{kbic}^{(2)} \bar{H}_{ackj}^{(2)}}{\epsilon_{ij}^{ab} \epsilon_{kj}^{ac}}.
 \end{aligned} \tag{3.83}$$

The complete set of non-canonical third-order contributions with only one- and two-body operators is given, among other places, in Ref. [51].

The inclusion of additional terms is not the only challenge when dealing with a non-canonical reference state. Choosing a different reference state than the HF determinant corresponds to choosing a worse partitioning for H , that is, more information is held in the perturbation H_1 , as the HF determinant is the best possible single Slater determinant approximation to the ground state. This less optimal choice can lead to poor convergence behavior of MBPT [49]. For instance, in Fig. 3.1 the ground-state energy of ^{16}O was calculated using a harmonic-oscillator determinant and a Hartree-Fock determinant for the reference state. While for the HF reference state MBPT converges nicely, for the HO reference state the calculation rapidly begins to diverge when going to higher orders in perturbation theory. Additionally, while MBPT benefits strongly from working with SRG-evolved Hamiltonians, it can have difficulty converging even when using an HF reference state for un-evolved nuclear Hamiltonians that are too “hard” [48].

3.5 Non-perturbative techniques

The convergence challenges of MBPT motivate us to consider non-perturbative many-body methods, which sum to all orders certain types of diagrams to produce a convergent result. Coupled cluster theory and the in-medium similarity renormalization group are two examples of such methods. Their non-perturbative nature makes them less sensitive to the choice of reference state (although convergence speed will be affected by a non-canonical choice of reference state) and better able to deal with “harder” nuclear Hamiltonians. We discuss the IMSRG in detail in the next chapter. Here, we aim to briefly introduce the coupled cluster many-body approach as it shares many similarities with the IMSRG.

The ansatz for the coupled cluster (CC) approach is describing the ground state as

$$|\Psi\rangle = \exp(T) |\Phi\rangle, \tag{3.84}$$

where T is the cluster operator, which when applied exponentially to the reference state $|\Phi\rangle$ yields the ground state [52]. T contains in general one- through A -body operators,

$$T = T^{(1)} + T^{(2)} + \dots + T^{(A)}, \tag{3.85}$$

which generate particle-hole excitations of the reference state.

The ground-state energy is then given by

$$E = \langle \Psi | H | \Psi \rangle \quad (3.86)$$

$$= \langle \Phi | \exp(-T) (\bar{H}^{(1)} + \bar{H}^{(2)} + \bar{H}^{(3)}) \exp(T) | \Phi \rangle + \bar{H}^{(0)} \quad (3.87)$$

$$\equiv \langle \Phi | \bar{H} | \Phi \rangle + \bar{H}^{(0)}, \quad (3.88)$$

where we have defined the similarity-transformed Hamiltonian \bar{H} . The task is to solve for matrix elements of the different A -body parts of T such that

$$0 = \langle \Phi_{ijk\dots}^{abc\dots} | \bar{H} | \Phi \rangle \quad (3.89)$$

for all n -particle n -hole excited states of the reference state. These are the coupled cluster equations.

One computes \bar{H} via the Baker-Campbell-Hausdorff expansion,

$$\bar{H} = H_N + [H_N, T] + \frac{1}{2!} [[H_N, T], T] + \dots, \quad (3.90)$$

where $H_N \equiv \bar{H}^{(1)} + \bar{H}^{(2)} + \bar{H}^{(3)}$. This commutator expansion ensures that only connected diagrams in the MBPT expansion are generated, ensuring the size extensivity of the method. A standard approach in nuclear physics is to truncate T , H_N , and the commutator at the two-body level, giving two coupled cluster equations

$$0 = \langle \Phi_i^a | \bar{H} | \Phi \rangle, \quad (3.91)$$

$$0 = \langle \Phi_{ij}^{ab} | \bar{H} | \Phi \rangle, \quad (3.92)$$

known as CCSD (SD for singles and doubles). Another variant approximately treats the so-called triples and is denoted CCSD(T). In the next chapter, when discussing the IMSRG, the many similarities of the methods will be quite obvious.

Chapter 4

The in-medium similarity renormalization group

The in-medium similarity renormalization group is a modern *ab initio* many-body method that extends the renormalization group approach of decoupling energy scales to many-body calculations. It is a non-perturbative many-body expansion method, in the same vein as coupled cluster, but it operates on the operators rather than the wave function. It is remarkably flexible, with favorable scaling with system size and the ability to target many different observables, and its invention and development has contributed strongly to the rapid expansion of *ab initio* theoretical calculations of medium-mass nuclei. In this chapter, we introduce the IMSRG formalism. We then discuss the topics of truncation scheme, generator selection, and approaches to solving the flow equations.

4.1 Basic formalism

As a reminder from Section 2.2, the idea behind the SRG is the construction of a continuous unitary transformation of the Hamiltonian

$$H(s) = U(s)H U^\dagger(s), \quad (4.1)$$

which can be obtained by solving the flow equation

$$\frac{dH(s)}{ds} = [\eta(s), H(s)], \quad (4.2)$$

with the anti-Hermitian generator $\eta(s)$. The solution of this flow equation with vacuum normal-ordered operators, the free-space SRG, is appealing in that the evolved operators are not system specific and can be generally used for many-body calculations of nuclei and nuclear matter. However, the free-space SRG evolution can only be done consistently in the two- and three-body spaces for nuclear systems, leaving out induced higher-body operators.

The idea behind the IMSRG is to solve Eq. (4.2) in-medium, that is, to normal order with respect to a reference state before solving the flow equations. Starting from a Hamiltonian with a one-, two- and three-body part

$$H = H^{(1)} + H^{(2)} + H^{(3)}, \quad (4.3)$$

our normal-ordered Hamiltonian matrix elements are given by

$$E \equiv \bar{H}^{(0)} = \sum_i H_{ii}^{(1)} + \frac{1}{2} \sum_{ij} H_{ijij}^{(2)} + \frac{1}{6} \sum_{ijk} H_{ijkijk}^{(3)}, \quad (4.4)$$

$$f_{pq} \equiv \bar{H}_{pq}^{(1)} = H_{pq}^{(1)} + \sum_i H_{piqi}^{(2)} + \frac{1}{2} \sum_{ij} H_{pijqij}^{(3)}, \quad (4.5)$$

$$\Gamma_{pqrs} \equiv \bar{H}_{pqrs}^{(2)} = H_{pqrs}^{(2)} + \sum_i H_{pqirsi}^{(3)}, \quad (4.6)$$

$$W_{pqrst} \equiv \bar{H}_{pqrst}^{(3)} = H_{pqrst}^{(3)}, \quad (4.7)$$

where we have introduced the conventional names for zero-, one-, two-, and three-body normal-ordered parts of the Hamiltonian, E , f , Γ , and W , used in the literature. As a reminder, indices p, q, r, \dots run over all single-particle states, indices i, j, k, \dots run over holes, single-particle states occupied in the reference state, and indices a, b, c, \dots run over particles, single-particle states unoccupied in the reference state.

In general, the generator $\eta(s)$ has one- through A -body normal-ordered parts

$$\eta(s) = \sum_{i=1}^A \eta^{(i)}(s). \quad (4.8)$$

For now, we leave $\eta(s)$ unspecified beyond its required anti-Hermiticity, which causes it to not have a zero-body part. We discuss the choice of generator in Section 4.3. Concretely, our initial normal-ordered Hamiltonian is

$$\begin{aligned} H = & E + \sum_{pq} f_{pq} \text{N}_\Phi [a_p^\dagger a_q] \\ & + \frac{1}{(2!)^2} \sum_{pqrs} \Gamma_{pqrs} \text{N}_\Phi [a_p^\dagger a_q^\dagger a_s a_r] \\ & + \frac{1}{(3!)^2} \sum_{pqrst} W_{pqrst} \text{N}_\Phi [a_p^\dagger a_q^\dagger a_r^\dagger a_u a_t a_s], \end{aligned} \quad (4.9)$$

and our generator is

$$\begin{aligned} \eta(s) = & \sum_{pq} \eta_{pq}^{(1)}(s) \text{N}_\Phi [a_p^\dagger a_q] \\ & + \frac{1}{(2!)^2} \sum_{pqrs} \eta_{pqrs}^{(2)}(s) \text{N}_\Phi [a_p^\dagger a_q^\dagger a_s a_r] \\ & + \frac{1}{(3!)^2} \sum_{pqrst} \eta_{pqrst}^{(3)}(s) \text{N}_\Phi [a_p^\dagger a_q^\dagger a_r^\dagger a_u a_t a_s] \\ & + \dots \end{aligned} \quad (4.10)$$

The evaluation of the right-hand side of Eq. (4.2) then reduces to the evaluation of commutators of normal-ordered products,

$$\left[N_{\Phi} \left[a_{p_1}^{\dagger} \dots a_{p_M}^{\dagger} a_{q_M} \dots a_{q_1} \right], N_{\Phi} \left[a_{r_1}^{\dagger} \dots a_{r_N}^{\dagger} a_{s_N} \dots a_{s_1} \right] \right], \quad (4.11)$$

which can be simplified into a sum of normal-ordered operators using the generalized Wick's theorem [see Eq. (3.23)]. The commutator of a K -body operator $A^{(K)}$ and an L -body operator $B^{(L)}$ will in general have contributions of $|K - L|$ -body operators through $K + L - 1$ -body operators,

$$[A^{(K)}, B^{(L)}] = \sum_{M=|K-L|}^{K+L-1} C^{(M)}. \quad (4.12)$$

The right-hand side can then be broken up into zero- through A -body parts. We then identify the zero-body part of the right-hand side with dE/ds , the one-body part with df_{pq}/ds , and so on. This makes it obvious that even if the initial Hamiltonian and generator contain only up to three-body operators the IMSRG evolution induces higher-body operators, all the way up to A -body operators after a couple integration steps, resulting in coupled flow equations for the zero- through A -body parts of the Hamiltonian. Note that one must also ensure the antisymmetry of the right-hand sides of the two-, three-, and higher-body flow equations so the matrix elements remain antisymmetric.

The discussion here has been focused on the Hamiltonian, but the IMSRG can also be used to evolve other operators,

$$\frac{dO}{ds} = [\eta(s), O(s)], \quad (4.13)$$

where O has also been normal ordered with respect to our reference state $|\Phi\rangle$. Since the generator $\eta(s)$ should be the same for the evolution of H and O and the reconstruction of the unitary transformation from the evolved form of H is not possible, H and O must naively be evolved simultaneously. In Section 4.4, we discuss an alternative approach to solving the IMSRG flow equations that allows for the construction of the unitary transformation, resulting in easy evolution of other operators along with the Hamiltonian.

4.2 Truncation schemes

As is the case with the free-space SRG, it is not feasible to do the full A -body evolution, and the flow equations must be truncated at some B -body level. However, the situation is not quite the same as with the free-space SRG. Because the initial normal ordering shifts information about higher-body operators into lower-body normal-ordered operators and the continuous normal ordering absorbs information about induced higher-body operators into lower-body normal-ordered operators, the truncated IMSRG flow equations still approximately evolve higher-body operators (in the free-space sense) using only the reduced B -body flow equations. In the following sections, we discuss truncating the IMSRG

at the two-body and three-body level, yielding the so-called IMSRG(2) and IMSRG(3) truncations respectively.

4.2.1 IMSRG(2)

Truncating the flow equation at the two-body level amounts to assuming

$$H(s) \approx E(s) + f(s) + \Gamma(s), \quad (4.14)$$

$$\eta(s) \approx \eta^{(1)}(s) + \eta^{(2)}(s). \quad (4.15)$$

In this approximation, we are not including the three-body part of the initial Hamiltonian exactly. However, the three-body force *does* contribute as it was used in obtaining the normal-ordered zero-, one-, and two-body parts of the Hamiltonian. The only part that is being discarded is the residual three-body part, W . This is known as the normal-ordered two-body (NO2B) approximation, which has been quite successful in nuclear many-body applications.

Using the generalized Wick's theorem, which yields the fundamental commutators in Appendix A or also in Appendix A of Ref. [3], one arrives at the flow equations for the Hamiltonian

$$\begin{aligned} \frac{dE}{ds} &= \sum_{ab} n_a \bar{n}_b (\eta_{ab}^{(1)} f_{ba} - f_{ab} \eta_{ba}^{(1)}) \\ &\quad + \frac{1}{4} \sum_{abcd} n_a n_b \bar{n}_c \bar{n}_d (\eta_{abcd}^{(2)} \Gamma_{cdab} - \Gamma_{abcd} \eta_{cdab}^{(2)}), \end{aligned} \quad (4.16)$$

$$\begin{aligned} \frac{df_{ij}}{ds} &= \sum_a (\eta_{ia}^{(1)} f_{aj} - f_{ia} \eta_{aj}^{(1)}) \\ &\quad + \sum_{ab} (n_a - n_b) (\eta_{ab}^{(1)} \Gamma_{biaj} - f_{ab} \eta_{biaj}^{(2)}) \\ &\quad + \frac{1}{2} \sum_{abc} (\bar{n}_a \bar{n}_b n_c + n_a n_b \bar{n}_c) (\eta_{ciab}^{(2)} \Gamma_{abcj} - \Gamma_{ciab} \eta_{abcj}^{(2)}), \end{aligned} \quad (4.17)$$

$$\begin{aligned} \frac{d\Gamma_{ijkl}}{ds} &= \sum_a (1 - P_{ij}) (\eta_{ia}^{(1)} \Gamma_{ajkl} - f_{ia} \eta_{ajkl}^{(2)}) \\ &\quad - \sum_a (1 - P_{kl}) (\eta_{ak}^{(1)} \Gamma_{ijal} - f_{ak} \eta_{ijal}^{(2)}) \\ &\quad + \frac{1}{2} \sum_{ab} (1 - n_a - n_b) (\eta_{ijab}^{(2)} \Gamma_{abkl} - \Gamma_{ijab} \eta_{abkl}^{(2)}) \\ &\quad + \sum_{ab} (n_a - n_b) (1 - P_{ij}) (1 - P_{kl}) \eta_{aibk}^{(2)} \Gamma_{bjal}, \end{aligned} \quad (4.18)$$

where n_p are the occupation numbers of the reference state, $\bar{n}_p \equiv 1 - n_p$, the s -dependence has been suppressed, and the permutation operator P_{pq} exchanges the indices p and q in the following expression. We have broken our usual notation for single-particle index

labels to adopt the following convention for the IMSRG flow equations: the indices i, j, \dots are for external indices (indices on the flowing Hamiltonian), and the indices a, b, \dots are for contracted indices, which are summed over in the flow equation.

Eqs. (4.16)-(4.18) are solved by integrating from $s = 0$ towards $s \rightarrow \infty$ with the initial conditions $E(0) = E$, $f(0) = f$, and $\Gamma(0) = \Gamma$. Given appropriate decoupling (see Section 4.3), $E(\infty)$ gives the energy of the state targeted by the reference state, for our applications typically the ground state. The cost of this integration is dominated by the final two terms in Eq. (4.18), which scale like $\mathcal{O}(N^6)$, where N is the size of the single-particle basis for the calculation. Another nice property is that the flow equation, due to being a commutator many-body expansion, generates only connected diagrams and thus ensures size extensivity [3]. This is true for any B -body truncation.

4.2.2 IMSRG(3)

Truncating at the three-body level allows one to exactly include initial three-body forces. One assumes

$$H(s) \approx E(s) + f(s) + \Gamma(s) + W(s), \quad (4.19)$$

$$\eta(s) \approx \eta^{(1)}(s) + \eta^{(2)}(s) + \eta^{(3)}(s), \quad (4.20)$$

yielding additional terms with commutators of $\eta^{(3)}$ and W with zero- through two-body operators and a commutator between $\eta^{(3)}$ and W . The flow equations are

$$\begin{aligned} \frac{dE}{ds} = & \sum_{ab} n_a \bar{n}_b (\eta_{ab}^{(1)} f_{ba} - f_{ab} \eta_{ba}^{(1)}) \\ & + \frac{1}{4} \sum_{abcd} n_a n_b \bar{n}_c \bar{n}_d (\eta_{abcd}^{(2)} \Gamma_{cdab} - \Gamma_{abcd} \eta_{cdab}^{(2)}) \\ & + \frac{1}{36} \sum_{abcdef} n_a n_b n_c \bar{n}_d \bar{n}_e \bar{n}_f (\eta_{abcdef}^{(3)} W_{defabc} - W_{abcdef} \eta_{defabc}^{(3)}), \end{aligned} \quad (4.21)$$

$$\begin{aligned} \frac{df_{ij}}{ds} = & \sum_a (\eta_{ia}^{(1)} f_{aj} - f_{ia} \eta_{aj}^{(1)}) \\ & + \sum_{ab} (n_a - n_b) (\eta_{ab}^{(1)} \Gamma_{biaj} - f_{ab} \eta_{biaj}^{(1)}) \\ & + \frac{1}{2} \sum_{abc} (\bar{n}_a \bar{n}_b n_c + n_a n_b \bar{n}_c) (\eta_{ciab}^{(2)} \Gamma_{abcj} - \Gamma_{ciab} \eta_{abcj}^{(2)}) \\ & - \frac{1}{4} \sum_{abcd} (n_a n_b \bar{n}_c \bar{n}_d - \bar{n}_a \bar{n}_b n_c n_d) (\eta_{cdab}^{(2)} W_{abijcd} - \Gamma_{cdab} \eta_{abijcd}^{(2)}) \\ & + \frac{1}{12} \sum_{abcde} (n_a n_b \bar{n}_c \bar{n}_d \bar{n}_e + \bar{n}_a \bar{n}_b n_c n_d n_e) (\eta_{abicide}^{(3)} W_{cdeabj} - W_{abicide} \eta_{cdeabj}^{(3)}), \end{aligned} \quad (4.22)$$

$$\begin{aligned}
\frac{d\Gamma_{ijkl}}{ds} = & \sum_a (1 - P_{ij})(\eta_{ia}^{(1)}\Gamma_{ajkl} - f_{ia}\eta_{ajkl}^{(2)}) \\
& - \sum_a (1 - P_{kl})(\eta_{ak}^{(1)}\Gamma_{ijal} - f_{ak}\eta_{ijal}^{(2)}) \\
& + \frac{1}{2} \sum_{ab} (1 - n_a - n_b)(\eta_{ijab}^{(2)}\Gamma_{abkl} - \Gamma_{ijab}\eta_{abkl}^{(2)}) \\
& + \sum_{ab} (n_a - n_b)(1 - P_{ij})(1 - P_{kl})\eta_{aibk}^{(2)}\Gamma_{bjal} \\
& + \sum_{ab} (n_a - n_b)(\eta_{ab}^{(1)}W_{bijakl} - f_{ab}\eta_{bijakl}^{(3)}) \\
& - \frac{1}{2} \sum_{abc} (n_a\bar{n}_b\bar{n}_c + \bar{n}_an_bn_c)(1 - P_{kl})(\eta_{bca}^{(2)}W_{aijbcl} - \Gamma_{bca}\eta_{aijbcl}^{(3)}) \\
& + \frac{1}{2} \sum_{abc} (n_a\bar{n}_b\bar{n}_c + \bar{n}_an_bn_c)(1 - P_{ij})(\eta_{bca}^{(2)}W_{aklbcl} - \Gamma_{bca}\eta_{aklbcl}^{(3)}) \\
& + \frac{1}{6} \sum_{abcd} (n_a\bar{n}_b\bar{n}_c\bar{n}_d - \bar{n}_an_bn_cn_d)(\eta_{aijbcd}^{(3)}W_{bcdakl} - W_{aijbcd}\eta_{bcdakl}^{(3)}) \\
& + \frac{1}{4} \sum_{abcd} (\bar{n}_a\bar{n}_bn_cn_d - n_an_b\bar{n}_c\bar{n}_d)(1 - P_{ij})(1 - P_{kl})\eta_{abikcd}^{(3)}W_{cdjabk},
\end{aligned} \tag{4.23}$$

$$\begin{aligned}
\frac{dW_{ijklmn}}{ds} = & \sum_a P(i/jk)(\eta_{ia}^{(1)}W_{ajklmn} - f_{ia}\eta_{ajklmn}^{(3)}) \\
& - \sum_a P(l/mn)(\eta_{al}^{(1)}W_{ijkamn} - f_{al}\eta_{ijkamn}^{(3)}) \\
& + \sum_a P(ij/k)P(l/mn)(\eta_{ijla}^{(2)}\Gamma_{akmn} - \Gamma_{ijla}\eta_{akmn}^{(2)}) \\
& + \frac{1}{2} \sum_{ab} (1 - n_a - n_b)P(ij/k)(\eta_{ijab}^{(2)}W_{abklmn} - \Gamma_{ijab}\eta_{abklmn}^{(3)}) \\
& - \frac{1}{2} \sum_{ab} (1 - n_a - n_b)P(l/mn)(\eta_{abmn}^{(2)}W_{ijklab} - \Gamma_{abmn}\eta_{ijklab}^{(3)}) \\
& + \frac{1}{6} \sum_{abc} (n_an_bn_c + \bar{n}_a\bar{n}_b\bar{n}_c)(\eta_{ijkabc}^{(3)}W_{abclmn} - W_{ijkabc}\eta_{abclmn}^{(3)}) \\
& + \frac{1}{2} \sum_{abc} (n_an_b\bar{n}_c + \bar{n}_a\bar{n}_bn_c)P(ij/k)P(l/mn) \\
& \quad \times (\eta_{abkcmn}^{(3)}W_{cijabl} - \eta_{cjkabn}^{(3)}W_{iablmc}),
\end{aligned} \tag{4.24}$$

Here, $P(pq/r) = 1 - P_{pr} - P_{qr}$ and $P(p/qr) = 1 - P_{pq} - P_{pr}$ ensure the antisymmetry of the three-body indices.

It is clear that the final two terms in Eq. (4.24) dominate the cost of the integration, scaling like $\mathcal{O}(N^9)$ in the size of our single-particle basis. In the absence of an initial three-body operator, the third term in Eq. (4.24), the three-body part of the commutator of two two-body operators, induces a three-body operator, which leads to the contribution

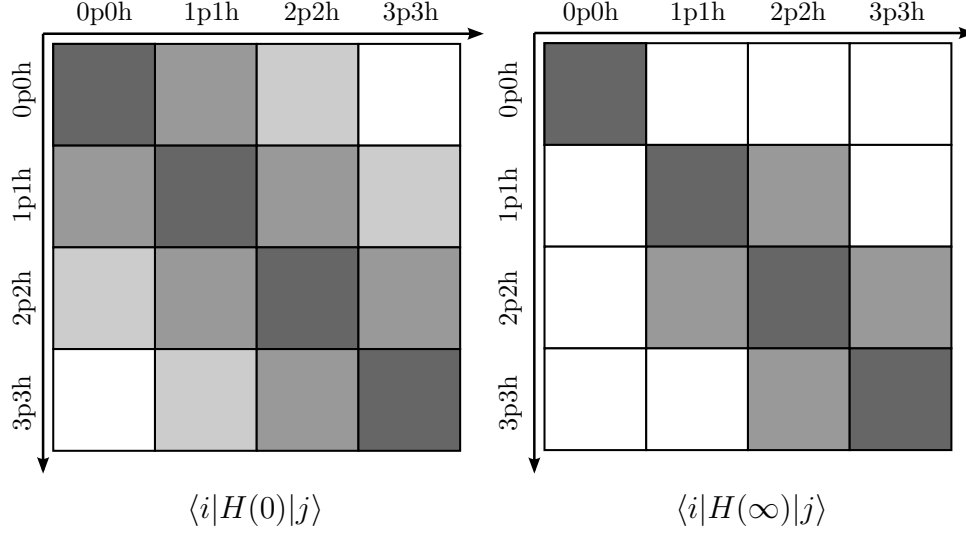


Figure 4.1: Schematic diagram showing the minimal decoupling scheme taken in the IMSRG. Figure taken from Ref. [3].

of all other terms later in the integration.

We would also like to note that in the derivation of the flow equations here the only assumption that was made was that two- and three-body matrix elements are appropriately antisymmetric. In particular, unlike several other references in the literature, for instance Refs. [3, 11], the flow equations here do not assume f , Γ , and W are Hermitian (which of course they are). While this assumption allows for the simplification of certain terms (nothing that changes the scaling of the terms however), it limits the expressions to only commutators of anti-Hermitian and Hermitian operators. In Section 4.4, we require the commutator of two anti-Hermitian operators, for which the right-hand sides of Eqs. (4.16)-(4.18) and Eqs. (4.21)-(4.24) are equally valid. For numerical implementations, it is a good idea to implement each of the fundamental commutators separately, to allow for validation and fine-grained optimization in the most expensive commutators.

4.3 Generator selection

So far, we have not discussed specific choices of our generator η . The possible definitions of η hinge on the specification of our so-called “off-diagonal” Hamiltonian H_{od} , the part of the Hamiltonian we wish to suppress to ensure appropriate decoupling in the remaining “diagonal” part. In Section 2.2, we saw that the generator choice $\eta(s) = [T_{\text{rel}}, H(s)]$ leads to the decoupling of any two states with a decay scale set by the difference in their kinetic energy expectation values. The result is that the Hamiltonian evolves towards a diagonal form, providing vastly improved convergence and allowing many-body calculations to use

significantly smaller model spaces.

To identify the desired decoupling for the IMSRG, we begin by considering the Hamiltonian in the basis spanned by our reference state $|\Phi\rangle$ and n -particle n -hole (nph) excitations of the reference state,

$$\{|\Phi\rangle, |\Phi_i^a\rangle, |\Phi_{ij}^{ab}\rangle, |\Phi_{ijk}^{abc}\rangle, \dots\}. \quad (4.25)$$

For a Hamiltonian with only one- and two-body operators, as is the approximation after normal ordering for the IMSRG(2) truncation, the Hamiltonian in this basis is schematically represented in the left panel of Fig. 4.1. It is band-diagonal and only able to couple an nph excitation to $(n \pm 2)p(n \pm 2)h$ excitations. For a Hamiltonian with a three-body part, the band diagonal grows to include $(n \pm 3)p(n \pm 3)h$ excitations.

For the IMSRG, a decoupling towards a true diagonal form is no longer a good idea, as one must avoid inducing significant three-body terms in the IMSRG(2) or four- and higher-body terms in the IMSRG(3) to maintain the validity of the truncation. The alternative is a minimal decoupling scheme, where the sole objective is to decouple the reference state $|\Phi\rangle$ from all nph excitations, as shown in the right panel of Fig. 4.1. Achieving this decoupling gives us the energy of the state E in the zero-body part of the normal-ordered Hamiltonian and the corresponding eigenstate by applying the unitary transformation to the reference state, $U^\dagger(\infty)|\Phi\rangle$. For some finite truncation of the flow equations, this result is of course only approximate.

Now that we know we want to suppress the matrix elements that couple $|\Phi\rangle$ to its excitations, we want to identify which parts of our normal-ordered Hamiltonian these matrix elements correspond to. For the couplings between $|\Phi\rangle$ and $1p1h$ excitations, we find

$$\langle\Phi|H|\Phi_i^a\rangle = \langle\Phi|HN_\Phi[a_a^\dagger a_i]|\Phi\rangle \quad (4.26)$$

$$\begin{aligned} &= E \langle\Phi|N_\Phi[a_a^\dagger a_i]|\Phi\rangle \\ &\quad + \sum_{pq} f_{pq} \langle\Phi|N_\Phi[a_p^\dagger a_q]N_\Phi[a_a^\dagger a_i]|\Phi\rangle \\ &\quad + \sum_{pqrs} \Gamma_{pqrs} \langle\Phi|N_\Phi[a_p^\dagger a_q^\dagger a_s a_r]N_\Phi[a_a^\dagger a_i]|\Phi\rangle \end{aligned} \quad (4.27)$$

$$= \sum_{pq} f_{pq} \delta_{pi} \delta_{qa} n_i \bar{n}_a \quad (4.28)$$

$$= f_{ia}. \quad (4.29)$$

Via similar calculations, one finds

$$\langle \Phi_i^a | H | \Phi \rangle = f_{ai} , \quad (4.30a)$$

$$\langle \Phi | H | \Phi_{ij}^{ab} \rangle = \Gamma_{ijab} , \quad (4.30b)$$

$$\langle \Phi_{ij}^{ab} | H | \Phi \rangle = \Gamma_{abij} , \quad (4.30c)$$

$$\langle \Phi | H | \Phi_{ijk}^{abc} \rangle = W_{ijkabc} , \quad (4.30d)$$

$$\langle \Phi_{ijk}^{abc} | H | \Phi \rangle = W_{abcijk} . \quad (4.30e)$$

We define our “off-diagonal” normal-ordered Hamiltonian then to be

$$\begin{aligned} H_{od} \equiv & \sum_{ia} \left(f_{ia} N_{\Phi} [a_i^{\dagger} a_a] + f_{ai} N_{\Phi} [a_a^{\dagger} a_i] \right) \\ & + \frac{1}{(2!)^2} \sum_{ijab} \left(\Gamma_{ijab} N_{\Phi} [a_i^{\dagger} a_j^{\dagger} a_b a_a] + \Gamma_{abij} N_{\Phi} [a_a^{\dagger} a_b^{\dagger} a_j a_i] \right) \\ & + \frac{1}{(3!)^2} \sum_{ijkabc} \left(W_{ijkabc} N_{\Phi} [a_i^{\dagger} a_j^{\dagger} a_k^{\dagger} a_c a_b a_a] + W_{abcijk} N_{\Phi} [a_a^{\dagger} a_b^{\dagger} a_c^{\dagger} a_k a_j a_i] \right) . \end{aligned} \quad (4.31)$$

We are now in a position where we can define generators that suppress these matrix elements over the course of the flow.

Wegner’s original ansatz for the generator of the SRG flow equation is

$$\eta(s) = [H_d(s), H_{od}(s)] , \quad (4.32)$$

where $H_d = H - H_{od}$ [35]. When using H_{od} as defined above, one can evaluate the commutator truncating at the two- or three-body level depending on the truncation scheme, giving the one-, two-, and three-body components of η in the same form as Eqs. (4.21)–(4.24). A perturbative analysis of the flow equations with this choice of generator, as is done in Ref. [53], reveals that the two-body “off-diagonal” matrix elements are suppressed like

$$\Gamma_{abij}(s) \approx \Gamma_{abij}(0) \exp(-(\Delta_{abij})^2 s) , \quad (4.33)$$

where Δ_{abij} are the energy denominators. There are multiple options for these energy denominators, corresponding to different partitionings in MBPT (see Section 3.4). We choose to focus on the Møller-Plesset denominators, with $\Delta_{abij} = \epsilon_{abij}$ from Eq. (3.79). Another alternative is the Epstein-Nesbet denominators (see Ref. [47] for details).

We have included the Wegner generator in this discussion for completeness but will not use it in any applications. One reason for this is that the Wegner generator is simply more expensive to construct than the alternatives, which give explicit expressions for the matrix elements of η , resulting in scaling of $\mathcal{O}(N^4)$ and $\mathcal{O}(N^6)$ for IMSRG(2) and IMSRG(3), respectively. This is to be contrasted with the evaluation of a full commutator, which scales like $\mathcal{O}(N^6)$ and $\mathcal{O}(N^9)$ for IMSRG(2) and IMSRG(3). Additionally, the Wegner generator causes the system of differential equations to be much more stiff, making the

integration much more expensive (in terms of storage and computational requirements) than for other generators.

The following generators directly construct the matrix elements of η , working with a basic form of

$$\begin{aligned} \eta \equiv & \sum_{ia} \left(\eta_{ia}^{(1)} N_{\Phi} [a_i^{\dagger} a_a] + \eta_{ai}^{(1)} N_{\Phi} [a_a^{\dagger} a_i] \right) \\ & + \frac{1}{(2!)^2} \sum_{ijab} \left(\eta_{ijab}^{(2)} N_{\Phi} [a_i^{\dagger} a_j^{\dagger} a_b a_a] + \eta_{abij}^{(2)} N_{\Phi} [a_a^{\dagger} a_b^{\dagger} a_j a_i] \right) \\ & + \frac{1}{(3!)^2} \sum_{ijkabc} \left(\eta_{ijkabc}^{(3)} N_{\Phi} [a_i^{\dagger} a_j^{\dagger} a_k^{\dagger} a_c a_b a_a] + \eta_{abcijk}^{(3)} N_{\Phi} [a_a^{\dagger} a_b^{\dagger} a_c^{\dagger} a_k a_j a_i] \right), \end{aligned} \quad (4.34)$$

where we note that for η to be anti-Hermitian, the matrix elements must fulfill

$$\eta_{ia}^{(1)} = -\eta_{ai}^{(1)}, \quad (4.35a)$$

$$\eta_{ijab}^{(2)} = -\eta_{abij}^{(2)}, \quad (4.35b)$$

$$\eta_{ijkabc}^{(3)} = -\eta_{abcijk}^{(3)}. \quad (4.35c)$$

The White generator corresponds to the choice

$$\eta_{ia}^{(1)}(s) = \frac{f_{ia}(s)}{\Delta_{ia}(s)}, \quad (4.36)$$

$$\eta_{ijab}^{(2)}(s) = \frac{\Gamma_{ijab}(s)}{\Delta_{ijab}(s)}, \quad (4.37)$$

$$\eta_{ijkabc}^{(3)}(s) = \frac{W_{ijkabc}(s)}{\Delta_{ijkabc}(s)}, \quad (4.38)$$

where the antisymmetry of the denominators automatically gives the desired anti-Hermiticity [54]. The White generator suppresses off-diagonal matrix elements like

$$\Gamma_{abij}(s) \approx \Gamma_{abij}(0) \exp(-s), \quad (4.39)$$

that is, it suppresses all off-diagonal matrix elements with the same decay scale, regardless of the energy differences between the states. This is unusual and not strictly speaking in line with the renormalization group approach, where large energy-difference modes are integrated out first. However, we are interested in $H(\infty)$ and $E(\infty)$, and in this limit all generators that suppress H_{od} produce identical results for $E(\infty)$ and $U^{\dagger}(\infty) |\Phi\rangle$, up to truncation effects.

A potential difficulty with the White generator arises when one of the energy denominators becomes very small, leading to large matrix elements of η and thus extremely large derivatives in the right-hand side of the flow equation. This can be mitigated by a

variation of the standard White generator, the arctan generator, with generator matrix elements defined as

$$\eta_{ia}^{(1)}(s) = \frac{1}{2} \arctan \left(\frac{2f_{ia}(s)}{\Delta_{ia}(s)} \right), \quad (4.40)$$

$$\eta_{ijab}^{(2)}(s) = \frac{1}{2} \arctan \left(\frac{2\Gamma_{ijab}(s)}{\Delta_{ijab}(s)} \right), \quad (4.41)$$

$$\eta_{ijkabc}^{(3)}(s) = \frac{1}{2} \arctan \left(\frac{2W_{ijkabc}(s)}{\Delta_{ijkabc}(s)} \right), \quad (4.42)$$

where the arctan function regularizes any possible large matrix elements that arise due to small energy denominators.

The final generator we discuss here is the imaginary-time generator, which was ostensibly inspired by imaginary-time evolution techniques in Quantum Monte Carlo methods [3]. Its matrix elements are defined as

$$\eta_{ia}^{(1)}(s) = \text{sign}(\Delta_{ia}(s)) f_{ia}(s), \quad (4.43)$$

$$\eta_{ijab}^{(2)}(s) = \text{sign}(\Delta_{ijab}(s)) \Gamma_{ijab}(s), \quad (4.44)$$

$$\eta_{ijkabc}^{(3)}(s) = \text{sign}(\Delta_{ijkabc}(s)) W_{ijkabc}(s). \quad (4.45)$$

A perturbative analysis of the flow equations with this generator choice shows that off-diagonal matrix elements are suppressed like

$$\Gamma_{abij}(s) \approx \Gamma_{abij}(0) \exp(-|\Delta_{abij}|s). \quad (4.46)$$

The sign function in the definition of the generator ensures that there is an absolute value around the energy denominator in the exponential, giving a suppression for all matrix elements instead of an enhancement for some. We also note here that the imaginary-time generator produces a “proper” RG flow, where matrix elements coupling large energy differences are suppressed before those coupling smaller energy differences.

4.4 The Magnus expansion

Working with Eqs. (4.16)-(4.18) and (4.21)-(4.24), one can solve the IMSRG by numerically integrating the system of ordinary differential equations (ODEs) to obtain the energy and the expectation values of other observables in the targeted state. This approach has two main challenges: First, the flow equations need to be solved to high precision, as otherwise numerical effects destroy the unitarity of the transformation even in the absence of any truncation. This necessitates the application of sophisticated ODE solvers to minimize this numerical error. These solvers require the allocation of several times the memory requirement of two- and three-body operators, which is already quite a lot (on the order of GB or tens of GB), and the evaluation of each integration step is substantially

more expensive (providing the benefit of reduced accumulated numerical error) than an Euler method. This is incidentally also a reason the White, arctan, and imaginary-time generators are preferred over the Wegner generator, as the stiffness of the flow equations with the Wegner generator requires the use of stiff ODE solvers, which are even more expensive in terms of storage and computational cost than their non-stiff counterparts.

Second, the evolution of other operators along with the Hamiltonian requires them to be evolved in parallel in this approach. This means that for every additional operator the memory and computational cost increases by the amount that it would cost to just solve the Hamiltonian. Furthermore, additional operators may increase the stiffness of the system of ODEs as the integration scales for their matrix elements may differ from the Hamiltonian. This challenge can be alleviated by the ability to construct the unitary transformation for the evolution, $U(s)$.

This is the goal of the Magnus expansion approach to solving the IMSRG flow equations [55]. Given our definition of $\eta(s)$ following Eq. (2.3), we get a differential equation for $U(s)$,

$$\frac{dU(s)}{ds} = -\eta(s)U(s), \quad (4.47)$$

where $U(0) = 1$. The formal integral of this differential equation is

$$U(s) = \mathcal{T}_s \left[\exp\left(-\int_0^s ds' \eta(s')\right) \right], \quad (4.48)$$

where \mathcal{T}_s is the time-ordering operator with respect to s [56].

The Magnus expansion postulates that a solution of the form

$$U(s) = \exp(\Omega(s)) \quad (4.49)$$

exists, where $\Omega(s)$ is anti-Hermitian and $\Omega(0) = 0$ [57]. To obtain $\Omega(s)$, one solves the differential equation of its expansion in $\eta(s)$,

$$\frac{d\Omega(s)}{ds} = \sum_{k=0}^{\infty} \frac{B_k}{k!} ad_{\Omega(s)}^k(\eta(s)), \quad (4.50)$$

where B_k are the Bernoulli numbers and ad_{Ω}^k are the recursively defined commutators,

$$ad_{\Omega(s)}^0(\eta(s)) = \eta(s), \quad (4.51)$$

$$ad_{\Omega(s)}^k(\eta(s)) = [\Omega(s), ad_{\Omega(s)}^{k-1}(\eta(s))]. \quad (4.52)$$

The interested reader may refer to Ref. [58] for detailed review of the Magnus expansion.

Here we note that $ad_{\Omega(s)}^k(\eta(s))$ is anti-Hermitian for all k , thus truncating Eq. (4.50) at any order gives an exactly anti-Hermitian approximation to $d\Omega(s)/ds$, which when integrated gives an exactly anti-Hermitian approximation to $\Omega(s)$. Thus $U(s) = \exp(\Omega(s))$ is always exactly unitary, regardless of accumulated numerical error in the solution for

$\Omega(s)$. This alleviates the requirement of using high-order ODE solvers to avoid numerical error, and the solution of the IMSRG flow equations in this approach can proceed using a cheap numerical integrator, for example a simple Euler method.

To apply the obtained unitary transformation to our Hamiltonian or some other operator, we use the Baker-Campbell-Hausdorff (BCH) formula,

$$H(s) = e^{\Omega(s)} H(0) e^{-\Omega(s)} = \sum_{k=0}^{\infty} \frac{1}{k!} \text{ad}_{\Omega(s)}^k (H(0)). \quad (4.53)$$

To be concrete, the evaluation of the IMSRG flow equations in the Magnus formalism proceeds as follows:

1. the generator $\eta(s)$ is constructed from $H(s)$,
2. the derivative $d\Omega(s)/ds$ is obtained via Eq. (4.50) and applied via a simple Euler method,
3. the new evolved Hamiltonian $H(s + ds)$ is obtained via Eq. (4.53),

repeating these steps until E is sufficiently converged. For practical calculations, a few truncations must be made. First, $H(s)$, $\eta(s)$, $\Omega(s)$, and all commutators must be truncated at the B -body level, leading to the Magnus(2) and Magnus(3) analogs to the IMSRG(2) and IMSRG(3) truncations. Additionally, the Magnus and BCH expansions [Eqs. (4.50) and (4.53)] must be truncated at some finite k . For the Magnus expansion, we truncate the series when the norm of the k -th term drops below a threshold ϵ_{deriv} ,

$$\left| \frac{B_k ||\text{ad}_{\Omega(s)}^k(\eta(s))||}{k! ||\Omega(s)||} \right| < \epsilon_{\text{deriv}}. \quad (4.54)$$

A similar condition can also be used for the truncation of the BCH expansion, with the threshold ϵ_{BCH} ,

$$\left| \frac{||\text{ad}_{\Omega(s)}^k(H(0))||}{k! ||\Omega(s)||} \right| < \epsilon_{\text{BCH}}. \quad (4.55)$$

An alternative, for when one is only interested in the zero-body part of the evolving Hamiltonian, is

$$\left| \frac{\text{ad}_{\Omega(s)}^k(H(0))^{(0)}}{k!} \right| < \epsilon_{\text{BCH}}. \quad (4.56)$$

The Magnus expansion makes very clear the similarities and differences between the IMSRG and coupled cluster. Both use a nested commutator expansion, ensuring the connected nature of the expansion and guaranteeing size extensivity. The IMSRG and CC seek to generate a similarity transformation that decouples the reference state expectation

value from the rest of the Hamiltonian. However, in coupled cluster the cluster operator T is non-Hermitian, meaning that the BCH expansion for the similarity transformation truncates at a finite order. The IMSRG generates a unitary transformation, which means Ω , the Magnus analog of the cluster operator, is anti-Hermitian. This leads to an infinite BCH expansion that must be truncated at some order.

In this thesis, we present various results for many-body calculations obtained using the IMSRG. Nearly all of these are done using the Magnus formalism, as its computational benefits are invaluable when doing calculations with three-body operators.

4.5 Application to ${}^4\text{He}$

Here we consider ${}^4\text{He}$, the lightest closed-shell nucleus. Before we begin a discussion about the details of the system, a few comments are in order. The following calculation is restricted to a very small model space, one insufficient to achieve converged results for observables, and is also only for the IMSRG(2) truncation. In Chapter 5, we discuss the formalism that exploits the spherical symmetry of closed-shell systems like ${}^4\text{He}$ to cast the IMSRG flow equations into a more computationally tractable form, which allows us to reach larger model spaces for the IMSRG(2) and compute results for small model spaces for the IMSRG(3). Thus, this implementation is a benchmark implementation for the IMSRG(2), which we have compared against an existing publicly available IMSRG(2) implementation [59]. This serves as a validation of our implementation in addition to some IMSRG(2) and IMSRG(3) results for the pairing Hamiltonian discussed in Appendix C.

As input into our calculation, we start with the intrinsic A -body Hamiltonian with only an initial two-body interaction,

$$H_{\text{int}} = T_{\text{int}} + V^{(2)}, \quad (4.57)$$

with the intrinsic kinetic energy

$$T_{\text{int}} = T - T_{\text{cm}} \quad (4.58)$$

$$= \left(1 - \frac{1}{A}\right) \sum_i \frac{p_i^2}{2m} - \frac{1}{A} \sum_{i<j} \frac{p_i \cdot p_j}{m}. \quad (4.59)$$

We note that the first term gives us our one-body Hamiltonian and the second term contributes to the two-body Hamiltonian along with $V^{(2)}$ [60].

We work in the single-particle harmonic-oscillator basis at several different values of $\hbar\Omega$ (see Section 2.3.3), with the single-particle states

$$|n_a(l_a s_a) j_a m_{j_a} t_a m_{t_a}\rangle \equiv |\alpha_a\rangle, \quad (4.60)$$

where $s_a = 1/2$ and $t_a = 1/2$. A natural ordering of these states is according to their principal quantum number, $e = 2n + l$. For the following calculation, we truncate the

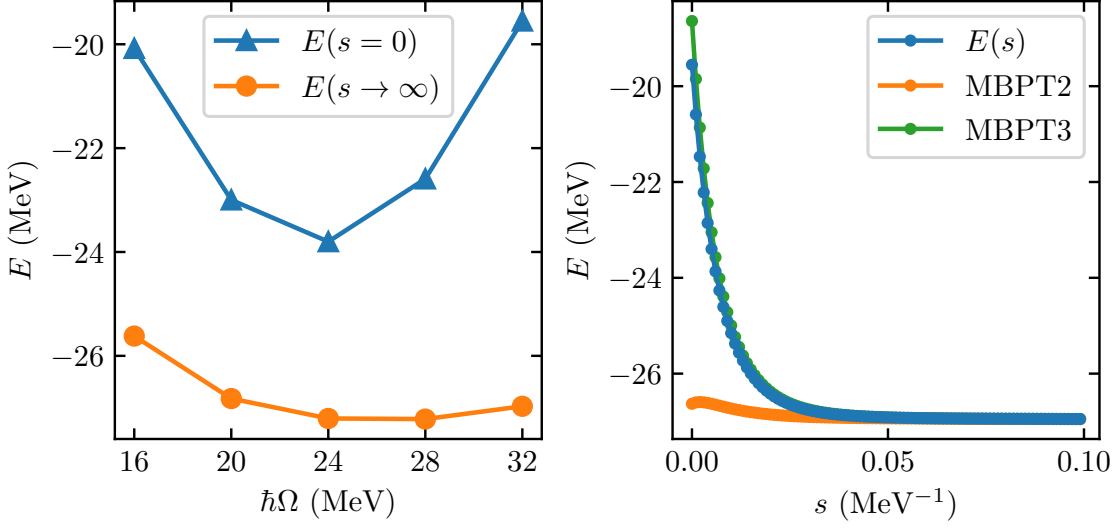


Figure 4.2: The left panel shows $E(s=0)$ and $E(s \rightarrow \infty)$ for an IMSRG(2) calculation of ${}^4\text{He}$ for $\hbar\Omega$ ranging from 16 MeV to 32 MeV. The interaction used is the EM NN interaction with a regulator cutoff $\Lambda = 500$ MeV and SRG-evolved to $\lambda = 1.8 \text{ fm}^{-1}$ [24]. The right panel shows the flowing energy $E(s)$ along with the energy with second- and third-order MBPT corrections included for $\hbar\Omega = 32$ MeV. The right panel is similar for the different $\hbar\Omega$ of the left panel.

single-particle basis at $e_{\text{max}} = 2$. The resulting size of our single-particle basis is $N = 40$. As our reference state for ${}^4\text{He}$ we choose to fill the four $e = 0$ HO states, the most reasonable choice to target the ground state without solving for and transforming to the Hartree-Fock basis.

For $V^{(2)}$, we use the EM NN potential from Ref. [24] at N³LO with a regulator cutoff at $\Lambda = 500$ MeV and SRG-evolved to $\lambda = 1.8 \text{ fm}^{-1}$. The results from normal ordering our Hamiltonians at the different $\hbar\Omega$ with respect to our HO reference state and evaluating the IMSRG(2) evolution are shown in the left panel of Fig. 4.2. We find that the unevolved energy $E(s=0)$, that is, the energy expectation value of the reference state, is already good to within 30% of the exact result, a consequence of the SRG-softened interaction we are using. Still, the IMSRG evolution absorbs up to 8 MeV of correlation energy into the ground-state energy. We also find that our implementation agrees with the implementation from Ref. [59] to within 10^{-5} MeV.

In the right panel of Fig. 4.2, we show the flowing ground-state energy as well as the ground-state energy with second- and third-order MBPT corrections. We find that these corrections vanish as the correlations are absorbed into the ground-state energy, indicating that we are achieving the desired decoupling. We emphasize once again that these results are intended to be interpreted as validation (for example, as a nuclear-like toy model) and not as physically meaningful. We consider the agreement between our implementation

and that of Ref. [59] to be *a posteriori* evidence of the correctness of our implementation.

Chapter 5

Angular-momentum coupling for the IMSRG

In theoretical physics, the exploitation of symmetries is essential to making the solution of certain problems computationally tractable. In many-body theories, general theories can be simplified (in terms of computational cost) by exploiting the symmetries present in the system and the chosen single-particle basis. For rotationally invariant systems, this symmetry exploitation is called angular-momentum reduction (AMR), which casts the many-body problem into the language of spherical tensors and angular-momentum eigenstates and analytically simplifies the angular-momentum-projection dependence related to the geometry of spherical systems. The angular-momentum reduction of a many-body approach can reduce the storage and computational cost by orders of magnitude, making it a very powerful tool to extend the range of the approach to larger model spaces or in some cases make calculations possible at all. The IMSRG is an excellent target for angular-momentum reduction, as one typically needs to push the model space to quite large single-particle basis truncations to achieve converged results. In this chapter, we give a brief overview of how angular-momentum reduction works and discuss its application to the IMSRG(3).

5.1 Wigner-Eckart theorem

Core to the angular-momentum reduction formalism are rotational symmetry, formally described by the $SU(2)$ Lie group, and the generator of rotations, the angular momentum \vec{J} . The prerequisites for AMR are [61]: a rotationally invariant Hamiltonian, which commutes with \vec{J} ; a spherical single-particle basis, which consists of eigenstates of J^2 and J_z ; and a spherical reference state, which has good angular momentum $J = 0$. In this case, the Hamiltonian, the single-particle basis, and the reference state share the symmetry group $SU(2)$, and one can cast the working equations of the theory into a spherically symmetric form and perform the analytical simplifications to allow one to profit from AMR.

An operator O can be expanded in spherical tensors \mathbf{O}^J of rank J , each with $2J + 1$ components O_M^J [62]. These spherical tensors have definite transformation behavior under rotations. Specifically, for a given unitary transformation $U(R)$ that corresponds to a rotation R , the spherical tensor components transform like [62]

$$U(R)O_M^J U^\dagger(R) = \sum_{M'=-J}^J D_{M'M}^J(R) O_{M'}^J, \quad (5.1)$$

where $D_{M'M}^J(R)$ are the Wigner D functions, which also give the transformation of the spherical harmonics under the same rotation [62]:

$$U(R)|jm\rangle = \sum_{m'=-j}^j D_{m'm}^j(R) |jm'\rangle. \quad (5.2)$$

Spherical tensors can be further simplified by the Wigner-Eckart theorem. The Wigner-Eckart theorem states that the matrix elements of a spherical tensor can be factorized into a reduced matrix element that is operator-specific and independent of any angular-momentum projection (in the bra state, ket state, and the tensor component) and a projection-dependent part that contains only geometric information and is independent of the specific operator [63, 64]:

$$\langle \xi_1 j_1 m_1 | O_M^J | \xi_2 j_2 m_2 \rangle = (-1)^{2J} \frac{1}{\hat{j}_1} \begin{pmatrix} j_2 & J \\ m_2 & M \end{pmatrix} \begin{pmatrix} j_1 \\ m_1 \end{pmatrix} \langle \xi_1 j_1 || \mathbf{O}^J || \xi_2 j_2 \rangle, \quad (5.3)$$

where $\hat{j} \equiv \sqrt{2j+1}$. The states $|\xi jm\rangle$ are eigenstates of angular momentum squared J^2 and angular-momentum projection J_z , with all other relevant quantum numbers contained in ξ . We generally use the shorthand $|p\rangle = |\tilde{p}m_p\rangle$, where $\tilde{p} \equiv \xi_p j_p$, for simplicity. Occasionally, we need time-reversed states with flipped angular-momentum projections, which we denote by $|\bar{p}\rangle \equiv |\tilde{p}(-m_p)\rangle$. Note that the reduced single-particle index \tilde{p} is the same for normal states and time-reversed states. Note that in Eq. (5.3) we have chosen the ‘‘Wigner’’ convention for reduced matrix elements, which is also used by Suhonen, Edmonds, Racah, and Varshalovich and which differs from the convention used by, for example, Sakurai.

Equipped with the factorization provided by the Wigner-Eckart theorem and the choice of spherical reference state and single-particle basis, one can in principle analytically perform the summations over all the angular-momentum-projection quantum numbers in a given expression. Intuitively, for every reduced index \tilde{p} in a many-body expression, one knows that both the reduced matrix elements and the reference state do not depend on m_p , so one is able to treat the entire ‘‘shell’’ of $2j_p + 1$ states collectively. This is where the ‘‘reduction’’ part of angular-momentum reduction takes place, since the resulting expressions are completely independent of projection quantum numbers, and one can use a reduced representation for the remaining operator-specific information that does not depend on the projection quantum numbers.

One particularly convenient approach to doing angular-momentum reduction is the diagrammatic expansion of an expression in a so-called Jucys graph and the simplification of the graph using various identities [65–67]. This approach was automated in the `amc` code published in Ref. [61]. The `amc` program automatically converts an uncoupled expression provided to it via an input file written in the AMC language into an equivalent m -independent reduced expression. Accomplishing this reduction by hand is tedious and error-prone, so we used this program as the primary workhorse for the angular-momentum reduction in Section 5.2.

5.2 Angular-momentum reduction for scalar operators

We will now apply angular-momentum reduction to the in-medium similarity renormalization group. The result of this symmetry reduction is the so-called J -scheme IMSRG, where the flow equations are formulated in terms of coupled or reduced matrix elements and the expressions have been reduced such that all dependence on angular-momentum projections has been analytically simplified. In the nuclear case, scalar operators play a special role in the IMSRG as the Hamiltonian and the generator are both scalar operators. This means that the many-body formalisms discussed in Chapters 3 and 4 can be symmetry reduced for closed-shell systems by considering only the case of scalar spherical tensors. As a result, the J -scheme IMSRG can access energies and charge radii without needing to consider the more complicated case of general spherical tensor operators (which we give an outlook on in Section 5.3).

5.2.1 Operator representation

Since spherical scalars are invariant under rotations and do not depend on any angular-momentum projection numbers, one can work with coupled matrix elements rather than reduced matrix elements [as in Eq. (5.3)], which differ by a simple factor (shown here for a one-body operator):

$$\langle \tilde{p} | T_0^0 | \tilde{q} \rangle = \frac{1}{\hat{j}_p} \langle \tilde{p} || \mathbf{T}^0 || \tilde{q} \rangle. \quad (5.4)$$

For the IMSRG(3), we need coupled matrix elements for up to three-body operators. Thus, we need to couple our A -body basis to be made up of eigenstates of the A -body total angular momentum squared J^2 and the z -component of the total angular momentum J_z . Since our chosen single-particle basis $|p\rangle = |\tilde{p}m_p\rangle$ consists of eigenstates of J_{1B}^2 and $J_{1B,z}$ for the one-body angular momentum \vec{J}_{1B} , the coupled matrix elements of a scalar one-body operator are simply the uncoupled matrix elements ¹,

$$O_{\tilde{p}\tilde{q}} = \langle \tilde{p}m_p = 1/2 | O | \tilde{q}m_q = 1/2 \rangle \delta_{j_p j_q} = O_{pq}, \quad (5.5)$$

¹ In Eq. (5.5), p and q have their angular-momentum projections implicitly fixed to $m_p = m_q = 1/2$.

where we have explicitly denoted that O is diagonal in j_p ². Note that $m_p = m_q$ could be any other value within the range given by j_p ; the matrix elements of a scalar operator will not change due to a different choice. We used $m_p = 1/2$ here simply because it will always be a valid choice for all j_p in our single-particle basis.

The representation of one-body operators can be made a bit more clear by adding an angular-momentum “channel” to the notation:

$$O_{pq}^j. \quad (5.6)$$

The channel j indicates that the matrix elements of O_{pq} are diagonal in $j_p = j_q$, and in this channel only the indices p and q with $j_p = j_q = j$ have non-zero matrix elements. We will stick with this notation for coupled one-body matrix elements going forward.

Our antisymmetrized two-body states

$$|pq\rangle = a_p^\dagger a_q^\dagger |0\rangle \quad (5.7)$$

are not eigenstates of J_{2B}^2 , only of $J_{2B,z}$. Coupling the states to two-body angular momentum J_{pq} gives the coupled two-body basis,

$$|(\tilde{p}\tilde{q})J_{pq}M_{pq}\rangle \equiv \sum_{m_p, m_q} \begin{pmatrix} j_p & j_q \\ m_p & m_q \end{pmatrix} \begin{pmatrix} J_{pq} \\ M_{pq} \end{pmatrix} |pq\rangle, \quad (5.8)$$

where the coupling brackets in $|(\tilde{p}\tilde{q})J_{pq}M_{pq}\rangle$ indicate that j_p and j_q are coupled to J_{pq} (and the rest of the quantum numbers in \tilde{p} and \tilde{q} are not involved). Note that the Clebsch-Gordan coefficients

$$\begin{pmatrix} j_p & j_q \\ m_p & m_q \end{pmatrix} \begin{pmatrix} J_{pq} \\ M_{pq} \end{pmatrix} \quad (5.9)$$

are defined such that they are 0 if $M_{pq} \neq m_p + m_q$, collapsing one of the sums over angular-momentum projections. The two-body states in Eq. (5.8) are not normalized, which can be remedied by multiplying them with the following factor [62]:

$$N_{pq(J_{pq})} \equiv \frac{\sqrt{1 + (-1)^{J_{pq}} \delta_{\tilde{p}\tilde{q}}}}{1 + \delta_{\tilde{p}\tilde{q}}}. \quad (5.10)$$

However, the coupled many-body expressions (and their numerical implementations) are simpler when using unnormalized coupled two- and three-body matrix elements.

²We previously denoted A -body operators by $O^{(A)}$. From this point on, we will leave off the (redundant) superscript to reduce notational clutter, as the many-body rank of an operator can be inferred from the number of indices on its matrix elements.

The unnormalized coupled two-body matrix elements of a scalar two-body operator O are given by

$$O_{\tilde{p}\tilde{q}\tilde{r}\tilde{s}}^{J_{pq}} \equiv \langle (\tilde{p}\tilde{q})J_{pq}M_{pq} = 0 | O | (\tilde{r}\tilde{s})J_{pq}M_{pq} = 0 \rangle \quad (5.11)$$

$$= \sum_{\substack{m_p, m_q \\ m_r, m_s}} \begin{pmatrix} j_p & j_q \\ m_p & m_q \end{pmatrix} \begin{pmatrix} J_{pq} \\ M_{pq} = 0 \end{pmatrix} \begin{pmatrix} j_r & j_s \\ m_r & m_s \end{pmatrix} \begin{pmatrix} J_{pq} \\ M_{pq} = 0 \end{pmatrix} O_{pqrs}. \quad (5.12)$$

Our representation builds the diagonality of the matrix elements in $J_{pq} = J_{rs}$ into the notation, as indicated by the J_{pq} channel in the superscript. Again, $M_{pq} = 0$ is a choice we have made that works for all sets of \tilde{p} and \tilde{q} . It is worth noting that not all $\tilde{p}\tilde{q}$ (or $\tilde{r}\tilde{s}$) combinations can couple to a given J_{pq} . This is not a problem, because in Eq. (5.12) the Clebsch-Gordan coefficients cause those matrix elements to be 0. This means they do not unphysically contribute in any many-body expressions. In numerical implementations, the exploitation of this reduction in the number of valid two-body states in a given angular-momentum channel is essential to improving performance to the point where calculations in large model spaces are possible.

The definition of the coupled three-body basis follows analogously,

$$|[(\tilde{p}\tilde{q})J_{pq}\tilde{r}]J_{pqr}M_{pqr}\rangle \equiv \sum_{m_r, M_{pq}} \begin{pmatrix} J_{pq} & j_r \\ M_{pq} & m_r \end{pmatrix} \begin{pmatrix} J_{pqr} \\ M_{pqr} \end{pmatrix} \sum_{m_p, m_q} \begin{pmatrix} j_p & j_q \\ m_p & m_q \end{pmatrix} \begin{pmatrix} J_{pq} \\ M_{pq} \end{pmatrix} |pqr\rangle, \quad (5.13)$$

where we have selected the “standard” coupling order with j_p and j_q coupled first to J_{pq} and then J_{pq} and j_r coupled to J_{pqr} . Once again, these states are not normalized, but working with unnormalized states is more convenient.

The unnormalized coupled matrix elements of a three-body operator O are given by

$$O_{\tilde{p}\tilde{q}\tilde{r}\tilde{s}\tilde{t}\tilde{u}}^{(J_{pqr}, J_{pq}, J_{st})} \equiv \langle [(\tilde{p}\tilde{q})J_{pq}\tilde{r}]J_{pqr}M_{pqr} = 1/2 | O | [(\tilde{s}\tilde{t})J_{st}\tilde{u}]J_{pqr}M_{pqr} = 1/2 \rangle \quad (5.14)$$

$$= \sum_{\substack{m_p, m_q, m_r, M_{pq} \\ m_s, m_t, m_u, M_{st}}} \begin{pmatrix} j_p & j_q \\ m_p & m_q \end{pmatrix} \begin{pmatrix} J_{pq} \\ M_{pq} \end{pmatrix} \begin{pmatrix} j_s & j_t \\ m_s & m_t \end{pmatrix} \begin{pmatrix} J_{st} \\ M_{st} \end{pmatrix} \begin{pmatrix} J_{pq} & j_r \\ M_{pq} & m_r \end{pmatrix} \begin{pmatrix} J_{pqr} \\ M_{pqr} = 1/2 \end{pmatrix} \begin{pmatrix} J_{st} & j_u \\ M_{st} & m_u \end{pmatrix} \begin{pmatrix} J_{pqr} \\ M_{pqr} = 1/2 \end{pmatrix} O_{pqrstu}. \quad (5.15)$$

The channel structure of the three-body matrix elements has grown more complicated, with the channel including the diagonal total three-body angular momentum $J_{pqr} = J_{stu}$ and the intermediate couplings J_{pq} and J_{st} . These intermediate couplings can take on different values, substantially increasing the number of three-body channels for which we need to handle matrix elements. Again, $M_{pqr} = 1/2$ is a choice we have made that works for all sets of \tilde{p} , \tilde{q} , and \tilde{r} .

At this point, it is useful to discuss the symmetry properties of these matrix elements. For a Hermitian operator the coupled matrix elements have the following properties:

$$O_{\tilde{p}\tilde{q}} = O_{\tilde{q}\tilde{p}}, \quad (5.16a)$$

$$O_{\tilde{p}\tilde{q}\tilde{r}\tilde{s}}^{J_{pq}} = O_{\tilde{r}\tilde{s}\tilde{p}\tilde{q}}^{J_{pq}}, \quad (5.16b)$$

$$O_{\tilde{p}\tilde{q}\tilde{r}\tilde{s}\tilde{t}\tilde{u}}^{(J_{pqr}, J_{pq}, J_{st})} = O_{\tilde{s}\tilde{t}\tilde{u}\tilde{p}\tilde{q}\tilde{r}}^{(J_{pqr}, J_{st}, J_{pq})}. \quad (5.16c)$$

Note the transposition of the intermediate couplings in the three-body channel in Eq. (5.16c). For an anti-Hermitian operator the coupled matrix elements have the following properties:

$$O_{\tilde{p}\tilde{q}} = -O_{\tilde{q}\tilde{p}}, \quad (5.17a)$$

$$O_{\tilde{p}\tilde{q}\tilde{r}\tilde{s}}^{J_{pq}} = -O_{\tilde{r}\tilde{s}\tilde{p}\tilde{q}}^{J_{pq}}, \quad (5.17b)$$

$$O_{\tilde{p}\tilde{q}\tilde{r}\tilde{s}\tilde{t}\tilde{u}}^{(J_{pqr}, J_{pq}, J_{st})} = -O_{\tilde{s}\tilde{t}\tilde{u}\tilde{p}\tilde{q}\tilde{r}}^{(J_{pqr}, J_{st}, J_{pq})}. \quad (5.17c)$$

Our two- and three-body matrix elements are also antisymmetric, although this symmetry is not realized as simply for coupled matrix elements as it is for uncoupled matrix elements. Two-body matrix elements have the following properties:

$$O_{\tilde{p}\tilde{q}\tilde{r}\tilde{s}}^{J_{pq}} = -(-1)^{j_p+j_q-J_{pq}} O_{\tilde{q}\tilde{p}\tilde{r}\tilde{s}}^{J_{pq}}, \quad (5.18a)$$

$$O_{\tilde{p}\tilde{q}\tilde{r}\tilde{s}}^{J_{pq}} = -(-1)^{j_r+j_s-J_{pq}} O_{\tilde{p}\tilde{q}\tilde{s}\tilde{r}}^{J_{pq}}. \quad (5.18b)$$

Three-body matrix elements have the following properties:

$$O_{\tilde{p}\tilde{q}\tilde{r}\tilde{s}\tilde{t}\tilde{u}}^{(J_{pqr}, J_{pq}, J_{st})} = -(-1)^{j_p+j_q-J_{pq}} O_{\tilde{q}\tilde{p}\tilde{r}\tilde{s}\tilde{t}\tilde{u}}^{(J_{pqr}, J_{pq}, J_{st})}, \quad (5.19a)$$

$$O_{\tilde{p}\tilde{q}\tilde{r}\tilde{s}\tilde{t}\tilde{u}}^{(J_{pqr}, J_{pq}, J_{st})} = \hat{J}_{pq} \sum_{J_2} \hat{J}_2 \begin{Bmatrix} j_p & j_q & J_{pq} \\ j_r & J_{pqr} & J_2 \end{Bmatrix} O_{\tilde{r}\tilde{q}\tilde{p}\tilde{s}\tilde{t}\tilde{u}}^{(J_{pqr}, J_2, J_{st})}, \quad (5.19b)$$

$$O_{\tilde{p}\tilde{q}\tilde{r}\tilde{s}\tilde{t}\tilde{u}}^{(J_{pqr}, J_{pq}, J_{st})} = -(-1)^{j_q+j_r-J_{pq}} \hat{J}_{pq} \sum_{J_2} \hat{J}_2 (-1)^{J_2} \begin{Bmatrix} j_q & j_p & J_{pq} \\ j_r & J_{pqr} & J_2 \end{Bmatrix} O_{\tilde{p}\tilde{r}\tilde{q}\tilde{s}\tilde{t}\tilde{u}}^{(J_{pqr}, J_2, J_{st})}, \quad (5.19c)$$

$$O_{\tilde{p}\tilde{q}\tilde{r}\tilde{s}\tilde{t}\tilde{u}}^{(J_{pqr}, J_{pq}, J_{st})} = -(-1)^{j_s+j_t-J_{st}} O_{\tilde{p}\tilde{q}\tilde{r}\tilde{t}\tilde{s}\tilde{u}}^{(J_{pqr}, J_{pq}, J_{st})}, \quad (5.19d)$$

$$O_{\tilde{p}\tilde{q}\tilde{r}\tilde{s}\tilde{t}\tilde{u}}^{(J_{pqr}, J_{pq}, J_{st})} = \hat{J}_{st} \sum_{J_2} \hat{J}_2 \begin{Bmatrix} j_s & j_t & J_{st} \\ j_u & J_{pqr} & J_2 \end{Bmatrix} O_{\tilde{p}\tilde{q}\tilde{r}\tilde{u}\tilde{t}\tilde{s}}^{(J_{pqr}, J_{pq}, J_2)}, \quad (5.19e)$$

$$O_{\tilde{p}\tilde{q}\tilde{r}\tilde{s}\tilde{t}\tilde{u}}^{(J_{pqr}, J_{pq}, J_{st})} = -(-1)^{j_t+j_u-J_{st}} \hat{J}_{st} \sum_{J_2} \hat{J}_2 (-1)^{J_2} \begin{Bmatrix} j_t & j_s & J_{st} \\ j_u & J_{pqr} & J_2 \end{Bmatrix} O_{\tilde{p}\tilde{q}\tilde{r}\tilde{s}\tilde{u}\tilde{t}}^{(J_{pqr}, J_{pq}, J_2)}. \quad (5.19f)$$

We provide only the pairwise antisymmetry properties, as the relations for the remaining permutations can be obtained by applying pairwise permutations.

At this point, we drop the cumbersome “tilde” notation for reduced state indices. The channels on matrix elements should make it clear whether the matrix elements are coupled or not. Additionally, in the surrounding text, we make it clear whether an expression is coupled or uncoupled.

5.2.2 Coupled many-body expressions

In addition to the fundamental commutators, IMSRG calculations typically employ a couple standard operations, which we discuss here. The first is bringing the initial Hamiltonian into normal order with respect to the employed A -body reference state. Given a Hamiltonian H with one- through three-body parts, the coupled expressions for the matrix elements of the normal-ordered Hamiltonian are

$$E = \bar{H} = \sum_{j_a} \hat{j}_a^2 \sum_a H_{aa}^{j_a} + \frac{1}{2} \sum_{J_{ab}} \hat{J}_{ab}^2 \sum_{ab} H_{abab}^{J_{ab}} + \frac{1}{6} \sum_{J_{ab} J_{abc}} \hat{J}_{abc}^2 \sum_{abc} H_{abcbac}^{(J_{abc}, J_{ab}, J_{ab})}, \quad (5.20a)$$

$$f_{pq}^{j_p} = \bar{H}_{pq}^{j_p} = H_{pq}^{j_p} + \frac{1}{\hat{j}_p^2} \sum_{J_{pa}} \hat{J}_{pa}^2 \sum_a H_{paqa}^{J_{pa}} + \frac{1}{2\hat{j}_p^2} \sum_{J_{pa} J_{pab}} \hat{J}_{pab}^2 \sum_{ab} H_{pabqab}^{(J_{pab}, J_{pa}, J_{pa})}, \quad (5.20b)$$

$$\Gamma_{pqrs}^{J_{pq}} = \bar{H}_{pqrs}^{J_{pq}} = H_{pqrs}^{J_{pq}} + \frac{1}{\hat{j}_{pq}^2} \sum_{J_{pqa}} \hat{J}_{pqa}^2 \sum_a H_{pqarsa}^{(J_{pqa}, J_{pq}, J_{pq})}, \quad (5.20c)$$

$$W_{pqrstu}^{(J_{pqr}, J_{pq}, J_{st})} = \bar{H}_{pqrstu}^{(J_{pqr}, J_{pq}, J_{st})} = H_{pqrstu}^{(J_{pqr}, J_{pq}, J_{st})}. \quad (5.20d)$$

Recall our previous convention that the indices p, q, r, \dots run over all single-particle states, the indices i, j, k, \dots run over hole states, and the indices a, b, c, \dots run over particle states.

Next, we need an antisymmetrizer for our two- and three-body matrix elements. This is because the fundamental commutators in Section 5.2.3 are not antisymmetrized to simplify the expressions and the numerical implementations. Thus, we need to explicitly restore the antisymmetry of some index combinations after evaluating the non-antisymmetrized fundamental commutators. In the two-body case, the antisymmetrizer is

$$\mathcal{A}_{2B} \equiv \mathcal{A}_{pq} \mathcal{A}_{rs}, \quad (5.21)$$

with

$$\mathcal{A}_{pq} \equiv \frac{1}{2}(1 - P_{pq}). \quad (5.22)$$

Recall that in the uncoupled expressions in Chapter 4 the permutation operator P_{pq} simply exchanged the indices p and q in the following expression. Now that indices are coupled, the action of permutation operators is complicated by the fact that they also change the coupling order. To implement \mathcal{A}_{2B} , all we need are the expressions for the action of P_{pq} and P_{rs} on two-body matrix elements:

$$O_{pqrs}^{J_{pq}} \xleftarrow{P_{pq}} (-1)^{j_p+j_q-J_{pq}} O_{qprs}^{J_{pq}}, \quad (5.23a)$$

$$O_{pqrs}^{J_{pq}} \xleftarrow{P_{rs}} (-1)^{j_r+j_s-J_{pq}} O_{pqsr}^{J_{pq}}. \quad (5.23b)$$

Using these operations along with scalar multiplication of and addition of matrix elements, the implementation of a two-body antisymmetrizer is simple.

In the three-body case, the antisymmetrizer is

$$\mathcal{A}_{3B} \equiv \mathcal{A}_{pqr} \mathcal{A}_{stu}, \quad (5.24)$$

with

$$\mathcal{A}_{pqr} \equiv \frac{1}{6}(1 + P_{prq} + P_{prq}^2)(1 - P_{pq}). \quad (5.25)$$

Here P_{prq} cyclically permutes the indices p , q , and r such that

$$(p, q, r) \xrightarrow{P_{prq}} (q, r, p) \xrightarrow{P_{prq}} (r, p, q) \xrightarrow{P_{prq}} (p, q, r). \quad (5.26)$$

There are other ways to define \mathcal{A}_{pqr} , for example in terms of P_{pq} and P_{qr} . They are all equivalent, and which one one chooses is a matter of preference. The action of P_{prq} , P_{pq} , P_{sut} , and P_{st} on three-body matrix elements is given by

$$O_{pqrstu}^{(J_{pqr}, J_{pq}, J_{st})} \xleftarrow{P_{prq}} -1(-1)^{j_p+j_q-J_{pq}} \hat{J}_{pq} \sum_{J_2} \hat{J}_2 \begin{Bmatrix} j_q & j_p & J_{pq} \\ j_r & J_{pqr} & J_2 \end{Bmatrix} O_{rpqstu}^{(J_{pqr}, J_2, J_{st})}, \quad (5.27a)$$

$$O_{pqrstu}^{(J_{pqr}, J_{pq}, J_{st})} \xleftarrow{P_{pq}} (-1)^{j_p+j_q-J_{pq}} O_{qprrtu}^{(J_{pqr}, J_{pq}, J_{st})}, \quad (5.27b)$$

$$O_{pqrstu}^{(J_{pqr}, J_{pq}, J_{st})} \xleftarrow{P_{sut}} -1(-1)^{j_s+j_t-J_{st}} \hat{J}_{st} \sum_{J_2} \hat{J}_2 \begin{Bmatrix} j_t & j_s & J_{st} \\ j_u & J_{pqr} & J_2 \end{Bmatrix} O_{pqrust}^{(J_{pqr}, J_{pq}, J_2)}, \quad (5.27c)$$

$$O_{pqrstu}^{(J_{pqr}, J_{pq}, J_{st})} \xleftarrow{P_{st}} (-1)^{j_s+j_t-J_{st}} O_{pqrtus}^{(J_{pqr}, J_{pq}, J_{st})}. \quad (5.27d)$$

With these basic operations in hand, one can implement a general three-body antisymmetrizer.

Finally, the second-order Møller-Plesset MBPT (MP2) energy correction is a critical diagnostic for the IMSRG as it is directly proportional to the matrix elements that the IMSRG evolution should suppress. The coupled expression for the MP2 energy correction is

$$E_{\text{MP2}} = - \sum_{ja} \hat{J}_a^2 \sum_{ai} \frac{|f_{ai}^{ja}|^2}{\epsilon_i^a} - \frac{1}{4} \sum_{J_{ab}} \hat{J}_{ab}^2 \sum_{abij} \frac{|\Gamma_{abij}^{J_{ab}}|^2}{\epsilon_{ij}^{ab}} - \frac{1}{36} \sum_{J_{abc} J_{ab} J_{ij}} \hat{J}_{abc}^2 \sum_{abcijk} \frac{|W_{abcijk}^{(J_{abc}, J_{ab}, J_{ij})}|^2}{\epsilon_{ijk}^{abc}}, \quad (5.28)$$

with

$$\epsilon_{ij\cdots}^{ab\cdots} = e_a + e_b + \cdots - (e_i + e_j + \cdots), \quad (5.29)$$

$$e_p = f_{pp}, \quad (5.30)$$

as in Eq. (3.79).

5.2.3 Coupled fundamental commutators

In this section, we present the coupled expressions for the fundamental commutators of two scalar operators. These expressions were obtained using the `amc` code from Ref. [61] on the uncoupled commutator expressions given in Appendix A. While this approach immediately produced desirable results for some commutators, for many it was possible to simplify the resulting expressions by exploiting symmetries of the uncoupled expressions. We discuss examples of these simplifications in Appendix B. Here, we will only show the simplest expressions we were able to produce.

The commutator expressions are “fundamental” in the sense that they are the basic operations required for any IMSRG(3) implementation. Using these expressions, one can quickly combine and expand them to produce the full IMSRG(3) flow equations (see Section 4.2.2), and one can also easily implement the series of nested commutators required by the Magnus and BCH expansions (see Section 4.4). Thus, correctly and efficiently implementing these expressions constitutes the main challenge of any IMSRG implementation.

The commutator of a K -body and an L -body operator gives an operator with $|K - L|$ - to $(K + L - 1)$ -body parts:

$$[A^{(K)}, B^{(L)}] = \sum_{M=|K-L|}^{K+L-1} C^{(M)}. \quad (5.31)$$

The expressions we give below are for the coupled matrix elements of the different M -body terms. In the IMSRG(3), we discard any four- and five-body parts induced, which appear in principle in the commutator of a two-body and a three-body operator and in the commutator of two three-body operators. We focus on the case where A and B and thus the resulting C are scalar operators.

Note that expressions for two- and three-body matrix elements are not antisymmetrized, so the appropriate antisymmetrizer must be applied [see Eqs. (5.21) and (5.24)] to the matrix elements after evaluating the commutator. We break our typical index label convention to use the convention that the index labels i, j, k, \dots are reserved for external indices, that is, indices appearing on the matrix elements of the resulting operator, and the index labels a, b, c, \dots are reserved for contracted indices, that is, indices that are summed over in the matrix elements of the input operators. As in Chapter 4, $\bar{n}_a = 1 - n_a$.

5.2.3.1 $[A^{(1)}, B^{(1)}]$

The commutator of two one-body operators has zero- and one-body parts.

The resulting zero-body contribution is given by the coupled expression

$$C = \sum_{j_a} \hat{j}_a^2 \sum_{ab} (n_a - n_b) A_{ab}^{j_a} B_{ba}^{j_a}. \quad (5.32)$$

The resulting coupled one-body matrix elements are given by the coupled expression

$$C_{ij}^{j_i} = \sum_a (A_{ia}^{j_i} B_{aj}^{j_i} - B_{ia}^{j_i} A_{aj}^{j_i}). \quad (5.33)$$

5.2.3.2 $[A^{(1)}, B^{(2)}]$

The commutator of a one-body operator and a two-body operator has one- and two-body parts.

The resulting coupled one-body matrix elements are given by the coupled expression

$$C_{ij}^{j_i} = \frac{1}{\hat{j}_i^2} \sum_{j_a} \sum_{J_2} \hat{J}_2^2 \sum_{ab} (n_a \bar{n}_b - \bar{n}_a n_b) A_{ab}^{j_a} B_{iajb}^{J_2}. \quad (5.34)$$

The resulting coupled two-body matrix elements are given by the coupled expression

$$C_{ijkl}^{J_C} = 2 \sum_{j_a} \sum_a (A_{ia}^{j_a} B_{ajkl}^{J_C} - A_{ak}^{j_a} B_{ijal}^{J_C}). \quad (5.35)$$

5.2.3.3 $[A^{(2)}, B^{(2)}]$

The commutator of two two-body operators has zero- through three-body parts.

The resulting zero-body contribution is given by the coupled expression

$$C = \frac{1}{4} \sum_{J_{ab}} \hat{J}_{ab}^2 \sum_{abcd} (n_a n_b \bar{n}_c \bar{n}_d - \bar{n}_a \bar{n}_b n_c n_d) A_{abcd}^{J_{ab}} B_{cdab}^{J_{ab}}. \quad (5.36)$$

The resulting coupled one-body matrix elements are given by the coupled expression

$$C_{ij}^{j_i} = \frac{1}{2} \frac{1}{\hat{j}_i^2} \sum_{J_{ab}} \hat{J}_{ab}^2 \sum_{abc} (\bar{n}_a \bar{n}_b n_c + n_a n_b \bar{n}_c) (A_{ciab}^{J_{ab}} B_{abcj}^{J_{ab}} - B_{ciab}^{J_{ab}} A_{abcj}^{J_{ab}}). \quad (5.37)$$

The resulting coupled two-body matrix elements are given by the coupled expression

$$C_{ijkl}^{J_C} = D_{ijkl}^{J_C} + E_{ijkl}^{J_C}, \quad (5.38)$$

with

$$D_{ijkl}^{J_C} \equiv \frac{1}{2} \sum_{ab} (\bar{n}_a \bar{n}_b - n_a n_b) (A_{ijab}^{J_C} B_{abkl}^{J_C} - B_{ijab}^{J_C} A_{abkl}^{J_C}), \quad (5.39)$$

$$\bar{E}_{ilkj}^{J_C} \equiv 4 \sum_{ab} (n_a \bar{n}_b - \bar{n}_a n_b) \bar{A}_{abk\bar{j}}^{J_C} \bar{B}_{ilab}^{J_C}. \quad (5.40)$$

The expression in Eq. (5.40) is written in terms of Pandya-transformed matrix elements, where the two-body Pandya transformation is given by [68]

$$\overline{O}_{p\bar{q}r\bar{s}}^{J_2} \equiv - \sum_{J'_2} \hat{J}_2'^2 \begin{Bmatrix} j_p & j_q & J_2 \\ j_r & j_s & J'_2 \end{Bmatrix} O_{p\bar{r}q\bar{s}}^{J'_2}. \quad (5.41)$$

The indices \bar{q} and \bar{s} are time reversed, that is, their angular-momentum projections are flipped. Since we are working with reduced indices without angular-momentum projections everywhere, this distinction is irrelevant, but we keep the modified indices around to be formally precise. The Pandya-transformed matrix elements are useful intermediates that isolate recoupling on A , B , and E that can be done independently. The resulting \bar{E} must be converted back to normal coupled matrix elements by a final Pandya transformation before being added to D to give C .

The resulting coupled three-body matrix elements are given by the coupled expression

$$\begin{aligned} C_{ijklmn}^{(J_{C,3}, J_{C,ij}, J_{C,lm})} &= -9(-1)^{J_{C,lm}} \hat{J}_{C,ij} \hat{J}_{C,lm} \sum_a (-1)^{j_a+j_k} \begin{Bmatrix} j_k & j_a & J_{C,lm} \\ j_n & J_{C,3} & J_{C,ij} \end{Bmatrix} \\ &\times (A_{ijn a}^{J_{C,ij}} B_{aklm}^{J_{C,lm}} - B_{ijn a}^{J_{C,ij}} A_{aklm}^{J_{C,lm}}). \end{aligned} \quad (5.42)$$

5.2.3.4 $[A^{(1)}, B^{(3)}]$

The commutator of a one-body operator and a three-body operator has two- and three-body parts.

The resulting coupled two-body matrix elements are given by the coupled expression

$$C_{ijkl}^{J_C} = \frac{1}{\hat{J}_C^2} \sum_{j_a} \sum_{J_{B,3}} \hat{J}_{B,3}^2 \sum_{ab} (n_a \bar{n}_b - \bar{n}_a n_b) A_{ab}^{j_a} B_{ijbkla}^{(J_{B,3}, J_C, J_C)}. \quad (5.43)$$

The resulting coupled three-body matrix elements are given by the coupled expression

$$C_{ijklmn}^{(J_{C,3}, J_{C,ij}, J_{C,lm})} = 3 \sum_{j_a} \sum_a (A_{ia}^{j_a} B_{ajklmn}^{(J_{C,3}, J_{C,ij}, J_{C,lm})} - A_{la}^{j_a} B_{ijkamn}^{(J_{C,3}, J_{C,ij}, J_{C,lm})}). \quad (5.44)$$

5.2.3.5 $[A^{(2)}, B^{(3)}]$

The commutator of a two-body operator and a three-body operator has one- through three-body parts.

The resulting coupled one-body matrix elements are given by the coupled expression

$$C_{ij}^{j_i} = -\frac{1}{4} \frac{1}{\hat{J}_i^2} \sum_{(J_{B,3}, J_{ab})} \hat{J}_{B,3}^2 \sum_{abcd} (n_a n_b \bar{n}_c \bar{n}_d - \bar{n}_a \bar{n}_b n_c n_d) A_{cdab}^{j_{ab}} B_{abijcd}^{(J_{B,3}, J_{ab}, J_{ab})}. \quad (5.45)$$

The resulting coupled two-body matrix elements are given by the coupled expression

$$C_{ijkl}^{J_C} = \frac{(-1)^{J_C}}{\hat{J}_C} \sum_{J_A, J_{B,3}} \hat{J}_A \hat{J}_{B,3}^2 \sum_{abc} (n_a \bar{n}_b \bar{n}_c + \bar{n}_a n_b n_c) \left((-1)^{j_k+j_l} \begin{Bmatrix} j_l & j_k & J_C \\ j_a & J_{B,3} & J_A \end{Bmatrix} A_{bcak}^{J_A} B_{ijabcl}^{(J_{B,3}, J_C, J_A)} + (-1)^{j_i+j_j} \begin{Bmatrix} j_j & j_i & J_C \\ j_a & J_{B,3} & J_A \end{Bmatrix} A_{bcai}^{J_A} B_{klabcj}^{(J_{B,3}, J_C, J_A)} \right). \quad (5.46)$$

The resulting coupled three-body matrix elements are given by the coupled expression

$$C_{ijklmn}^{(J_C, 3, J_C, ij, J_C, lm)} = D_{ijklmn}^{(J_C, 3, J_C, ij, J_C, lm)} + E_{ijklmn}^{(J_C, 3, J_C, ij, J_C, lm)}, \quad (5.47)$$

with

$$D_{ijklmn}^{(J_C, 3, J_C, ij, J_C, lm)} \equiv \frac{3}{2} \sum_{ab} (\bar{n}_a \bar{n}_b - n_a n_b) A_{ijab}^{J_C, ij} B_{abklmn}^{(J_C, 3, J_C, ij, J_C, lm)}, \quad (5.48)$$

$$E_{ijklmn}^{(J_C, 3, J_C, ij, J_C, lm)} \equiv -\frac{3}{2} \sum_{ab} (\bar{n}_a \bar{n}_b - n_a n_b) A_{ablm}^{J_C, lm} B_{ijkabn}^{(J_C, 3, J_C, ij, J_C, lm)}. \quad (5.49)$$

5.2.3.6 $[A^{(3)}, B^{(3)}]$

The commutator of two three-body operators has zero- through three-body parts.

The resulting zero-body contribution is given by the coupled expression

$$C = \frac{1}{36} \sum_{(J_3, J_{ab}, J_{de})} \hat{J}_3^2 \sum_{abcdef} (n_a n_b n_c \bar{n}_d \bar{n}_e \bar{n}_f - \bar{n}_a \bar{n}_b \bar{n}_c n_d n_e n_f) A_{abcdef}^{(J_3, J_{ab}, J_{de})} B_{defabc}^{(J_3, J_{de}, J_{ab})}. \quad (5.50)$$

The resulting coupled one-body matrix elements are given by the coupled expression

$$C_{ij}^{j_i} = \frac{1}{12} \frac{1}{\hat{J}_i^2} \sum_{(J_3, J_{ab}, J_{cd})} \hat{J}_3^2 \sum_{abcde} (n_a n_b \bar{n}_c \bar{n}_d \bar{n}_e + \bar{n}_a \bar{n}_b n_c n_d n_e) \left(A_{abcde}^{(J_3, J_{ab}, J_{cd})} B_{cdeabj}^{(J_3, J_{cd}, J_{ab})} - B_{abcde}^{(J_3, J_{ab}, J_{cd})} A_{cdeabj}^{(J_3, J_{cd}, J_{ab})} \right). \quad (5.51)$$

The resulting coupled two-body matrix elements are given by the coupled expression

$$C_{ijkl}^{J_C} = D_{ijkl}^{J_C} + E_{ijkl}^{J_C}, \quad (5.52)$$

with

$$D_{ijkl}^{J_C} \equiv \frac{1}{6} \frac{1}{\hat{J}_C^2} \sum_{(J_3, J_{bc})} \sum_{abcd} (n_a \bar{n}_b \bar{n}_c \bar{n}_d - \bar{n}_a n_b n_c n_d) \left(A_{ijabcd}^{(J_3, J_C, J_{bc})} B_{bcdkla}^{(J_3, J_{bc}, J_C)} - B_{ijabcd}^{(J_3, J_C, J_{bc})} A_{bcdkla}^{(J_3, J_{bc}, J_C)} \right), \quad (5.53)$$

$$\begin{aligned}
E_{ijkl}^{J_C} \equiv & (-1)^{j_j+j_l} \sum_{(J_{A,3}, J_{ab}, J_{cd})} (-1)^{J_{ab}+J_{cd}} \hat{J}_{A,3}^2 \sum_{J_{B,3}} \hat{J}_{B,3}^2 \\
& \left\{ \begin{matrix} j_i & J_{A,3} & J_{ab} \\ j_j & J_{cd} & J_{B,3} \\ J_C & j_l & j_k \end{matrix} \right\} \sum_{abcd} (\bar{n}_a \bar{n}_b n_c n_d - n_a n_b \bar{n}_c \bar{n}_d) \\
& A_{abickd}^{(J_{A,3}, J_{ab}, J_{cd})} B_{cdjabl}^{(J_{B,3}, J_{cd}, J_{ab})}.
\end{aligned} \tag{5.54}$$

The resulting coupled three-body matrix elements are given by the coupled expression

$$C_{ijklmn}^{(J_C, 3, J_C, ij, J_C, lm)} = D_{ijklmn}^{(J_C, 3, J_C, ij, J_C, lm)} + E_{ijklmn}^{(J_C, 3, J_C, ij, J_C, lm)} + F_{ijklmn}^{(J_C, 3, J_C, ij, J_C, lm)}, \tag{5.55}$$

with

$$\begin{aligned}
D_{ijklmn}^{(J_C, 3, J_C, ij, J_C, lm)} \equiv & \frac{1}{6} \sum_{J_{ab}} \sum_{ab} (n_a n_b n_c + \bar{n}_a \bar{n}_b \bar{n}_c) \\
& \left(A_{ijkabc}^{(J_C, 3, J_C, ij, J_{ab})} B_{abclmn}^{(J_C, 3, J_{ab}, J_C, lm)} - B_{ijkabc}^{(J_C, 3, J_C, ij, J_{ab})} A_{abclmn}^{(J_C, 3, J_{ab}, J_C, lm)} \right).
\end{aligned} \tag{5.56}$$

$$\bar{E}_{ijnlm\bar{k}}^{(J_3, J_C, ij, J_C, lm)} \equiv \frac{9}{2} \sum_{J_{ab}} \sum_{abc} (n_a n_b \bar{n}_c + \bar{n}_a \bar{n}_b n_c) \bar{B}_{ijnab\bar{c}}^{(J_3, J_C, ij, J_{ab})} \bar{A}_{abclm\bar{k}}^{(J_3, J_{ab}, J_C, lm)}, \tag{5.57}$$

$$\bar{F}_{ijnlm\bar{k}}^{(J_3, J_C, ij, J_C, lm)} \equiv -\frac{9}{2} \sum_{J_{ab}} \sum_{abc} (n_a n_b \bar{n}_c + \bar{n}_a \bar{n}_b n_c) \bar{A}_{ijnab\bar{c}}^{(J_3, J_C, ij, J_{ab})} \bar{B}_{abclm\bar{k}}^{(J_3, J_{ab}, J_C, lm)}. \tag{5.58}$$

The expressions in Eqs. (5.57) and (5.58) are written in terms of Pandya-transformed matrix elements, where the three-body Pandya transformation is given by

$$\bar{O}_{pq\bar{r}st\bar{u}}^{(J_3, J_{pq}, J_{st})} \equiv - \sum_{J'_3} \hat{J}_3'^2 \left\{ \begin{matrix} J_{pq} & j_r & J_3 \\ J_{st} & j_u & J_3 \end{matrix} \right\} O_{pqustr}^{(J'_3, J_{pq}, J_{st})}. \tag{5.59}$$

The indices \bar{r} and \bar{u} are time reversed, that is, their angular-momentum projections are flipped. Since we are working with reduced indices without angular-momentum projections everywhere, this distinction is irrelevant, but we keep the modified indices around to be formally precise. The Pandya-transformed matrix elements are useful intermediates that isolate recoupling on A , B , and E/F that can be done independently. The resulting \bar{E} and \bar{F} must be converted back to normal coupled matrix elements by a final Pandya transformation before being added to D to give C .

5.2.4 Validation of numerical implementation

With any numerical implementation, there is the question of how we can ensure that the code correctly implements the underlying formalism. With the J -scheme IMSRG, one has the advantage that there is the (more transparent) m -scheme formalism that one can compare against. This means one can uncouple the initial Hamiltonian fed into the J -scheme implementation, solve the IMSRG(3) flow equations via an m -scheme implementation,

and compare the results with those of the J -scheme IMSRG(3) solver. This can be done by looking at the ground-state energy or the second-order MBPT energy correction or by recoupling the resulting Hamiltonian matrix elements and checking that they match the J -scheme matrix elements to within the expected precision.

We take a more fine-grained approach to validating our J -scheme IMSRG(3) implementation, but using the same overall strategy. Working with the same initial matrix elements (in coupled and uncoupled form), we evaluate the fundamental commutators (and some many-body operations like the second-order MBPT energy correction and the two- and three-body antisymmetrizers) in our J -scheme implementation and an independent m -scheme implementation (used in Section 4.5 and Appendix C). The resulting uncoupled matrix elements provided by the m -scheme implementation are then recoupled and compared with the coupled matrix elements provided by the J -scheme implementation. With this strategy, we can demand stringent numerical agreement between the results, because accumulated numerical error should be low. We find all tested operations, which includes all fundamental commutators with antisymmetrization, the second-order MBPT energy corrections, and the normal ordering methods, pass this check.

5.3 Outlook towards tensor operators

Implementing tensor operator support in the IMSRG provides access to the full range of observables. Examples of observable tensor operators are electric and magnetic multipole operators, which when implemented give access to low-lying spectroscopy [69].

The implementation of tensor operators is a bit more challenging than that of scalar operators for a couple of reasons. First, the coupled matrix elements of tensor operators are no longer diagonal in total angular momentum J and angular-momentum projection M [61]. The M -dependence is taken care of by the factorization provided by the Wigner-Eckart theorem. However, when using the reduced matrix elements the non-diagonality in J remains, so the representation that worked for scalar operators needs to be generalized to support this (along with the inclusion of the tensor rank).

Additionally, one requires a whole new set of fundamental commutators, specifically those of a scalar operator (either the generator η or the Magnus operator Ω) and a tensor operator. The `amc` code has no trouble generating the coupled/reduced expressions for these fundamental commutators [61], but the implementation effort for these additional commutators will be similar to (probably greater than) that for the scalar-scalar commutators. Ultimately, in order to explore electroweak observables in nuclei, additional work in this direction must be done to implement these more general tensor-scalar commutators.

Chapter 6

Results

In this chapter, we discuss the application of the IMSRG(3) to two closed-shell nuclei, ^4He and ^{16}O . We are broadly interested in seeing what the three-body contributions of the IMSRG(3) are and if or how these change for different bases and reference states. For reasons of available computational time, we use various truncated schemes that do not include the most expensive terms in the IMSRG(3).

6.1 Model space and Hamiltonian details

For both ^4He and ^{16}O , we use spherical HO-like basis states

$$|n(ls)jm_jtm_t\rangle, \quad (6.1)$$

where $s = 1/2$ and $t = 1/2$. For the many-body calculations discussed here, we truncate the model space at $e_{\text{max}} = 2$, with the principal quantum number $e = 2n + l$. In an m -scheme implementation, this corresponds to 40 single-particle states, putting the computational cost of the IMSRG(3) in the order of $40^9 \sim \mathcal{O}(10^{17})$ floating-point operations. For a J -scheme implementation, there are “only” 12 reduced single-particle orbitals to consider, giving a naive cost on the order of $\mathcal{O}(10^{12})$.

In the following applications, we will use two bases, the Hartree-Fock basis and the natural orbitals (NAT) basis. For the HF single-particle states, the HF equation [see Eq. (3.59)] is solved in a spherically constrained way to give spherical HF orbitals. The solution of the HF equation takes place in the same $e_{\text{max}} = 2$ model space as the many-body calculation.

The natural orbitals are defined as the eigenbasis of the one-body density ρ . Diagonalizing an approximation to ρ yields approximate natural orbitals, which is done here with a second-order MBPT approximation to the one-body density. This was first presented for nuclear structure calculations in Ref. [70], where one saw that the natural orbitals led to strongly reduced frequency dependence in no-core shell model (NCSM) calculations of nuclear properties. In Ref. [71], it was shown that to achieve the same for the IMSRG,

the natural orbitals should be constructed in a large model space. After applying the resulting unitary transformation to the Hamiltonian, one can then truncate the Hamiltonian to a smaller model space for many-body calculations and profit from the improved single-particle orbitals optimized in the large model-space NAT calculation.

We use the same approach to including the NAT basis in our calculation. The natural orbitals are solved for in an $e_{\max} = 14$ model space. When 3N forces are included, an additional truncation is imposed such that only three-body states with $e_1 + e_2 + e_3 \leq E_{3\max} = 16$ are included. The resulting Hamiltonian is truncated down to $e_{\max} = 2$ for the many-body calculation. In Ref. [71], we envisioned that natural orbitals could enable expensive many-body methods, such as the IMSRG(3), to achieve converged results in much smaller model spaces than would be required for HF-based many-body calculations. While $e_{\max} = 2$ is not sufficient to achieve converged results, we expect that the NAT basis in $e_{\max} = 2$ will deliver essentially frequency independent results, saving us the trouble of scanning for the optimal HF frequency. Additionally, the NAT basis results are expected to lie closer to the converged results that one would obtain in larger model spaces than the HF basis results.

For the following calculations, we use two Hamiltonians. The first is the EM NN-only N³LO potential, with a regular cutoff of $\Lambda = 500$ MeV and SRG-evolved to $\lambda = 1.8 \text{ fm}^{-1}$ [24]. We will refer to this Hamiltonian as the “EM 1.8” Hamiltonian. The second Hamiltonian we use is the NN+3N N³LO potential presented in Ref. [72]. The NN force is the same as in the EM 1.8 potential. The two free parameters of the 3N force are fit such that resulting Hamiltonian reproduces experimental values for the ³H binding energy and the ⁴He point proton radius. The momentum-space regulator for the 3N force is $\Lambda_{3\text{NF}} = 2.0 \text{ fm}^{-1}$. We will refer to this Hamiltonian as the “EM 1.8/2.0” Hamiltonian.

For the many-body Hamiltonian, we use the intrinsic A -body Hamiltonian with a two-body potential (and in some cases a three-body potential),

$$H_{\text{int}} = T_{\text{int}} + V^{(2)}(+V^{(3)}), \quad (6.2)$$

with the intrinsic kinetic energy (written here in one- plus two-body form)

$$T_{\text{int}} = T - T_{\text{cm}} \quad (6.3)$$

$$= \left(1 - \frac{1}{A}\right) \sum_i \frac{p_i^2}{2m} - \frac{1}{A} \sum_{i < j} \frac{p_i \cdot p_j}{m}. \quad (6.4)$$

After normal-ordering the intrinsic Hamiltonian with respect to the appropriate reference state, we have a normal-ordered Hamiltonian with zero- up to three-body parts. In the NN+3N case, we discard the normal-ordered three-body part and work in the normal-ordered two-body approximation. This allows us to compare IMSRG(2) and IMSRG(3) results and see only the effect of induced three-body contributions that are kept in the IMSRG(3). In the future, it will also be interesting to see what the effect of the inclusion of the residual three-body force discarded in the NO2B approximation is.

Commutator	Cost	Included in IMSRG(3)-...?					
		A	B	C	D	E	F
$[1, 3] \rightarrow 2$	$\mathcal{O}(N^6)$		✓	✓	✓	✓	✓
$[2, 3] \rightarrow 1$	$\mathcal{O}(N^6)$		✓	✓	✓	✓	✓
$[3, 3] \rightarrow 0$	$\mathcal{O}(N^6)$		✓	✓	✓	✓	✓
$[2, 2] \rightarrow 3$	$\mathcal{O}(N^7)$	✓	✓	✓	✓	✓	✓
$[1, 3] \rightarrow 3$	$\mathcal{O}(N^7)$	✓	✓	✓	✓	✓	✓
$[2, 3] \rightarrow 2$	$\mathcal{O}(N^7)$	✓	✓	✓	✓	✓	✓
$[3, 3] \rightarrow 1$	$\mathcal{O}(N^7)$			✓	✓	✓	✓
$[2, 3] \rightarrow 3$	$\mathcal{O}(N^8)$				✓	✓	✓
$[3, 3] \rightarrow 2$	$\mathcal{O}(N^8)$					✓	✓
$[3, 3] \rightarrow 3$	$\mathcal{O}(N^9)$						✓

Table 6.1: List of IMSRG(3) fundamental commutators ordered by computational cost. Right columns indicate whether the commutator is included in various approximate IMSRG(3) truncation schemes (see text for details).

6.2 Truncation schemes

For the purposes of this thesis, we will work with numerous truncation schemes that partially include the commutators from the IMSRG(3) truncation on top of the IMSRG(2). This was done to allow for a broad range of calculations for different bases, basis frequencies, and Hamiltonians to take place in a relatively small amount of time. The fundamental commutators for the IMSRG are schematically of the form

$$[A^{(K)}, B^{(L)}] \rightarrow C^{(M)}, \quad (6.5)$$

with $|K - L| \leq M \leq K + L - 1$. The computational cost of such a commutator is $\mathcal{O}(N^{K+L+M})$, where N is the dimension of the (reduced) single-particle basis. For notational simplicity, we will use the simpler shorthand version of Eq. (6.5),

$$[K, L] \rightarrow M. \quad (6.6)$$

The commutators new to the IMSRG(3) are those where at least one of K , L , and M is 3, and none are greater than 3. A complete list of all of the new commutators and their computational costs is given in Table 6.1, along with whether they are included in the approximate truncation schemes discussed below.

The truncation schemes we use selectively add in fundamental commutators to the previous truncation scheme, starting from the IMSRG(2). The first truncation beyond IMSRG(2) is given by

$$\text{IMSRG(3)-A} \equiv \text{IMSRG(2)} + [2, 2] \rightarrow 3 + [2, 3] \rightarrow 2 + [1, 3] \rightarrow 3. \quad (6.7)$$

In the NO2B approximation, where the initial three-body Hamiltonian is 0, the $[2, 2] \rightarrow 3$ commutator is the only one that induces a three-body part. This alone is insufficient, because there is no way for the three-body part to feed back into the zero- through two-body parts, which is what the $[2, 3] \rightarrow 2$ commutator accomplishes. The reason this commutator is chosen and not a cheaper $\mathcal{O}(N^6)$ commutator is because of the work done in Ref. [73]. Here it was shown that the inclusion of a nested $[2, [2, 2] \rightarrow 3] \rightarrow 2$ commutator in the Magnus expansion alleviated undercounting in the IMSRG(2) truncation, giving the so-called IMSRG(2*) truncation. The IMSRG(3)-A scheme above naturally includes this nested commutator, but also includes a flowing three-body operator and thus includes contributions absent in the IMSRG(2*) truncation.

With just those two commutators added, the IMSRG would induce a three-body part to the Hamiltonian and allow it to feed back into lower-body parts, but it would not suppress the $ppphhh$ blocks, which couple the reference state to its $3p3h$ excitations. This suppression is achieved by terms proportional to $\eta^{(3)}$ in the three-body flow equation. These come in principle out of the $[1, 3] \rightarrow 3$ and $[2, 3] \rightarrow 3$ commutators. In practice, we see that the dominant diagonal of the one-body Hamiltonian f works best with $\eta^{(3)}$ to effectively drive the suppression. The two-body Hamiltonian Γ seems to have too much off-diagonal structure to stably suppress the relevant three-body matrix elements. Thus we include the $[1, 3] \rightarrow 3$ commutator in the IMSRG(3)-A truncation scheme. In this truncation scheme, we expect a three-body part of the Hamiltonian to be induced and properly feed back into the two-body part over the course of the evolution, and we expect the three-body $ppphhh$ blocks in the Hamiltonian, which contribute in the three-body generator, to be appropriately suppressed and the reference state to properly decouple from its excitations.

For the following truncations, we choose to organize them by cost, including cheaper commutators before including more expensive commutators. The hierarchy of commutator contributions and the development of improved truncation schemes will be studied in detail in future work. The next truncation scheme adds the $\mathcal{O}(N^6)$ IMSRG(3) fundamental commutators:

$$\text{IMSRG(3)-B} \equiv \text{IMSRG(3)-A} + [3, 3] \rightarrow 0 + [2, 3] \rightarrow 1 + [1, 3] \rightarrow 2. \quad (6.8)$$

The motivation to include these instead of some more expensive commutators is driven by cost, and they are added all together as there does not seem to be a reason to prefer a specific ordering among the $\mathcal{O}(N^6)$ commutators. Continuing to add commutators in order of cost, the next truncation scheme includes the final remaining $\mathcal{O}(N^7)$ commutator,

$$\text{IMSRG(3)-C} \equiv \text{IMSRG(3)-B} + [3, 3] \rightarrow 1, \quad (6.9)$$

and the final three truncation schemes include first the $\mathcal{O}(N^8)$ commutators,

$$\text{IMSRG(3)-D} \equiv \text{IMSRG(3)-C} + [2, 3] \rightarrow 3, \quad (6.10)$$

$$\text{IMSRG(3)-E} \equiv \text{IMSRG(3)-D} + [3, 3] \rightarrow 2, \quad (6.11)$$

N_{\max}	$E_{^4\text{He}}$ (MeV)	
	EM 1.8	EM 1.8/2.0
0	-8.81320	-8.6427
2	-23.5758	-23.6755
4	-26.6500	-27.2420
6	-27.6024	-28.2752
8	-28.0584	-28.7386
10	-28.2676	-28.9448
12	-28.3584	-29.0290
14	-28.4016	-29.0677
16	-28.4241	-29.0884
18	-28.4362	-29.0996
20	-28.4428	-29.1056
∞ (extrap.)	-28.4499	-29.1125

Table 6.2: Jacobi-NCSM results for the ground-state energy of ^4He as a function of the truncation parameter N_{\max} for the NN-only EM 1.8 potential and the NN+3N EM 1.8/2.0 potential [77]. $N_{\max} = \infty$ values are based on an exponential extrapolation using the values of $E_{^4\text{He}}$ for $N_{\max} \geq 12$.

and finally the $\mathcal{O}(N^9)$ commutator,

$$\text{IMSRG(3)-F} \equiv \text{IMSRG(3)-E} + [3, 3] \rightarrow 3. \quad (6.12)$$

We also call IMSRG(3)-C IMSRG(3)- N^7 as it includes all terms that cost up to $\mathcal{O}(N^7)$. For comparison, the approximate treatment of triples in coupled-cluster calculations used in nuclear structure theory [for example in $\Lambda\text{CCSD(T)}$, CR-CC(2,3)] also scales like $\mathcal{O}(N^7)$ [74–76]. In the next two sections, we first compare IMSRG(3)- N^7 to the IMSRG(2). We then study the magnitude of the contributions when we use the different truncation schemes discussed above.

6.3 IMSRG(3)- N^7 results

In this section, we take a careful look at what happens to calculations for ^4He when we apply the IMSRG(3)- N^7 truncation. For reference, we show in Fig. 6.1 the results for the ground-state energy and charge radius obtained via the IMSRG(2) for HF and NAT reference states at various oscillator frequencies. For the charge radius, we use the square root of the point-proton mean-square radius operator expectation value and a spin-orbit correction [78] added in quadrature. We observe that the NAT basis gives essentially frequency-independent results for energies and radii in both the NN-only and NN+3N cases. The relatively strong frequency dependence of the HF results is a consequence of

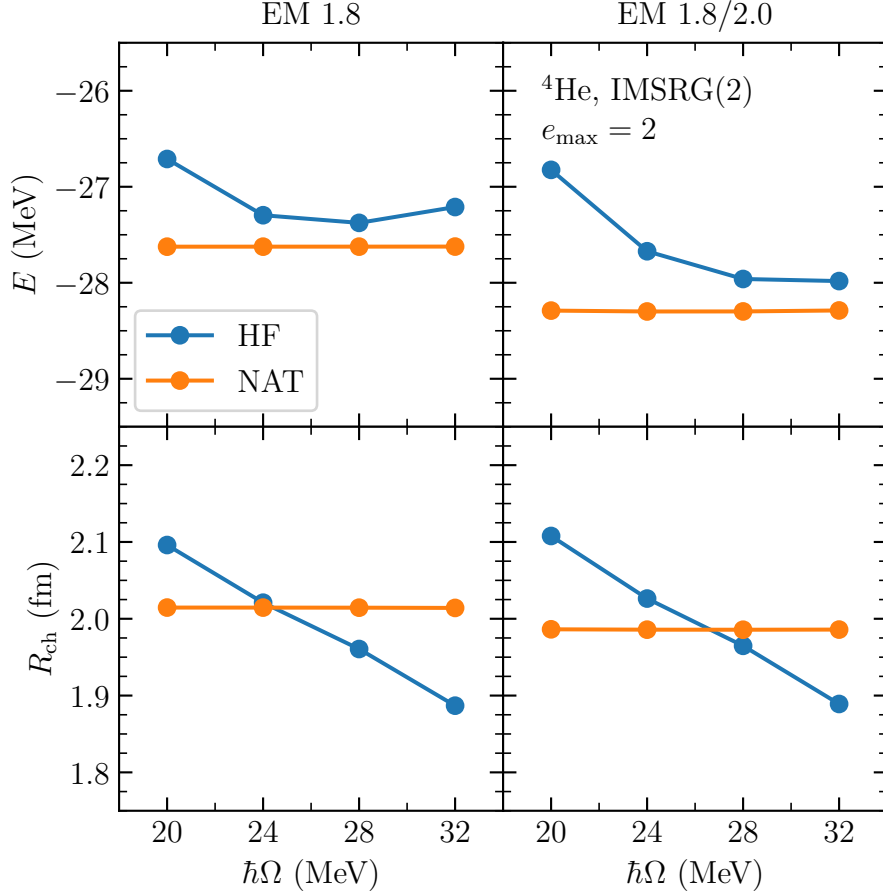


Figure 6.1: IMSRG(2) ground-state energies (top row) and charge radii (bottom row) of ${}^4\text{He}$ for the NN-only EM 1.8 potential (left column) and the NN+3N EM 1.8/2.0 potential (right column) as a function of the oscillator frequency $\hbar\Omega$ for the HF and NAT bases. The HF basis is constructed in $e_{\text{max}} = 2$, and the NAT basis is constructed in $e_{\text{max}} = 14$, with $E_{3\text{max}} = 16$ for the NN+3N case, before being truncated to $e_{\text{max}} = 2$ for the IMSRG(2) calculation.

the construction of the HF basis in $e_{\text{max}} = 2$. The correlation energy

$$E_{\text{corr}} \equiv E(s \rightarrow \infty) - E(s = 0), \quad (6.13)$$

which is the contribution to the ground-state energy generated by the many-body expansion, is around 4 MeV for the NN-only calculations and around 5 MeV for the NN+3N calculations. When we compare the IMSRG(2) and IMSRG(3)- N^7 results, it is sometimes illustrative to consider their differences relative to E_{corr} , since $E(s = 0)$ is the same in both truncations and they only differ in their many-body expansion order. As a concrete example, for the HF NN+3N case at $\hbar\Omega = 28$ MeV, $E(s = 0) = -22.8145$ MeV. For

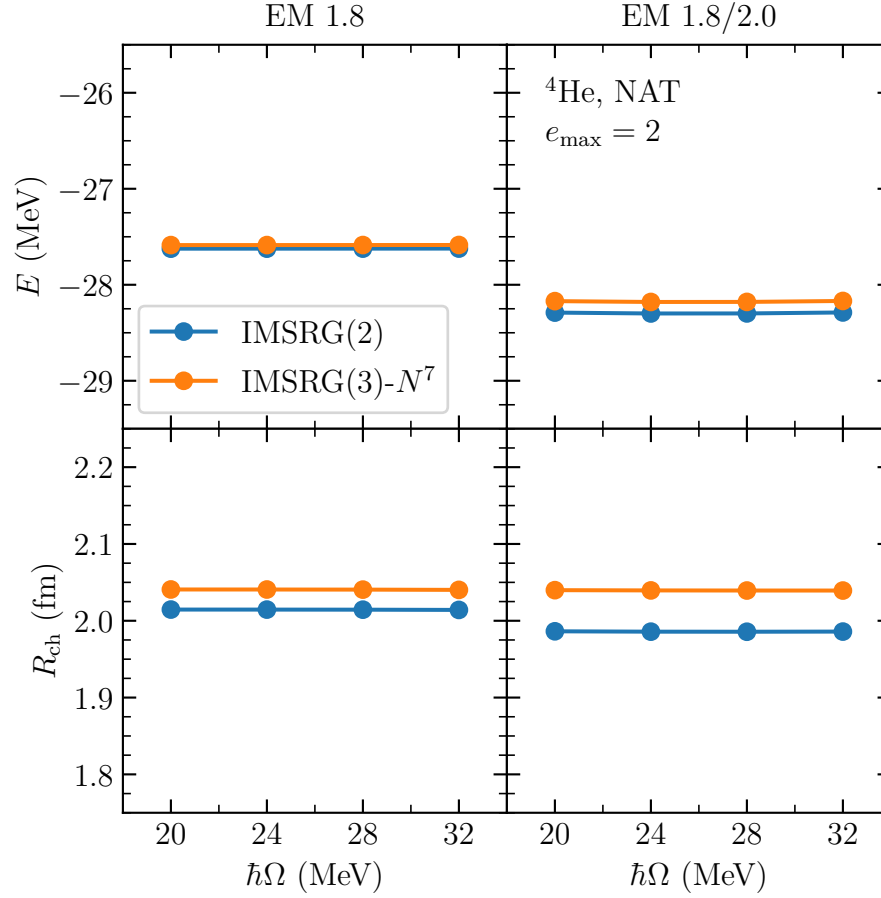


Figure 6.2: Ground-state energies (top row) and charge radii (bottom row) of ${}^4\text{He}$ for the NN-only EM 1.8 potential (left column) and the NN+3N EM 1.8/2.0 potential (right column) as a function of the oscillator frequency $\hbar\Omega$ for the NAT basis obtained via IMSRG(2) and IMSRG(3)- N^7 calculations. The NAT basis is constructed in $e_{\text{max}} = 14$, with $E_{3\text{max}} = 16$ for the NN+3N case, before being truncated to $e_{\text{max}} = 2$ for the IMSRG calculations.

the IMSRG(2) calculation, $E(s \rightarrow \infty) = -27.9606 \text{ MeV}$ giving a correlation energy of $E_{\text{corr}} = -5.1461 \text{ MeV}$.

The inclusion of 3N forces at the NO2B level gives (in this system and for this model space) a slightly larger binding energy and accordingly a slightly smaller radius. We emphasize that just the results from $e_{\text{max}} = 2$ are not sufficient to make a statement about the effect of 3N forces in ${}^4\text{He}$. This is because in this model space the Hamiltonian is not fully converged with respect to model-space size and so parts of the Hamiltonian could be cut out by the truncation that would change the effect of 3N forces. Thus, to make

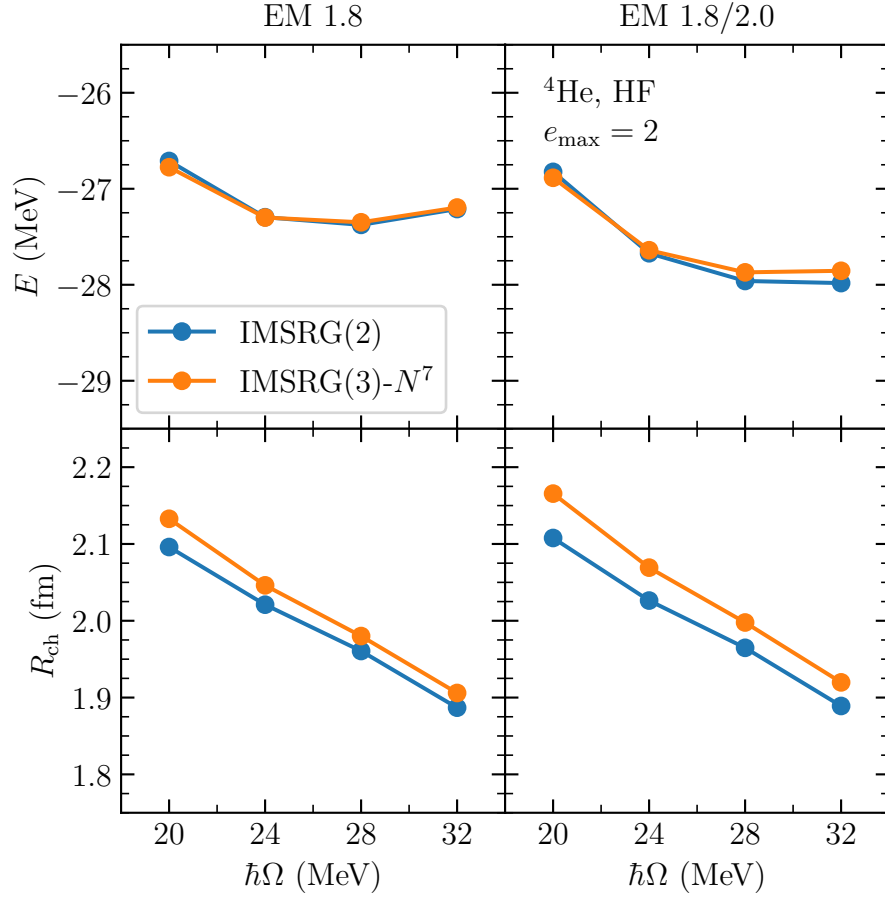


Figure 6.3: Ground-state energies (top row) and charge radii (bottom row) of ^4He for the NN-only EM 1.8 potential (left column) and the NN+3N EM 1.8/2.0 potential (right column) as a function of the oscillator frequency $\hbar\Omega$ for the HF basis obtained via IMSRG(2) and IMSRG(3)- N^7 calculations. The HF basis is constructed in $e_{\text{max}} = 2$.

a concrete claim, one must also do calculations for larger model spaces (currently out of reach) and observe that the converged energies change little as a function of $e_{\text{max}} = 2$ to draw conclusions about the contributions of 3N forces.

Incidentally, in Jacobi-NCSM calculations, shown in Table 6.2, one sees that 3N forces do in fact give a little bit more binding in ^4He [77]. These values should not be compared with those from our IMSRG calculations as the extrapolated values are converged with respect to model-space size while our $e_{\text{max}} = 2$ IMSRG results are not, the N_{max} truncation used in NCSM calculations is different from the e_{max} truncation used in many-body expansion methods, and the calculation is based additionally on a Jacobi HO basis instead of a single-particle basis like the single-particle NCSM and the IMSRG. Additionally, we

use the NO2B approximation here, which was seen to perform relatively poorly in ^4He in NCSM calculations [79] and is not present in the Jacobi-NCSM calculations discussed above.

In Fig. 6.2, we compare the results for the ground-state energy and charge radius of ^4He for IMSRG(2) and IMSRG(3)- N^7 calculations based on NAT reference states. The frequency independence of the IMSRG(2) results is preserved in the IMSRG(3)- N^7 results. The three-body contributions to the ground-state energy in the IMSRG(3)- N^7 are small, 37 keV in the NN-only case and 120 keV in the NN+3N case. The effect on the charge radius is more pronounced, with a shift of 0.026 fm in the NN-only case and 0.054 fm in the NN+3N case.

In Fig. 6.3, we see that the same trends are generally seen for calculations based on HF reference states. We see that the IMSRG(3)- N^7 results for the energy are slightly flatter as a function of oscillator frequency than the IMSRG(2) results. This may be a sign that the inclusion of three-body operators in the IMSRG(3)- N^7 makes the IMSRG evolution less sensitive to reference-state deficiencies. However, to be able to conclude this, this trend must be seen also for larger model spaces, for other bases, and for other closed-shell systems.

6.4 Approximate IMSRG(3) truncation-scheme analysis

Now we turn our attention to what happens when we turn on selected fundamental commutators from the IMSRG(3) relative to the IMSRG(2) starting point. For the purposes of this first exploration, we consider ^{16}O in an $e_{\text{max}} = 2$ model space. We use the optimized NAT basis, which delivers essentially frequency-independent results for IMSRG(2) calculations of ^{16}O .

In Fig. 6.4, we show the ground-state energy of ^{16}O for various different truncation schemes (see Sec. 6.2 for details). For all of these calculations, $E_{\text{corr}} \sim 10$ MeV. We see that the first stable IMSRG(3) approximation, the IMSRG(3)-A truncation, produces a sizable shift in the energy of 42 keV. This is to be contrasted with the next two truncations, IMSRG(3)-B, which adds all $\mathcal{O}(N^6)$ IMSRG(3) fundamental commutators to IMSRG(3)-A, and IMSRG(3)-C (or IMSRG(3)- N^7), which adds the final remaining $\mathcal{O}(N^7)$ IMSRG(3) fundamental commutator to IMSRG(3)-B, where the energy shifts by 9 keV and 0.2 keV respectively. In this sense, it seems as though the IMSRG(3)- N^7 truncation is dominated by the commutators included in the IMSRG(3)-A truncation and the commutators included in the IMSRG(3)-B and IMSRG(3)-C truncations do relatively little. We note that for the three commutators added in the IMSRG(3)-B truncation each commutator separately has a small contribution, and it is not the case that two commutators have relatively large contributions that cancel to give an overall small contribution.

The organization outlined in Section 6.2 is primarily based on computational cost.

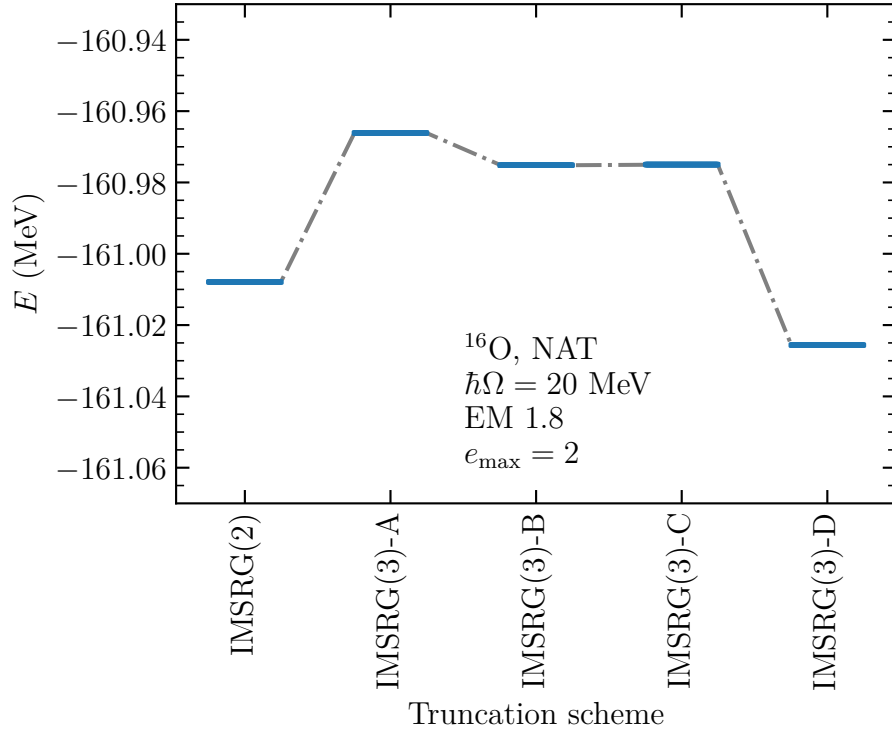


Figure 6.4: Ground-state energies of ^{16}O for the NN-only EM 1.8 potential resulting from IMSRG calculations using the IMSRG(2) and various approximated IMSRG(3) truncation schemes (see text for details). Calculations were done at an oscillator frequency of 20 MeV, and a NAT reference state was used. The NAT basis is constructed in $e_{\text{max}} = 14$ before being truncated to $e_{\text{max}} = 2$ for the various many-body calculations.

In light of this organization, it is interesting that the contribution from the first $\mathcal{O}(N^8)$ commutator included in the IMSRG(3)-D truncation scheme is quite large, producing a 51 keV shift in the ground-state energy. This suggests that the organization by cost may not be well motivated and in practice does not behave desirably when going from IMSRG(2) to IMSRG(3). To develop better approximated IMSRG(3) truncation schemes, one could perform a perturbative analysis as is done in Chapter 7 of Ref. [3] for IMSRG(2), where it is shown that IMSRG(2) is exact up to third order in MBPT. Doing this for IMSRG(3) would allow one to determine which commutators to include to make an approximate IMSRG(3) truncation complete up to some order in MBPT.

Chapter 7

Summary and outlook

The aim of this thesis was to investigate the contributions of induced three-body operators in the IMSRG. To this end, we studied the IMSRG(3) truncation of the IMSRG. The uncoupled (m -scheme) implementation of the IMSRG(3) is too expensive for nuclear applications, so we exploited the spherical symmetry of the IMSRG when applied to closed-shell nuclei to arrive at the J -scheme IMSRG(3) fundamental commutators. We implemented an IMSRG(2)/(3) solver using these fundamental commutators that is more performant than the previous m -scheme implementation. With this implementation in hand, we were able to do first explorations of the effects of approximations to the IMSRG(3) truncation when compared with the IMSRG(2) truncation in ${}^4\text{He}$ and ${}^{16}\text{O}$.

To allow for the exploration of different single-particle bases, Hamiltonians, and oscillator frequencies, we introduced several approximate IMSRG(3) truncation schemes that leave out the most expensive fundamental commutators, one of which was the IMSRG(3)- N^7 . We find that in ${}^4\text{He}$, the IMSRG(3)- N^7 truncation offers a small correction at the sub-percent level to the IMSRG(2) result for the ground-state energy in the $e_{\text{max}} = 2$ model space considered. The corrections to the charge radius are larger, on the order of a few percent. We see that the IMSRG(3)- N^7 performs somewhat better than the IMSRG(2) away from the optimal HF oscillator frequency, a trend that needs to be verified for larger model spaces and different systems.

For ${}^{16}\text{O}$, we considered various approximate IMSRG(3) truncation schemes. These schemes were set up to include one or several fundamental commutators on top of the previous truncation scheme, starting from the IMSRG(2). The organization of these schemes was partially physically motivated (in particular the IMSRG(3)-A scheme), but most commutator inclusions were organized by computational cost. We found that this organization did not deliver the desired results. While the IMSRG(3)-A truncation provided a relatively significant shift from the IMSRG(2) results, the inclusion of the remaining $\mathcal{O}(N^6)$ and $\mathcal{O}(N^7)$ commutators provided only small corrections to the ground-state energy of ${}^{16}\text{O}$. The final truncation scheme we considered, which included the first $\mathcal{O}(N^8)$ commutator, produced another large shift over the previous truncation. This suggests that computational cost is not a good proxy for importance in the formation of an approximate

IMSRG(3) truncation.

Looking to the future, there are clear objectives for our IMSRG(3) implementation. The first is tuning the performance of the implementation to put full IMSRG(3) $e_{\max} = 6$ and hopefully $e_{\max} = 8$ within reach. Additional restrictions can be placed on for example the range of three-body channels, potentially allowing IMSRG(3) calculations to reach even larger single-particle model space sizes. This will allow us to perform converged IMSRG(3) calculations for medium-mass nuclei and investigate what effects it has on observables. Parallel to this, obtaining exact (full configuration interaction) results in $e_{\max} = 2$ would allow us to see how IMSRG(3) compares with IMSRG(2) relative to the exact solution of the Schrödinger equation in $e_{\max} = 2$. A secondary implementation goal is the support of tensor operators, which would give our implementation access to many more observables, such as low-lying spectroscopy.

A key result of this thesis is that the organization by computational cost, at least for the limited calculations discussed here for which we lack exact results provided by full configuration interaction calculations, is not a good strategy for developing an IMSRG(3) approximation. To develop the IMSRG(3) further, a more careful look into the behavior and structure of the fundamental commutators is important to understand the deficiencies in the naive organization by cost. One path to doing this is the perturbative analysis of the IMSRG(3) flow equations. This could allow one to develop an approximate IMSRG(3) truncation that is potentially fourth- or fifth-order exact in MBPT. This analysis will need to be adapted to account for non-HF reference states and also cases beyond the NO2B approximation where the residual normal-ordered three-body Hamiltonian is included at the start of the IMSRG calculation. In this analysis of the IMSRG(3), it will be interesting to look at how the IMSRG(3) performs relative to the IMSRG(2) under variation of the reference state. If one finds that the IMSRG(3) is more successful for sub-optimal reference states, understanding this feature of the IMSRG(3) may allow for constructions of IMSRG(3) approximations that share this behavior.

This thesis represents a first step towards full IMSRG(3) calculations of light and medium-mass nuclei and the systematic development and testing of approximate IMSRG(3) truncation schemes. Accessing full IMSRG(3) calculations will provide access to high-precision many-body results, hopefully bringing the many-body uncertainty error for ground-state energies robustly into the per-mille range. Well-motivated approximations of the IMSRG(3) will make most of the accuracy benefits of the IMSRG(3) available at a lower computational cost, necessary for calculations where large model spaces are required to converge calculations, for example for heavy nuclei or hard, unevolved nuclear Hamiltonians.

Appendix A

m -scheme fundamental commutators for the IMSRG(3)

We list the m -scheme fundamental commutators needed for the IMSRG(3), taken from Ref. [3]. The commutator of a K -body and an L -body operator gives $|K-L|$ - to $(K+L-1)$ -body terms:

$$\left[A^{(K)}, B^{(L)}\right] = \sum_{M=|K-L|}^{K+L-1} C^{(M)}. \quad (\text{A.1})$$

Note that the expressions we give below are for the matrix elements of the different M -body terms. Also note that expressions for two- and three-body matrix elements are not antisymmetrized, so the appropriate antisymmetrizer must be applied to the matrix elements after evaluating the commutator. We use the convention that the index labels i, j, k, \dots are reserved for external indices, that is, indices appearing on the matrix elements of the resulting operator, and the index labels a, b, c, \dots are reserved for contracted indices, that is, indices that are summed over in the matrix elements of the input operators. n_a are the occupation numbers, and $\bar{n}_a = 1 - n_a$.

A.1 $[A^{(1)}, B^{(1)}]$

The commutator of two one-body operators has a zero-body part,

$$C = \sum_{ab} (n_a - n_b) A_{ab} B_{ba}, \quad (\text{A.2})$$

and a one-body part

$$C_{ij} = \sum_a (A_{ia} B_{aj} - B_{ia} A_{aj}). \quad (\text{A.3})$$

A.2 $[A^{(1)}, B^{(2)}]$

The commutator of a one-body operator and a two-body operator has a one-body part,

$$C_{ij} = \sum_{ab} (n_a - n_b) A_{ab} B_{biaj}, \quad (\text{A.4})$$

and a two-body part,

$$C_{ijkl} = 2 \sum_a (A_{ia} B_{ajkl} - A_{ak} B_{ijal}). \quad (\text{A.5})$$

A.3 $[A^{(2)}, B^{(2)}]$

The commutator of two two-body operators has a zero-body part,

$$C = \frac{1}{4} \sum_{abcd} (n_a n_b \bar{n}_c \bar{n}_d - \bar{n}_a \bar{n}_b n_c n_d) A_{abcd} B_{cdab}, \quad (\text{A.6})$$

a one-body part,

$$C_{ij} = \frac{1}{2} \sum_{abc} (\bar{n}_a \bar{n}_b n_c + n_a n_b \bar{n}_c) (A_{ciab} B_{abcj} - B_{ciab} A_{abcj}), \quad (\text{A.7})$$

a two-body part,

$$C_{ijkl} = D_{ijkl} + E_{ijkl}, \quad (\text{A.8})$$

with

$$D_{ijkl} \equiv \frac{1}{2} \sum_{ab} (\bar{n}_a - n_b) (A_{ijab} B_{abkl} - B_{ijab} A_{abkl}), \quad (\text{A.9})$$

$$E_{ijkl} \equiv 4 \sum_{ab} (n_a - n_b) A_{aibk} B_{bjal}, \quad (\text{A.10})$$

and a three-body part,

$$C_{ijklmn} = 9 \sum_a (A_{ijla} B_{akmn} - B_{ijla} A_{akmn}). \quad (\text{A.11})$$

A.4 $[A^{(1)}, B^{(3)}]$

The commutator of a one-body operator and a three-body operator has a two-body part,

$$C_{ijkl} = \sum_{ab} (n_a - n_b) A_{ab} B_{bijakl}, \quad (\text{A.12})$$

and a three-body part,

$$C_{ijklmn} = 3 \sum_a (A_{ia} B_{ajklmn} - A_{al} B_{ijkamn}). \quad (\text{A.13})$$

A.5 $[A^{(2)}, B^{(3)}]$

The commutator of a two-body operator and a three-body operator has a one-body part,

$$C_{ij} = -\frac{1}{4} \sum_{abcd} (n_a n_b \bar{n}_c \bar{n}_d - \bar{n}_a \bar{n}_b n_c n_d) A_{cdab} B_{abijcd}, \quad (\text{A.14})$$

a two-body part,

$$C_{ijkl} = -\sum_{ab} (n_a \bar{n}_b \bar{n}_c + \bar{n}_a n_b n_c) (A_{bcak} B_{aijbcl} + A_{bcai} B_{aklbcl}), \quad (\text{A.15})$$

and a three-body part,

$$C_{ijklmn} = \frac{3}{2} \sum_{ab} (\bar{n}_a - n_b) (A_{ijab} B_{abklmn} - A_{abmn} B_{ijklab}). \quad (\text{A.16})$$

A.6 $[A^{(3)}, B^{(3)}]$

The commutator of two three-body operators has a zero-body part,

$$C = \frac{1}{36} \sum_{abcdef} (n_a n_b n_c \bar{n}_d \bar{n}_e \bar{n}_f - \bar{n}_a \bar{n}_b \bar{n}_c n_d n_e n_f) A_{abcdef} B_{defabc}, \quad (\text{A.17})$$

a one-body part,

$$C_{ij} = \frac{1}{12} \sum_{abcde} (n_a n_b \bar{n}_c \bar{n}_d \bar{n}_e + \bar{n}_a \bar{n}_b n_c n_d n_e) (A_{abcide} B_{cdeabj} - B_{abcide} A_{cdeabj}), \quad (\text{A.18})$$

a two-body part,

$$C_{ijkl} = D_{ijkl} + E_{ijkl}, \quad (\text{A.19})$$

with

$$D_{ijkl} \equiv \frac{1}{6} \sum_{abcd} (n_a \bar{n}_b \bar{n}_c \bar{n}_d - \bar{n}_a n_b n_c n_d) (A_{aijbcd} B_{bcdakl} - B_{aijbcd} A_{bcdakl}), \quad (\text{A.20})$$

$$E_{ijkl} \equiv \sum_{abcd} (\bar{n}_a \bar{n}_b n_c n_d - n_a n_b \bar{n}_c \bar{n}_d) A_{abikcl} B_{cdjabk}, \quad (\text{A.21})$$

and a three-body part,

$$C_{ijklmn} = D_{ijklmn} + E_{ijklmn} + F_{ijklmn}, \quad (\text{A.22})$$

with

$$D_{ijklmn} \equiv \frac{1}{6} \sum_{abc} (n_a n_b n_c + \bar{n}_a \bar{n}_b \bar{n}_c) (A_{ijkabc} B_{abclmn} - B_{ijkabc} A_{abclmn}), \quad (\text{A.23})$$

$$E_{ijklmn} \equiv \frac{9}{2} \sum_{abc} (n_a n_b \bar{n}_c + \bar{n}_a \bar{n}_b n_c) A_{abkcmn} B_{cijabl}, \quad (\text{A.24})$$

$$F_{ijklmn} \equiv -\frac{9}{2} \sum_{abc} (n_a n_b \bar{n}_c + \bar{n}_a \bar{n}_b n_c) A_{cjkabn} B_{iablmc}. \quad (\text{A.25})$$

Appendix B

Simplification strategies for coupled fundamental commutators

For the coupled fundamental commutators, the key to arriving at the simplest expressions is to avoid unnecessary recoupling. Recoupling, where bra or ket couplings have to be broken and recreated to relate matrix elements on both sides of the expression, is unnecessary when symmetries of the matrix elements or of the expression can be exploited to bring the uncoupled expression into a form where its coupled analog no longer requires recoupling. Recoupling comes at the cost of an additional sum over an angular momentum and the inclusion of a Wigner $6j$ or $9j$ symbol. Thus avoiding unnecessary recoupling is essential for achieving better performance for implementations of the coupled expressions. In the following, we discuss two strategies for avoiding recoupling and apply them each to one example.

B.1 Using antisymmetry of input operator matrix elements

The uncoupled matrix elements are antisymmetric under exchange of any two bra or ket indices. This symmetry can easily be exploited to permute indices into a form that minimizes recoupling.

Consider the $[A^{(1)}, B^{(3)}] \rightarrow C^{(2)}$ fundamental commutator. The uncoupled expression for the matrix elements of C is

$$C_{ijkl} = \sum_{ab} (n_a - n_b) A_{ab} B_{bijakl} , \quad (\text{B.1})$$

and the coupled expression is

$$C_{ijkl}^{J_C} = (-1)^{j_i+j_j+j_k+j_l} \sum_{j_a} \sum_{(J_{B,3}, J_{B,pq}, J_{B,st})} \hat{J}_{B,pq} \hat{J}_{B,st} \hat{J}_{B,3}^2$$

$$\sum_{ab} (n_a \bar{n}_b - \bar{n}_a n_b) \begin{Bmatrix} j_j & j_i & J_C \\ j_a & J_{B,3} & J_{B,pq} \end{Bmatrix} \begin{Bmatrix} j_l & j_k & J_C \\ j_a & J_{B,3} & J_{B,st} \end{Bmatrix} \quad (B.2)$$

$$A_{ab}^{j_a} B_{bijakl}^{(J_{B,3}, J_{B,pq}, J_{B,st})}.$$

The appearance of $6j$ symbols is a result of breaking the bi coupling on the right to form the ij coupling on the left and breaking the ak coupling on the right to form the kl coupling on the left. By exploiting antisymmetry in the uncoupled matrix elements of B , we can arrive at the uncoupled expression

$$C_{ijkl} = \sum_{ab} (n_a \bar{n}_b - \bar{n}_a n_b) A_{ab} B_{ijbkla}, \quad (B.3)$$

which yields the coupled expression

$$C_{ijkl}^{J_C} = \frac{1}{\hat{J}_C^2} \sum_{j_a} \sum_{J_{B,3}} \hat{J}_{B,3}^2 \sum_{ab} (n_a \bar{n}_b - \bar{n}_a n_b) A_{ab}^{j_a} B_{ijbkla}^{(J_{B,3}, J_C, J_C)}. \quad (B.4)$$

B.2 Using antisymmetry of output operator matrix elements

As a reminder, in this work we typically work with non-antisymmetrized expressions for the fundamental commutators, so one can not simply permute the indices on the output matrix elements. However, one can exploit that the output matrix elements will at some point be antisymmetrized and choose the term that contributes to the antisymmetrized result with the minimal recoupling.

To make this clear, consider the following example: Suppose the three-body uncoupled matrix elements O_{pqrstu} are already antisymmetric in stu , but not in pqr . Thus to get the final antisymmetrized matrix elements O_{pqrstu}^{as} , one needs to evaluate

$$O_{pqrstu}^{\text{as}} = \mathcal{A}_{pqr} O_{pqrstu}, \quad (B.5)$$

with

$$\mathcal{A}_{pqr} = \frac{1}{6} (1 + P_{prq} + P_{prq}^2) (1 - P_{pq}), \quad (B.6)$$

where P_{prq} cyclically permutes the indices p , q , and r and P_{pq} exchanges the indices p and q as discussed in Section 5.2.2.

Writing Eq. (B.5) out, one gets

$$O_{pqrstu}^{\text{as}} = \frac{1}{6} (O_{pqrstu} + O_{qrpstu} + O_{rpqstu} - O_{qprstu} - O_{rqpstu} - O_{prqstu}). \quad (B.7)$$

Now consider

$$\overline{O}_{pqrstu} \equiv O_{qrpstu}. \quad (\text{B.8})$$

Antisymmetrizing \overline{O}_{pqrstu} gives

$$\overline{O}_{pqrstu}^{\text{as}} = \frac{1}{6}(\overline{O}_{pqrstu} + \overline{O}_{qrpstu} + \overline{O}_{rpqstu} - \overline{O}_{qprstu} - \overline{O}_{rqpstu} - \overline{O}_{prqstu}), \quad (\text{B.9})$$

which one can rewrite in terms of the original matrix elements O_{pqrstu} :

$$\overline{O}_{pqrstu}^{\text{as}} = \frac{1}{6}(O_{qrpstu} + O_{rpqstu} + O_{pqrstu} - O_{rqpstu} - O_{prqstu} - O_{qprstu}). \quad (\text{B.10})$$

One can quickly see that Eqs. (B.7) and (B.10) contain the exact same terms, making them equal. Thus if O_{pqrstu} is given by some many-body expression, one can permute the indices p , q , and r on the right-hand (or left-hand) side of the expression, including an overall minus sign if the permutation is odd, and know that it will give the same result after antisymmetrization.

Again, it is useful to consider a concrete application to illustrate how this strategy can be applied. Consider the $[A^{(2)}, B^{(2)}] \rightarrow C^{(3)}$ fundamental commutator. The uncoupled non-antisymmetrized expression is

$$C_{ijklmn} = 9 \sum_a (A_{ijla} B_{akmn} - B_{ijla} A_{akmn}). \quad (\text{B.11})$$

which gives the coupled expression

$$\begin{aligned} C_{ijklmn}^{(J_{C,3}, J_{C,ij}, J_{C,lm})} &= 9 \hat{J}_{C,ij} \hat{J}_{C,lm} (-1)^{j_m + j_n} \sum_{J_{mn}} \hat{J}_{mn}^2 \sum_a (-1)^{j_a + j_k} \\ &\times \left\{ \begin{matrix} j_k & j_a & J_{mn} \\ j_l & J_{C,3} & J_{C,ij} \end{matrix} \right\} \left\{ \begin{matrix} j_l & j_m & J_{C,lm} \\ j_n & J_{C,3} & J_{mn} \end{matrix} \right\} \\ &\times (A_{ijla}^{J_{C,ij}} B_{akmn}^{J_{mn}} - B_{ijla}^{J_{C,ij}} A_{akmn}^{J_{mn}}). \end{aligned} \quad (\text{B.12})$$

One can immediately see that the mn coupling on the right in B and A needs to be broken up to form the lm coupling on the left, leading to some of the recoupling.

However, the uncoupled expression

$$D_{ijklmn} \equiv 9 \sum_a (A_{ijna} B_{aklm} - B_{ijna} A_{aklm}) \quad (\text{B.13})$$

has the indices l , m , and n on the right-hand side permuted cyclically, and it will no longer have this recoupling problem when the expression is coupled. The antisymmetrized matrix elements of C and D are equal, so one might as well simply calculate D instead of C and antisymmetrize that. The coupled expression for D is

$$\begin{aligned} D_{ijklmn}^{(J_{C,3}, J_{C,ij}, J_{C,lm})} &= -9 (-1)^{J_{C,lm}} \hat{J}_{C,ij} \hat{J}_{C,lm} \sum_a (-1)^{j_a + j_k} \left\{ \begin{matrix} j_k & j_a & J_{C,lm} \\ j_n & J_{C,3} & J_{C,ij} \end{matrix} \right\} \\ &\times (A_{ijna}^{J_{C,ij}} B_{aklm}^{J_{C,lm}} - B_{ijna}^{J_{C,ij}} A_{aklm}^{J_{C,lm}}). \end{aligned} \quad (\text{B.14})$$

The final $6j$ symbol cannot be avoided as it forms the three-body angular-momentum coupling that is not present on the right-hand side. Comparing Eq. (B.12) and Eq. (B.14), one can see the simplification afforded by carefully considering which quantity one actually wants to calculate.

Appendix C

IMSRG(3) for the pairing Hamiltonian

The pairing Hamiltonian is given by

$$H = \delta \sum_{p\sigma} (p-1) a_{p\sigma}^\dagger a_{p\sigma} - \frac{g}{2} \sum_{pq} a_{p+}^\dagger a_{p-}^\dagger a_{q-} a_{q+}, \quad (\text{C.1})$$

where we have equally-spaced two-fold degenerate levels indexed by the quantum number p and an attractive (for $g > 0$) pairing interaction. Cooper first considered this Hamiltonian in 1956 [80], which led to the successful Bardeen-Cooper-Schreifer (BCS) theory of superconductivity [81]. The exact eigenvalues of the pairing Hamiltonian were given by Richardson in 1963, where the solutions are obtained via the solution of the non-linear coupled Richardson equations [82].

We focus on a restricted case where $p = 1, \dots, 4$ and $\delta = 1 \text{ MeV}$, and we vary the strength of the pairing interaction g . We are interested in the ground state of four fermions, for which our reference state is the state with the two lowest levels completely filled,

$$|\Phi\rangle = a_{2-}^\dagger a_{2+}^\dagger a_{1-}^\dagger a_{1+}^\dagger |0\rangle. \quad (\text{C.2})$$

This system has a couple of useful properties: First, the number of single-particle states is only eight, making the IMSRG(3) calculation relatively tractable. Additionally, one can increase the number of levels p_{max} easily to get a handle on the performance for larger single-particle basis sizes. Second, in addition to the available exact solution, this system is easy to construct and diagonalize in the basis of the reference state and its particle-hole excitations,

$$\{|\Phi\rangle, |\Phi_{ij}^{ab}\rangle, |\Phi_{ijkl}^{abcd}\rangle\}, \quad (\text{C.3})$$

where the odd number particle-hole excitations do not contribute as Eq. (C.1) only couples pairs. This makes it easy to obtain an exact solution with which to compare the IMSRG(2) and IMSRG(3) solutions. Finally, after normal ordering the Hamiltonian with respect to our reference state, we find that $\bar{H}^{(1)}$ is diagonal, meaning our reference state is the

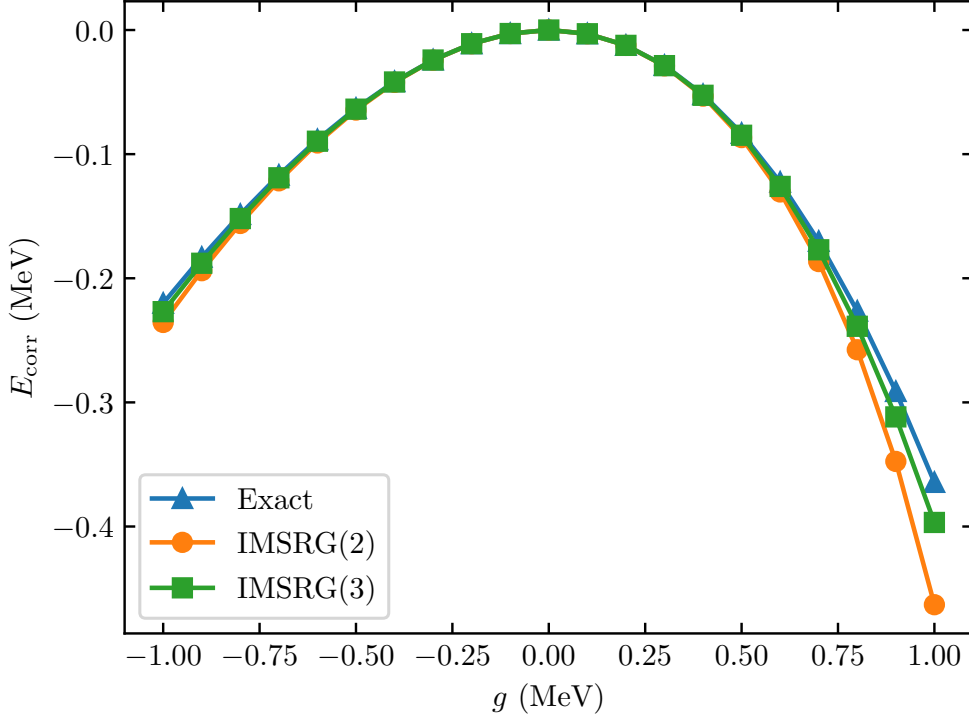


Figure C.1: The correlation energy E_{corr} for the solution of the pairing Hamiltonian obtained via exact diagonalization, IMSRG(2), and IMSRG(3) for $-1 \leq g \leq 1$. Exact diagonalization results obtained using code published with Ref. [83].

canonical Hartree-Fock reference state with the Hartree-Fock energy $\bar{H}^{(0)} = E_{\text{HF}} = 2 - g$. This means the IMSRG evolution must only bring in correlation corrections to the energy without needing to overcome any reference state deficiencies.

Thus, we are interested in the correlation energy obtained by the IMSRG(2) and IMSRG(3) solutions, defined as

$$E_{\text{corr}} \equiv E(s \rightarrow \infty) - E(s = 0). \quad (\text{C.4})$$

This is plotted in Fig. C.1 for $-1 \leq g \leq 1$. We find generally good agreement between the IMSRG correlation energy and the exact correlation energy, with the exception of the region for $0.5 \leq g \leq 1$. Here, the IMSRG(3) calculation improves upon the relatively large error in the IMSRG(2) correlation energy, which in Ref. [53] was explained as being due to an overcounting in the fourth-order diagrams in MBPT by a factor of 1/2 present in the IMSRG(2) truncation. It seems that this overcounting at fourth-order is lifted in the IMSRG(3). We note here that our results for IMSRG(2) match exactly with those from Ref. [53].

Bibliography

- [1] National Research Council, *Nuclear Physics: Exploring the Heart of Matter* (The National Academies Press, Washington, DC, 2013).
- [2] J. Erler, N. Birge, M. Kortelainen, W. Nazarewicz, E. Olsen, A. M. Perhac, and M. Stoitsov, “The limits of the nuclear landscape,” *Nature* **486**, 509 (2012).
- [3] H. Hergert, S. K. Bogner, T. D. Morris, A. Schwenk, and K. Tsukiyama, “The In-Medium Similarity Renormalization Group: A Novel Ab Initio Method for Nuclei,” *Phys. Rept.* **621**, 165 (2016).
- [4] S. Weinberg, “Phenomenological Lagrangians,” *Physica A* **96**, 327 (1979).
- [5] H.-W. Hammer, S. König, and U. van Kolck, “Nuclear effective field theory: status and perspectives,” *Rev. Mod. Phys.* **92**, 025004 (2020).
- [6] E. Epelbaum, H.-W. Hammer, and U.-G. Meißner, “Modern Theory of Nuclear Forces,” *Rev. Mod. Phys.* **81**, 1773 (2009).
- [7] R. Machleidt and D. R. Entem, “Chiral effective field theory and nuclear forces,” *Phys. Rept.* **503**, 1 (2011).
- [8] K. G. Wilson, “Renormalization group and critical phenomena. 1. Renormalization group and the Kadanoff scaling picture,” *Phys. Rev. B* **4**, 3174 (1971).
- [9] S. K. Bogner, R. J. Furnstahl, and R. J. Perry, “Similarity Renormalization Group for Nucleon-Nucleon Interactions,” *Phys. Rev. C* **75**, 061001 (2007).
- [10] S. K. Bogner, R. J. Furnstahl, and A. Schwenk, “From low-momentum interactions to nuclear structure,” *Prog. Part. Nucl. Phys.* **65**, 94 (2010).
- [11] K. Tsukiyama, S. K. Bogner, and A. Schwenk, “In-Medium Similarity Renormalization Group for Nuclei,” *Phys. Rev. Lett.* **106**, 222502 (2011).
- [12] S. R. Stroberg, A. Calci, H. Hergert, J. D. Holt, S. K. Bogner, R. Roth, and A. Schwenk, “A nucleus-dependent valence-space approach to nuclear structure,” *Phys. Rev. Lett.* **118**, 032502 (2017).

- [13] S. K. Bogner, H. Hergert, J. D. Holt, A. Schwenk, S. Binder, A. Calci, J. Langhammer, and R. Roth, “Nonperturbative shell-model interactions from the in-medium similarity renormalization group,” *Phys. Rev. Lett.* **113**, 142501 (2014).
- [14] H. Hergert, S. Binder, A. Calci, J. Langhammer, and R. Roth, “Ab Initio Calculations of Even Oxygen Isotopes with Chiral Two-Plus-Three-Nucleon Interactions,” *Phys. Rev. Lett.* **110**, 242501 (2013).
- [15] E. Gebrerufael, K. Vobig, H. Hergert, and R. Roth, “Ab Initio Description of Open-Shell Nuclei: Merging No-Core Shell Model and In-Medium Similarity Renormalization Group,” *Phys. Rev. Lett.* **118**, 152503 (2017).
- [16] J. M. Yao, J. Engel, L. J. Wang, C. F. Jiao, and H. Hergert, “Generator-coordinate reference states for spectra and $0\nu\beta\beta$ decay in the in-medium similarity renormalization group,” *Phys. Rev. C* **98**, 054311 (2018).
- [17] J. D. Holt, S. R. Stroberg, A. Schwenk, and J. Simonis, “Ab initio limits of atomic nuclei,” (2019), arXiv:1905.10475 .
- [18] R. B. Wiringa, V. G. J. Stoks, and R. Schiavilla, “Accurate nucleon-nucleon potential with charge independence breaking,” *Phys. Rev. C* **51**, 38 (1995).
- [19] K. Hebeler, “Three-Nucleon Forces: Implementation and Applications to Atomic Nuclei and Dense Matter,” (2020), arXiv:2002.09548 .
- [20] H. Pagels, “Departures from Chiral Symmetry: A Review,” *Phys. Rept.* **16**, 219 (1975).
- [21] R. J. Furnstahl, N. Klco, D. R. Phillips, and S. Wesolowski, “Quantifying truncation errors in effective field theory,” *Phys. Rev. C* **92**, 024005 (2015).
- [22] E. Epelbaum, H. Krebs, and U. G. Meißner, “Improved chiral nucleon-nucleon potential up to next-to-next-to-next-to-leading order,” *Eur. Phys. J.* **A51**, 53 (2015).
- [23] E. Epelbaum, H. Krebs, and U. G. Meißner, “Precision nucleon-nucleon potential at fifth order in the chiral expansion,” *Phys. Rev. Lett.* **115**, 122301 (2015).
- [24] D. R. Entem and R. Machleidt, “Accurate charge dependent nucleon nucleon potential at fourth order of chiral perturbation theory,” *Phys. Rev. C* **68**, 041001 (2003).
- [25] D. R. Entem, R. Machleidt, and Y. Nosyk, “High-quality two-nucleon potentials up to fifth order of the chiral expansion,” *Phys. Rev. C* **96**, 024004 (2017).
- [26] S. Ishikawa and M. R. Robilotta, “Two-pion exchange three-nucleon potential: $O(q^4)$ chiral expansion,” *Phys. Rev. C* **76**, 014006 (2007).
- [27] V. Bernard, E. Epelbaum, H. Krebs, and U.-G. Meißner, “Subleading contributions to the chiral three-nucleon force. I. Long-range terms,” *Phys. Rev. C* **77**, 064004 (2008).

- [28] V. Bernard, E. Epelbaum, H. Krebs, and U.-G. Meißner, “Subleading contributions to the chiral three-nucleon force II: Short-range terms and relativistic corrections,” *Phys. Rev. C* **84**, 054001 (2011).
- [29] K. Hebeler, H. Krebs, E. Epelbaum, J. Golak, and R. Skibinski, “Efficient calculation of chiral three-nucleon forces up to N3LO for ab initio studies,” *Phys. Rev. C* **91**, 044001 (2015).
- [30] I. Tews, T. Krüger, K. Hebeler, and A. Schwenk, “Neutron matter at next-to-next-to-next-to-leading order in chiral effective field theory,” *Phys. Rev. Lett.* **110**, 032504 (2013).
- [31] S. Schulz, *Four-Nucleon Forces in Ab Initio Nuclear Structure*, Ph.D. thesis, Technische Universität, Darmstadt (2018).
- [32] S. R. Beane, P. F. Bedaque, M. J. Savage, and U. van Kolck, “Towards a perturbative theory of nuclear forces,” *Nucl. Phys.* **A700**, 377 (2002).
- [33] A. Nogga, R. G. E. Timmermans, and U. van Kolck, “Renormalization of one-pion exchange and power counting,” *Phys. Rev. C* **72**, 054006 (2005).
- [34] E. Epelbaum, A. M. Gasparyan, J. Gegelia, and U.-G. Meißner, “How (not) to renormalize integral equations with singular potentials in effective field theory,” *Eur. Phys. J.* **A54**, 186 (2018).
- [35] F. Wegner, “Flow-equations for Hamiltonians,” *Ann. Phys.* **506**, 77 (1994).
- [36] S. D. Glazek and K. G. Wilson, “Renormalization of Hamiltonians,” *Phys. Rev. D* **48**, 5863 (1993).
- [37] K. Hebeler, “Momentum space evolution of chiral three-nucleon forces,” *Phys. Rev. C* **85**, 021002 (2012).
- [38] E. D. Jurgenson, S. K. Bogner, R. J. Furnstahl, and R. J. Perry, “Decoupling in the Similarity Renormalization Group for Nucleon-Nucleon Forces,” *Phys. Rev. C* **78**, 014003 (2008).
- [39] M. Moshinsky, “Transformation brackets for harmonic oscillator functions,” *Nucl. Phys.* **13**, 104 (1959).
- [40] B. Buck and A. C. Merchant, “A simple expression for the general oscillator bracket,” *Nucl. Phys.* **A600**, 387 (1996).
- [41] J. C. Slater, “The Theory of Complex Spectra,” *Phys. Rev.* **34**, 1293 (1929).
- [42] G. C. Wick, “The Evaluation of the Collision Matrix,” *Phys. Rev.* **80**, 268 (1950).
- [43] W. Kutzelnigg and D. Mukherjee, “Normal order and extended Wick theorem for a multiconfiguration reference wave function,” *J. Chem. Phys.* **107**, 432 (1997).

- [44] J. C. Slater, “The Self Consistent Field and the Structure of Atoms,” *Phys. Rev.* **32**, 339 (1928).
- [45] V. Fock, “Näherungsmethode zur Lösung des quantenmechanischen Mehrkörperproblems,” *Z. Phys.* **61**, 126 (1930).
- [46] D. R. Hartree, “The Wave Mechanics of an Atom with a Non-Coulomb Central Field. Part II. Some Results and Discussion,” *Math. Proc. Cambridge Philos. Soc.* **24**, 111–132 (1928).
- [47] I. Shavitt and R. J. Bartlett, *Many-Body Methods in Chemistry and Physics: MBPT and Coupled-Cluster Theory*, Cambridge Molecular Science (Cambridge University Press, 2009).
- [48] A. Tichai, R. Roth, and T. Duguet, “Many-body perturbation theories for finite nuclei,” *Front. in Phys.* **8**, 164 (2020).
- [49] A. Tichai, J. Langhammer, S. Binder, and R. Roth, “Hartree–Fock many-body perturbation theory for nuclear ground-states,” *Phys. Lett. B* **756**, 283 (2016).
- [50] B. S. Hu, T. Li, and F. R. Xu, “Ab initio Rayleigh–Schrödinger perturbation calculation including three-body force,” (2018), arXiv:1810.08804 .
- [51] A. Tichai, *Many-Body Perturbation Theory for Ab Initio Nuclear Structure*, Ph.D. thesis, Technische Universität, Darmstadt (2017).
- [52] G. Hagen, T. Papenbrock, M. Hjorth-Jensen, and D. J. Dean, “Coupled-cluster computations of atomic nuclei,” *Rept. Prog. Phys.* **77**, 096302 (2014).
- [53] H. Hergert, S. K. Bogner, J. G. Lietz, T. D. Morris, S. Novario, N. M. Parzuchowski, and F. Yuan, “In-Medium Similarity Renormalization Group Approach to the Nuclear Many-Body Problem,” *Lect. Notes Phys.* **936**, 477 (2017).
- [54] S. R. White, “Numerical canonical transformation approach to quantum many-body problems,” *J. Chem. Phys.* **117**, 7472 (2002).
- [55] T. D. Morris, N. M. Parzuchowski, and S. K. Bogner, “Magnus expansion and in-medium similarity renormalization group,” *Phys. Rev. C* **92**, 034331 (2015).
- [56] F. J. Dyson, “The Radiation Theories of Tomonaga, Schwinger, and Feynman,” *Phys. Rev.* **75**, 486 (1949).
- [57] W. Magnus, “On the exponential solution of differential equations for a linear operator,” *Commun. Pure Appl. Math.* **7**, 649 (1954).
- [58] S. Blanes, F. Casas, J. Oteo, and J. Ros, “The Magnus expansion and some of its applications,” *Phys. Rept.* **470**, 151 (2009).

- [59] S. R. Stroberg, H. Hergert, J. D. Holt, S. K. Bogner, and A. Schwenk, “Ground and excited states of doubly open-shell nuclei from ab initio valence-space Hamiltonians,” *Phys. Rev. C* **93**, 051301 (2016).
- [60] H. Hergert and R. Roth, “Treatment of the Intrinsic Hamiltonian in Particle-Number Nonconserving Theories,” *Phys. Lett. B* **682**, 27 (2009).
- [61] A. Tichai, R. Wirth, J. Ripoché, and T. Duguet, “Symmetry reduction of tensor networks in many-body theory I. Automated symbolic evaluation of $SU(2)$ algebra,” (2020), arXiv:2002.05011 .
- [62] J. Suhonen, *From Nucleons to Nucleus: Concepts of Microscopic Nuclear Theory* (Springer Berlin Heidelberg, Berlin, Heidelberg, 2007).
- [63] E. Wigner, “Einige Folgerungen aus der schrödingerschen Theorie für die Termstrukturen,” *Z. Phys.* **43**, 624 (1927).
- [64] C. Eckart, “The Application of Group theory to the Quantum Dynamics of Monatomic Systems,” *Rev. Mod. Phys.* **2**, 305 (1930).
- [65] D. A. Varshalovich, A. N. Moskalev, and V. K. Khersonskii, *Quantum Theory of Angular Momentum* (World Scientific, Singapore, 1988).
- [66] P. Wormer and J. Paldus, “Angular Momentum Diagrams,” in *Advances in Quantum Chemistry*, Vol. 51, edited by J. Sabin and E. Brändas (Academic Press, 2006) pp. 59 – 123.
- [67] I. Lindgren and J. Morrison, “Angular-Momentum Graphs,” in *Atomic Many-Body Theory* (Springer Berlin Heidelberg, Berlin, Heidelberg, 1986) pp. 47–79.
- [68] S. P. Pandya, “Nucleon-Hole Interaction in jj Coupling,” *Phys. Rev.* **103**, 956 (1956).
- [69] N. M. Parzuchowski, S. R. Stroberg, P. Navrátil, H. Hergert, and S. K. Bogner, “Ab initio electromagnetic observables with the in-medium similarity renormalization group,” *Phys. Rev. C* **96**, 034324 (2017).
- [70] A. Tichai, J. Müller, K. Vobig, and R. Roth, “Natural orbitals for ab initio no-core shell model calculations,” *Phys. Rev. C* **99**, 034321 (2019).
- [71] J. Hoppe, A. Tichai, M. Heinz, K. Hebeler, and A. Schwenk, “Natural orbitals for many-body expansion methods,” (2020), arXiv:2009.04701 .
- [72] K. Hebeler, S. K. Bogner, R. J. Furnstahl, A. Nogga, and A. Schwenk, “Improved nuclear matter calculations from chiral low-momentum interactions,” *Phys. Rev. C* **83**, 031301 (2011).
- [73] T. D. Morris, *Systematic improvements of ab-initio in-medium similarity renormalization group calculations*, Ph.D. thesis, Michigan State University, East Lansing (2016).

- [74] A. G. Taube and R. J. Bartlett, “Improving upon CCSD(T): ACCSD(T). I. Potential energy surfaces,” *J. Chem. Phys.* **128**, 044110 (2008).
- [75] A. G. Taube and R. J. Bartlett, “Improving upon CCSD(T): ACCSD(T). II. Stationary formulation and derivatives,” *J. Chem. Phys.* **128**, 044111 (2008).
- [76] S. Binder, P. Piecuch, A. Calci, J. Langhammer, P. Navrátil, and R. Roth, “Extension of coupled-cluster theory with a noniterative treatment of connected triply excited clusters to three-body Hamiltonians,” *Phys. Rev. C* **88**, 054319 (2013).
- [77] K. Hebeler, 2020 (personal communication).
- [78] A. Ong, J. C. Berengut, and V. V. Flambaum, “The Effect of spin-orbit nuclear charge density corrections due to the anomalous magnetic moment on halonuclei,” *Phys. Rev. C* **82**, 014320 (2010).
- [79] R. Roth, S. Binder, K. Vobig, A. Calci, J. Langhammer, and P. Navratil, “Ab Initio Calculations of Medium-Mass Nuclei with Normal-Ordered Chiral NN+3N Interactions,” *Phys. Rev. Lett.* **109**, 052501 (2012).
- [80] L. N. Cooper, “Bound electron pairs in a degenerate Fermi gas,” *Phys. Rev.* **104**, 1189 (1956).
- [81] J. Bardeen, L. N. Cooper, and J. R. Schrieffer, “Theory of superconductivity,” *Phys. Rev.* **108**, 1175 (1957).
- [82] R. Richardson, “A restricted class of exact eigenstates of the pairing-force Hamiltonian,” *Phys. Lett.* **3**, 277 (1963).
- [83] J. Lietz, S. Novario, G. R. Jansen, G. Hagen, and M. Hjorth-Jensen, “Computational Nuclear Physics and Post Hartree-Fock Methods,” *Lect. Notes Phys.* **936**, 293 (2017).